2020

IDENTIFICATION OF HEAT RELEASE SHAPES AND COMBUSTION CONTROL OF AN LTC ENGINE

Radhika Sitaraman
Michigan Technological University, rsitaram@mtu.edu

IDENTIFICATION OF HEAT RELEASE SHAPES AND COMBUSTION CONTROL OF AN LTC ENGINE

By

Radhika Sitaraman

A THESIS

Submitted in partial fulfillment of the requirements for the degree of

MASTER OF SCIENCE

In Mechanical Engineering

MICHIGAN TECHNOLOGICAL UNIVERSITY

2020

This thesis has been approved in partial fulfillment of the requirements for the Degree of MASTER OF SCIENCE in Mechanical Engineering.

Department of Mechanical Engineering - Engineering Mechanics

Thesis Co-advisor: *Dr. Mahdi Shahbakhti*

Thesis Co-advisor: *Dr. Jeffrey Naber*

Committee Member: *Dr. Hoseinali Borhan*

Department Chair: *Dr. William W Predebon*

Dedication

To My Parents & Sister

Contents

List of Figures

List of Tables

Preface

Work documented is in continuation of research by Kaveh Sadabadi [1], Kaushik Kannan [2], Nitin Kondipati [3], Akshat Raut [4] and Aditya Basina [5]. Engine data collected in [2, 3] was used in Chapter 3. The convolutional neural network developed by Yajie Bao was used for heat release rate classification in Section 3.2 and k-means developed by Aditya Basina was used in Section 3.4. Dr. Mahdi Shahbakhti provided guidance on the aspects of the thesis includign engine data analysis, heat release rate classification model based on machine learning approach, identification of scheduling parameter and building control architecture with scheduling variable. Dr. Jeffrey Naber provided guidance for proper analysis of the engine heat release data. Dr. Hoseinali Borhan and Dr. Javad Mohammadpour Velni provided technical advise on optimization tools for building data driven modelling for engine data and machine learning approach for classification of heat release rate traces. The LS-SVM code from the reference [6] was used in Chapter 4 to perform data driven modelling. RCCI engine plant developed in references [1, 2, 3, 4] is used to assess the performance of controller.

Acknowledgments

I wish to acknowledge the support of my family for letting me pursue my dream.

I would like to express my sincere thanks to Dr. Mahdi Shahbakhti for giving me an opportunity to be part of his research team, for guiding and encouraging me to understand machine learning techniques and explore further to improve the performance of the model and realize the goal of this project.

I wish to express my gratitude to Dr. Hoseinali Borhan and Dr. Javad Mohammadpour Velni for mentoring and guiding me closely on data driven modelling. Their continuous mentoring helped me to understand and make progress in it. I would like to thank Dr. Jeffrey Naber for serving as my co-advisor and Dr. Hoseinali Borhan for agreeing to be in my committee. I would like to acknowledge NSF for funding and Cummins inc. for an internship opportunity in Summer 2019 in relation to the work on data driven LPV modelling of a diesel engine charge flow and emissions.

I would also like to recognise the invaluable support provided by Yajie Bao, Aditya Basina, Sadaf Batool and Behrouz Khoshbakht Irdmousa during this study. They helped me out at a peer level on various research queries. I wish to express my deepest gratitude to my friend Shruti Amre for always being there as a moral support throughout this study .

List of Abbreviations

ANN	Artificial Neural Network
aTDC	after Top Dead Center
bTDC	before Top Dead Center
CAD	Crank Angle Degree
CFD	Computational Fluid Dynamics
CFR	Cooperative Fuel Research
CI	Compression Ignition
CNG	Compressed Natural Gas
CNN	Convolutional Neural Network
COV	Co-efficient., bcxz1 of Variation
DDM	Data Driven Modelling
DI	Direct Injection
DKL	Deep Learning Neural Network
ECU	Electronic Control Unit
EGR	Exhaust Gas Re circulation
ELM	Extreme Learning Machine
EOC	End of Combustion
EPA	Environmental Protection Agency

FPGA	Field Programmable Gate Array
GA	Genetic Algorithm
GDI	Gasoline Direct Injection
HCCI	Homogeneous Charge Compression Ignition
HDMR	High Dimensional Model Representation
IC	Internal Combustion
IMEP	Indicated Mean Effective Pressure
LPV	Linear Parameter Varying
LS-SVM	Least Square Support Vector Machine
LTC	Low Temperature Combustion
MABX	Micro Auto Box
MPC	Model Predictive Control
MPRR	Maximum Pressure Rise Rate
MSE	Mean Square Error
NO_x	Oxides of Nitrogen
NTEOFC	Not To Exceed Oxygen Fuel Control
PCA	Principal Component Analysis
PCCI	Premixed Charge Compression Ignition
PFI	Port Fuel Injection
PM	Particulate matter
PN	Particulate Number

PR	Premixed Ratio
PSO	Particle Swam Optimisation
RCCI	Reactivity Controlled Compression Ignition
RGS	Random Gaussian Signal
RMSE	Root Mean Square Error
RVM	Relevance Vector Machine
SA	Simulated Annealing
SI	Spark Ignition
SOC	Start of Combustion
SOI	Start of Injection
SVM	Support Verctor Machine
SVSF	Smooth Variable Structure Filter
VGT	Variable Geometry Turbocharger

Nomenclature

Symbol	**Variable**	**Units**
c_v	Specific heat at constant volume	kJ/kg.K
LHV	Lower Heating Value	MJ/kg
m'_{air}	Mass flow of air	g/s
m'_{fuel}	Mass flow of fuel	mg/cycle
mf_{iso}	Mass flow of iso- octane fuel	mg/cycle
mf_{nhep}	Mass flow of n-heptane fuel	mg/cycle
N	Engine speed	RPM
n_c	Polytropic coefficient for compression	-
n_e	Polytropic coefficient for expansion	-
P_{in}	Intake Pressure	kPa
P_{ivc}	Pressure at IVC	kPa
r_c	Compression Ratio	-
Sig	Spontaneous ignition front speed	m/s
T_{exh}	Exhaust gas Temperature	K
T_{in}	Intake Temperature	K
T_{ivc}	Temperature at IVC	K
T_{rg}	Temperature of residual gas	K

T_w	Temperature of cylinder wall	K
γ	Ratio of specific heat	-
ΔT	Temperature rise	K
ϕ	Equivalence ratio	-
θ	Crank Angle	CAD

Abstract

Low Temperature Combustion (LTC) regimes have gained attention in internal combustion engines since they deliver low nitrogen oxides (NO_x) and soot emissions with higher thermal efficiency and better combustion efficiency, compared to conventional combustion regimes. However, the operating region of these high-efficiency combustion regimes is limited as it is prone to knocking and high in-cylinder pressure rise rate outside the engine safe zone. By allowing multi-regime operation, high-efficiency region of the engine is extended. To control these complex engines, understanding and identification of heat release rate shapes is essential. Experimental data collected from a 2 liter 4 cylinder LTC engine with in-cylinder pressure measurements, is used in this study to calculate Heat Release Rate (HRR). Fractions of early and late heat release are calculated from HRR as a ratio of cumulative heat release in the early or late window to the total energy of the fuel injected into the cylinder. Three specific HRR patterns and two transition zones are identified. A rule based algorithm is developed to classify these patterns as a function of fraction of early and late heat release percentages. Combustion parameters evaluated also showed evidence on characteristics of classification. Supervised and unsupervised machine learning approaches are also evaluated to classify the HRR shapes. Supervised learning method (Decision Tree)is studied to develop an automatic classifier based on the control inputs to the engine. In addition, supervised learning method (Convolutional

Neural Network (CNN)) and unsupervised learning method (k-means clustering) are studied to develop an automatic classifier based on HRR trace obtained from the engine. The unsupervised learning approach wasn't successful in classification as the arrived k-means centroids didn't clearly represent a particular combustion regime. Supervised learning techniques, CNN method is found with a classifier accuracy of 70% for identifying heat release shapes and Decision Tree with the accuracy of 74.5% as a function of control inputs.

On rule based classified traces with the use of principle component analysis (PCA) and linear regression, heat release rate classifiers are built as a function of engine input parameters including, Engine speed, Start of injection (SOI), Fuel quantity (FQ) and Premixed ratio (PR). The results are then used to build a linear parameter varying (LPV) model as a function of the modelled combustion classifiers by using the least square support vector machine (LS-SVM) approach. LPV model could predict CA_{50}(Combustion phasing), IMEP (indicated mean effective pressure) and MPRR (maximum pressure rise rate) with a RMSE of 0.4 CAD, 16.6 kPa and 0.4 bar/CAD respectively. The designed LPV model is then incorporated in a model predictive control (MPC) platform to adjust CA_{50}, IMEP and MPRR. The results show the designed LTC engine controller could track CA_{50} and IMEP with average error of 1.2 CAD and 6.2 kPa while limiting MPRR to 6 bar/CAD. The controller uses three engine inputs including, SOI, PR and FQ as manipulated variables, that are optimally changed to control the LTC engine.

Chapter 1

Introduction

Greenhouse gas emissions in atmosphere have increased world wide. In the latest report by the United States Environmental Protection Agency (EPA), it is evident that transportation sector is one of the major contributors of greenhouse gas emissions in the United States [7]. EPA and other emission regulating agencies across the world have taken measures to curb the pollutants. They have imposed stringent emission norms and higher fuel economy targets. Automotive manufacturers and researchers have continuously worked to innovate new techniques in order to achieve emission and fuel economy targets. Many concepts have been developed to eliminate the drawback observed on a conventional injection technique. In the conceptual model of conventional direct injection (DI) combustion in [8] the process involved in creation of NO_x and soot is described. NO_x gets created at the contact of diffusion flame front with premixed charge. Soot gets generated at the fuel rich zones of the fuel plume. Based on this understanding a recent technique of low temperature combustion(LTC) was developed. It results in ultra low NO_x and soot as significant amount of fuel is pre-mixed with air before the actual combustion begins. Soot is eliminated by having a premixed mixture of fuel and air. NO_x is reduced by having a premixed volumetric combustion [9].Multiple concepts of LTC demonstrated by researchers [2, 9, 10, 11], either used single fuel or combination of two fuels.

Some of the prominent techniques of LTC are shown in the Figure 1.1, in local equivalence ratio and temperature space.

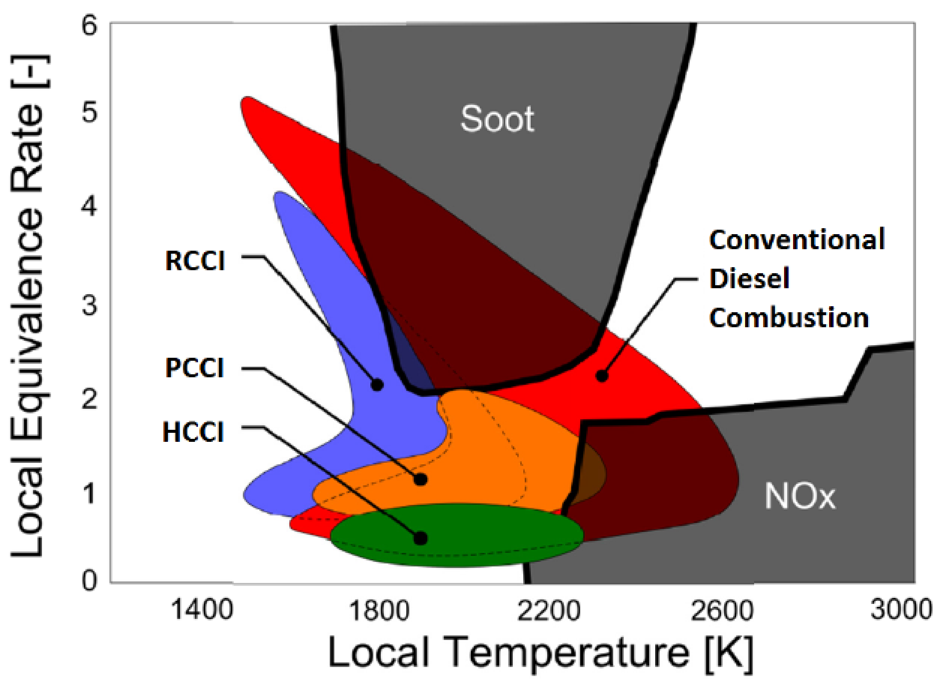

Figure 1.1: Soot and NO_x in equivalence ratio to Temperature space reference [12] Adapted from reference [13]

Interestingly, conventional diesel operates in a zone which is prone for higher NO_x and soot. Advanced combustion techniques depicted, predominantly operate on a lower NO_x and soot zone. Various Combustion regimes of interest and research work is described below.

† Homogeneous charge compression ignition (HCCI) is a concept in which fuel is injected into intake manifold to achieve a homogeneous premixed charge. Charge is compressed in the compression stroke. It results in controlled auto ignition (CAI). So, a volumetric combustion with a small burn duration is achieved [14, 15]. It results in high in cylinder pressure rise rate.

† Premixed charge compression ignition (PCCI) was developed from HCCI concept to reduce its drawbacks of higher pressure rise rate. In PCCI, fuel is injected partially in the manifold and in-cylinder in order to reduce homogeneity of fuel and air, [16, 17, 18]. Secondary fuel injection timing adds more control on combustion phasing.

† Reactivity controlled compression ignition (RCCI) works on the principle of difference in reactivity rates of two different fuels being used for combustion. The low reactivity fuel is injected into the intake ports. In the homogeneous mixture of low reactivity fuel and air, the high reactivity fuel is injected inside the cylinder. Studies in references, [19, 20, 21] discuss additional control levers for governing combustion phasing such as difference in reactivity of both fuels,

start of injection timing of the higher reactivity fuel and the ratio of both low reactivity and high reactivity fuel on the engine.

Understanding of these low temperature combustion techniques play critical role in order to study the heat release traces of the engine and incorporate the dynamics involved while developing engine models.

1.1 Engine modelling for controls

Internal combustion (IC) engine modelling techniques have gained attention as it could improve engine performance. It could predict engine performance parameter without physically running the engine and also estimate parameters which are difficult to be measured [22]. Automotive manufacturers are keen to improve accuracy of engine model as it saves money and product development time. Control oriented models are advanced mathematical models suitable for control system design. It is built based on two fundamental methods

† First principle based approach

† Data driven approach

In first principle based approach, model is primarily based on physical principles.

Additionally engine experimental data is used to parameterize engine models. This helps to closely represent the engine. Input-output models and first principle based models are inter dependent on each other to ensure accuracy of the engine model. In [23] reviewed advancement in engine modelling. Improved engine model has resulted in better control of engine. The model was developed for performance optimisation of steady state calibration and dynamic corrections to calibration.

First principle based approach is time consuming to build. As an alternative, data driven approach has gained significance. In [24] data driven approach, the relationship between inputs and outputs of the system is modelled, without complex physics based modelling of the system. Data driven modelling represent the significant contribution made by the fields, artificial intelligence (AI), Computational intelligence (CI), soft computing (SC), machine learning (ML), data mining (DM) and intelligent data analysis (IDA). Data driven modelling approach focused in this research work is based on machine learning based techniques. Machine learning theory is about building a model capable of learning to improve its own performance based on its previous experience. It uses pattern recognition and statistical inference to come up with a conclusion. The study in [25] discussed approaches using machine learning to make engine modelling process faster. The results showed that data driven models demonstrated better performance than physical models by its ability to capture non-linear trends and pattern in the data. It is recommended in a scenarios where data is incomplete to build a physical model. Machine learning approach has been widely used in the literature for modelling engine by utilizing engine experimental data.

Next sections discuss on the current research work on identification of combustion events, system identification of the engine through machine learning approach and control of the engine.

1.2 Machine learning based approach for combustion classification

Combustion identification in ICEs can be studied by analyzing in-cylinder pressure data. In-cylinder pressure measurement with a piezoelectric sensor mounted on the engines, is a conventional approach for off-line analysis of combustion process.

Various combustion metrics listed in Figure 1.2 can be analysed with machine learning techniques. With machine learning algorithm, misfire event identification was done by analysing the vibration pattern associated with particular cylinder in [26]. Identification of misfire events is closely tied to identification of patterns in combustion trace, which corresponds to misfire. Linear model tree algorithm was suggested to have better classification accuracy compared to other algorithms considered in [26]. Similarly, with the vibration measurement data from the engine, classifier accuracy was compared in [27], between convention feature extraction approach with support

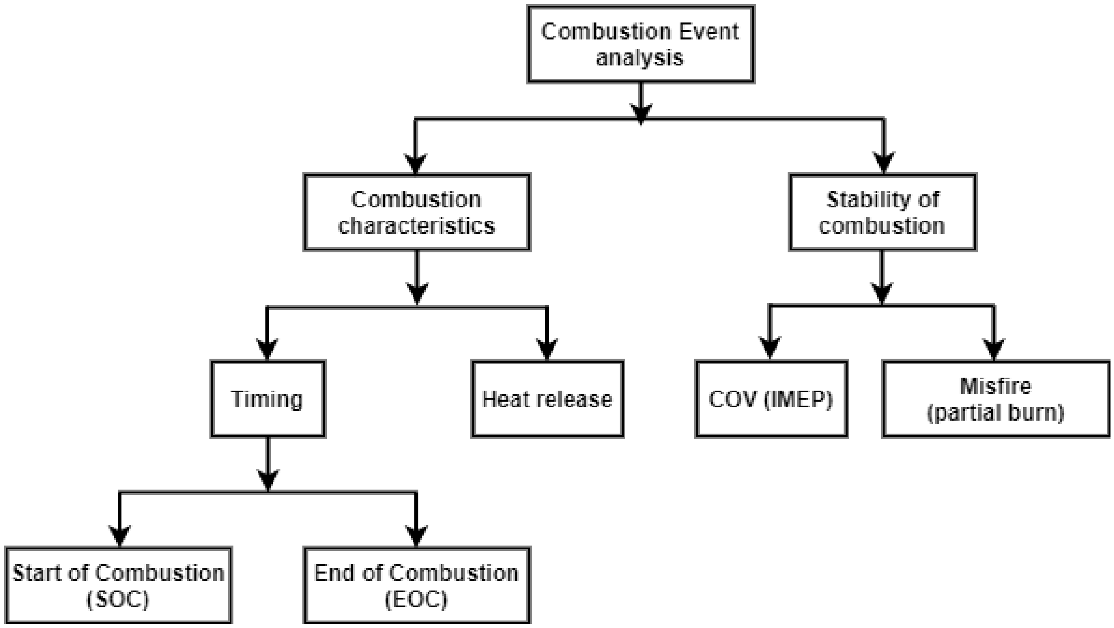

Figure 1.2: Combustion metrics

vector machine (SVM) and deep learning convolutional neural network (CNN) without feature extraction. Deep learning approach was observed to perform better better compared to CNN with feature extraction and SVM for multi-class misfire detection.

In [28] have listed deep learning techniques with 2-D convolutional neural network, which could extract features to identify combustion instability. This could help in identifying and preventing the occurrence of poor combustion. Discussed in [29] is a novel method of building adopted artificial neural network(ANN) model from the empirical model. The developed model showed an accuracy of 85% as mean prediction accuracy. In [30], developed a misfire detection technique for an HCCI engine. Misfire was created by cutting the fuel supply, varying air to fuel ratio (AFR) and low air intake temperature. Engine powered with ethanol by using experimental data to model ANN for misfire detection. ANN is modelled using the in-cylinder pressure value modeled using regression equation using maximum heat release rate (MHRR) at crank angles, 0, 5, 10, 15 and 20 aTDC. The ANN model developed with four hidden layers using in-cylinder pressure was able to detect the misfire with 100% accuracy.

In [31], a misfire identification technique for HCCI engine fueled with ethanol was carried out. Skewness and kurtosis of in cylinder pressure and crankshaft rotational speed were analysed. Result showed that on all misfire cycles, engine speed showed negative skew values. In [32], to improve the operating range of the HCCI engine, the authors studied cyclic variation of CA50 near misfire region to extend the range of operation. Return map and symbol sequence approach was used to statistically model the system and a joint prediction of CA50 one cycle ahead was conducted. The residual between predicted and actual data was in the 95% confidence interval and hence model prediction is acceptable.

In [33], the authors discussed about limited operating range of HCCI due to higher pressure rise rate and ringing. Ringing intensity (RI) increased with lower burn duration and advanced CA50. ANN model was built with in-cylinder pressure values at 5,10 and 15 CAD aTDC and Pmax to predict RI with prediction error of 4.2%. In [34], intense ringing in an HCCI engine, which limits the range of operation was studied. To this end a ANN based approach was designed to predict the combustion noise level to identify ringing regions. The model was able to predict with an error of less than 0.5% from the actual combustion noise level.

Extreme learning machine (ELM) are feed forward neural networks for classification [35] with extremely fast learning speed. So, was named as "Extreme learning machine". ELM is single hidden layer feedforward neural networks which randomly chooses hidden nodes and analytically determines the output weight. In theory [35], algorithm provides good generalization performance at extremely fast learning speed. ELM was used to model a bio-diesel engine performance. In [36], optimisation of engine was carried out using logarithmic transformation to reduce the impact of data scarcity in real time. The result was concluded based on the comparison of engine model between two optimization techniques, simulated annealing (SA) and particle swam optimisation (PSO).

Engine ignition pattern analysis is one of the diagnostic method for gasoline engines. In [37], wavelet packet transform was used to extract features from the ignition pattern. Based on identified features, then a multi-class least square support vector machine (MCLS-SVM) was used to identify fault related to malfunctioning parts of engine. Diagnosis accuracy of MCLS-SVM was higher than the typical MLP (multi layer perceptron) approach in the experimental results.

In [38], studied about fault diagnosis for process monitoring in industrial environment. In process monitoring, unsupervised learning approach on multi dimensional data for clustering result was slow due to the curse of dimensionality and result in unrelated features existence. Dimensionality reduction was carried out using Principal Component Analysis (PCA). PCA is an approach for feature extraction by creation of new independent variable which is a combination of the old variables. Engine output parameters are dependent on many input variables. PCA can help reduce dimensionality of the data by generating new independent variables,also known as principal axes. Multi-linear extensions of PCA was observed to be effective in reducing the dimensionality to result in better separation of clusters. Also, the study in the reference article[39] show that vibration measurement from the engine was used to identify fault on engine related to defective lash adjuster and chain tensioner. Based on the severity of measured vibration, it could identify and classify fault into specific fault domain. The smooth variable structure filter (SVSF) algorithm outperformed in comparison with other approaches and showed a success rate of 97% in the detecting the faults.

With the study on reference articles, *its evident that a lot of research has been done in order to identify misfire and fault diagnostics on engine, but significant study hasn't happened in terms of characterizing the combustion traces to identify heat release patterns.* This in turn opens up a large scope of work in terms of classification of combustion traces on a multi-mode engine. Once classification of combustion traces is done, an effective method of integration of this information into real-time system identification is done and the combustion control for the engine will be required.

Thus, in the subsequent section prior studies in terms of system identification and control of engine combustion are reviewed.

1.3 Machine learning approaches for ICE combustion modeling and control

Multiple machine learning techniques have been explored to build engine models that are compatible for ICE controls. In [40], HCCI engine powered with butanol and ethanol was studied. Engine powered with butanol, n-heptane and ethanol was modelled with feed forward neural network (FFNN) and radial basis function neural network (RBFNN). Multiple-input and multiple-output (MIMO) neural network developed showed that both approaches were able to predict the engine performance metrics including indicated mean effective pressure (IMEP), thermal efficiency, in-cylinder pressure, net total heat released, nitrogen oxides (NO_x), carbon monoxide (CO), and total hydrocarbon (THC) concentrations with error less than 4%. With the fact that FFNN involved less complex equation in comparison to RBFNN, which involved complex equations but needed less training time.

In [41], a high accuracy models with low computational effort for HCCI engine was built. The authors in reference [41] developed a gray box modelling technique that used a combination of physical model with artificial neural network (ANN) feed forward model for the prediction of CA50, IMEP and exhaust gas temperature (Texh). Developed model predicted CA50, IMEP and Texh with an accuracy of less than 1 crank angle degree, 0.2 bar and 6°C, respectively. In [42], prediction of engine rotational dynamics was done using a gray box model that consisted of a physical mode and a black box ANN. The authors studied 2 gray box architectures: series and parallel. Gray box model with series structure was identified and found to perform better than the parallel approach. In [43], discussed that HCCI engines could be brought to practical use if the drawbacks on high THC and CO is reduced by controlling CA_{50} for lower emissions and higher thermal efficiency. Gray box modeling as a combination of both physical and feed forward artificial neural network (FFANN). Model was build for two different HCCI engines. The model could predict combustion phasing, load, exhaust gas temperature and emissions (THC, CO, NO_x) with the validation on steady state and transient test prediction error resulted in less than 10%.

In [44], optimisation of bio diesel engine engine model was built using kernel based ELM technique. By use of cuckoo search (CS), optimal bio-diesel ratio with minimization cost function for both fuel cost and emissions. The results were compared with LS-SVM. It was concluded that K-ELM achieves comparable result and optimisation with CS results in reliable prediction and optimisation. In [36], optimisation of bio-diesel engine with less emissions was evaluated with ELM, least-squares support vector machine (LS-SVM) and RBFNN approach to model the engine. It was evaluated with two optimization methods, namely simulated annealing (SA) and particle swarm optimization (PSO) as optimisation function to result in optimal bio-diesel ratio. ELM with logarithmic transformation model was observed to perform faster and better. PSO as an optimisation algorithm performed better with cost function on fuel cost and lower emissions.

In [45], evaluated the prediction capability of the ANN model built for an engine operated with exhaust gas re-circulation (EGR) strategies. It was built with 70% experimental data, 15% for cross validation to avoid overfitting and other 15% for testing the model accuracy in prediction. With the inputs- load, rail pressure, EGR% and fuel, model could predict the performance and emission parameters with high correlation, it was also able to map the trade off between PM-NO_x-brake specific fuel consumption (BSFC) under operation with EGR. In [46], authors studied that engine operating on transient condition based on steady state tuned tables may not result in optimal performance. To mitigate this issue, authors built a real time system capable of perceiving driver, driving pattern and optimize performance by using Markov decision process. It resulted resulted in overall 9.3% improvement in fuel economy compared to baseline calibration by the use of decentralised learning to optimize fuel economy and emission by varying variable geometry turbocharger (VGT) position and injection timing, .

In [47], a control oriented model was built to control combustion timing, engine load and combustion efficiency for an HCCI engine. Detailed physics based model was developed including effect of residual gases and rate of fueling on model out put parameters (combustion timing, engine load and combustion efficiency). Model could perform with acceptable accuracy in both steady state and transient validation. [48] is based on combustion timing and load control of HCCI engine. Nonlinear control oriented model (NCOM) developed was linearized and integral discrete time sliding mode controller (IDSMC) was built to control load and combustion timing. Its performance was compared to manually tuned proportional- integral (PI) controller. IDSMC showed better tracking efficiency and also responded well to the introduction of disturbance in equivalence ratio and intake temperature. In [49], combustion analysis comparison of performance between DI engine and bio-diesel with waste vegetable oil was compared on similar operating conditions. ANN model was built to model the engine characteristics operated with waste vegetable oil from the experimental results and IDSMC performed better in tracking efficiency.

RCCI promising for its high thermal efficiency but comes with a need of high accuracy control oriented model and control technique. Approach of data driven linear parameter varying model, built based on support vector machine was developed in [50]. The model could be built fast and model could track CA_{50} for change in load with less than 1 CAD when built with a model predictive controller (MPC). The linear parameter varying (LPV) model is built as a function of fuel quantity. In [51], model based control was developed and trajectory optimised for lower emissions was fed as reference. The computational requirement of the gray box model was 1 ms in a 2.67GHz processor. Controller ability to track optimum trajectory for IMEP and CA50 was tested and verified. In [52], automated the proportional–integral–derivative (PID) system tuning by using simulator CARLA, an open source simulator . Model was evaluated for performance on the governing the engine idle speed. The method performed better than typical tuning process of the PID parameters and better results both in simulation and in practice.

LPV modelling approximates the non linear system with a state space structure suitable to build linear controller on it. In [6, 50], method of developing LPV model based on support vector machine is proposed. The study in [50] demonstrated system identification capability using the above technique for control of combustion phasing of the RCCI engine. In addition to [50], capability of this technique for modelling maximum pressure rise rate (MPRR) is discussed in [5]. The limitation of this approach is only 2 manipulated variables start of injection (SOI) and fuel quantity were available to achieve control on combustion phasing and IMEP.

1.4 Shortcomings of literature

The review in Section 1.2 and 1.3, showed prior studies into extracting features of combustion parameters from the in-cylinder pressure traces, vibration measurements or identifying engine combustion related fault, but the area of identifying the heat release rate patterns from engine data for the control of a multi-mode LTC engine remains under explored. Identifying pattern of heat release rate in combustion events will be critical to optimally control operation of multi-mode LTC engines.

The review in Section 1.3, discussed various machine learning and deep learning approaches in practice for ICE modelling and control. However there is no integrated machine learning and control method based on engine heat release shapes for LTC engines. In particular one promising area is the application of machine learning based LPV models for MPC control of LTC engines based in identifying varying heat release shapes.

1.5 Scope of Research

Based on the shortcomings listed in Section 1.4, the scope of the thesis is defined as: Machine learning approach is suggested for building accurate model of IC engine.

Numerical simulation capability of the technique will help to improve modelling capability. A real time predictive control on a cycle to cycle basis, to optimize combustion mixture formation and improve stability of combustion.

Scope of the research is listed as :-

† Study machine learning algorithm and develop an algorithm to classify the heat release rate patterns in an LTC engine. This would form the basis in identification of heat release rate patterns which can be used for engine combustion control. Model classification with machine learning technique would also help assess if the classification problem could be solved with higher prediction accuracy.

† Analyze experimental data from an LTC engine to determine between heat release pattern and engine control variables. The results from this study will be used to determine optimum scheduling parameters for engine controls.

† Create a machine learning based control oriented model to predict CA_{50}, IMEP and MPRR for an LTC engine

† Design and verify optimal predictive combustion controller for a LTC engine to adjust engine load and combustion phasing, while meeting MPRR and actuators constraints.

1.6 Organization of Thesis

Experimental setup of engine is discussed in Chapter 2. Machine learning approach used for classification, results and its accuracy are discussed in Chapter 3. Identification of combustion classifier, discussed in Chapter 4 and building of LPV- SVM model as a function of it as scheduling parameter is discussed in Chapter 5. Building a MPC control structure to control combustion phasing, IMEP with MPRR limitation is covered in Chapter 6. Conclusion and future work are listed in Chapter 7, followed by sections of appendix including data files and other relevant details of the thesis.

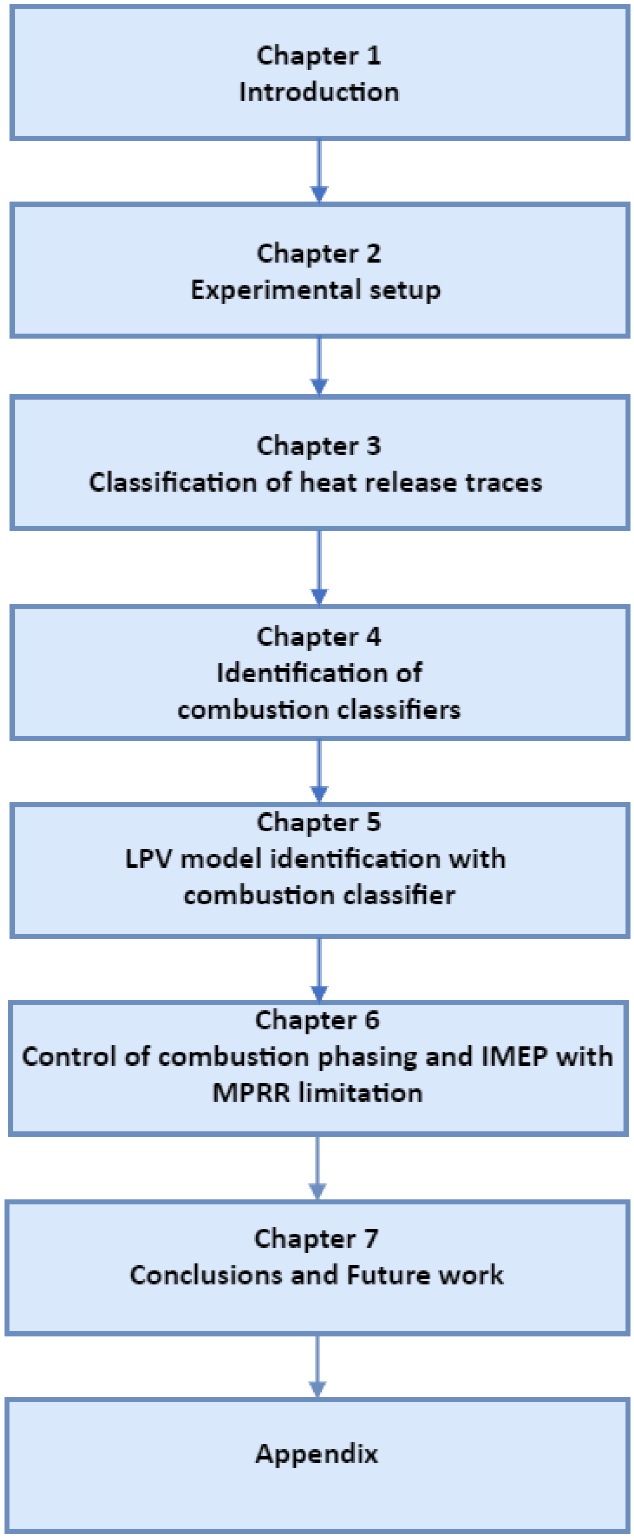

Figure 1.3: Thesis Organization

Chapter 2

Experimental Setup

Engine experimental data is required in order to study and classify LTC heat release shapes and identify appropriate schedulign parameters for LTC engine control. Specifications of the engine, test cell layout and data acquisition are explained in this chapter.

2.1 Engine Specification

This thesis uses a 2 Liter GM Ecotec engine with the specification listed in Table 2.1. The engine is located at Michigan tech's Advanced Propulsion Systems Research Center (APSRC).

Table 2.1
Engine Specifications

Make	General Motors
Model	Ecotec 2.0L Turbocharged
Engine Type	4 stroke,Gasoline
Fuel System	Direct Injection
Number of Cylinders	4 Cylinders
Displaced Volume	1998 [cc]
Bore	86 [mm]
Stroke	86 [mm]
Compression Ratio	9.2:1
Max Engine Power	164 @ 5300 [kW @rpm]
Max Engine Torque	353 @ 2400 [Nm @rpm]
Firing Order	1-3-4-2
IVO	25.5/-24.5 [°CAD bTDC]
IVC	2/-48 [°CAD bBDC]
EVO	36/-14 [°CAD bBDC]
EVC	22/-28 [°CAD bTDC]
Valve lift	10.3[mm]

2.1.1 Engine Modifications

The engine is modified to demonstrate low temperature combustion concepts Figure 2.1. To this end, a dual fuel injection system is added to the engine as part of the modifications. Engine is modified to have both iso-octane port fuel injection (PFI) system and a n-heptane direct injection (DI) system. In the data used for this research work, both fuels are used to vary the reactivity of the charge inside the cylinder. Injection system calibration was carried out and documented in [2, 3].

The engine setup also has a heater upstream of air intake, in order to vary intake air temperature.

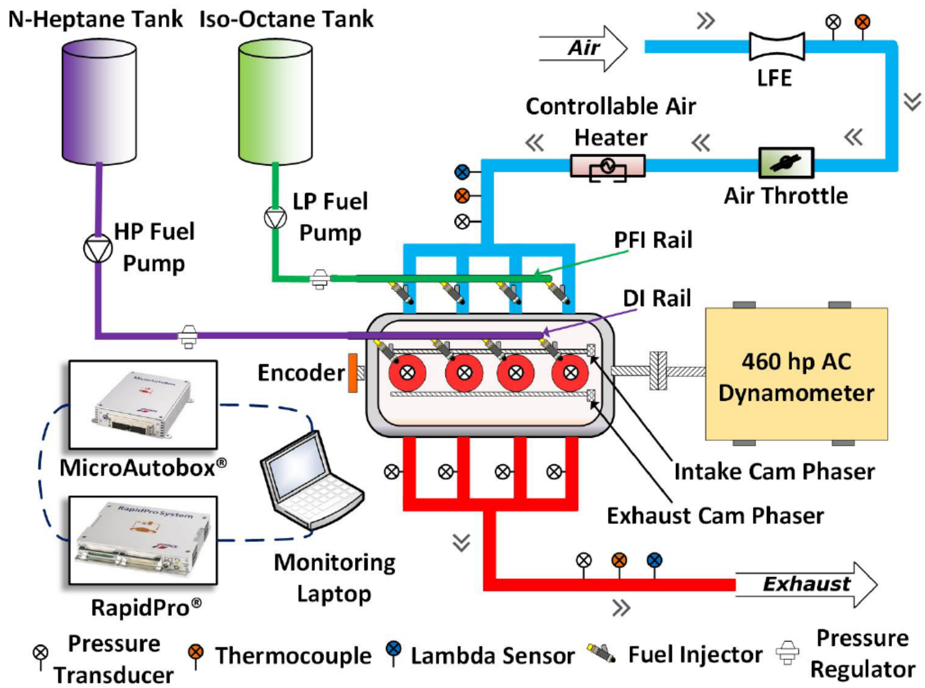

Figure 2.1: LTC engine setup in this work [4]

Iso-octane is the low reactivity fuel and n-heptane is the high reactivity fuel. Properties of these two fuels are summarized in Table 2.2.

Table 2.2
Fuel Specifications

Property	Iso-Octane	N-Heptane
Higher Heating Value [MJ/kg]	47.77	48.07
Lower Heating Value [MJ/kg]	44.30	44.56
Density [kg/m^3]	693.8	686.6
Octane Number [-]	100	0

2.2 Data Acquisition

Data from the engine is captured using 3 subsystems including, National Instruments Labview, dSPACE and ACAP combustion analyser. The NI Labview gathered temperature data from the engine. It also sends control commands to dynamometer and the air intake temperature. dSPACE helped in sending control signals to various actuators on the engine. Injectors, spark plug and EGR valve control signals are also provided by dSPACE. Calculations are preformed in Field Programmable Gate Array(FPGA) as shown in [3] and communicated to RapidPro through a CAN. dSpace also has a slave controller named micro auto box (MABX). Both RapidPro and MABX together assist to control the engine.

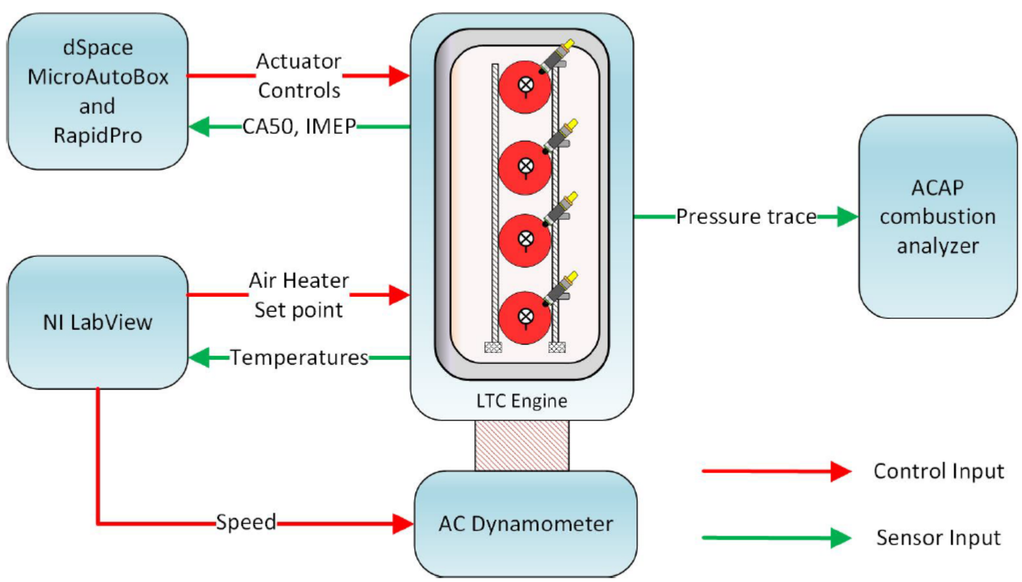

Figure 2.2: LTC Engine Data Acquisition from reference [5]

ACAP is used to collect in-cylinder pressure traces from the piezo electric transducers-115A04 transducers. The crank angle reference is gathered by encoder mounted on the crankshaft of the engine.

2.3 Test data and Analysis

Engine data analysed in this research work was collected by varying independent parameters like engine speed, fuel quantity, pre-mixed ratio, start of injection of n-heptane, intake manifold temperature and intake manifold pressure. Pre-mixed ratio (PR) is defined as the ratio of the energy of the low reactivity fuel to the energy of the total fuel. The low reactivity fuel in current experiment is iso-octane and the high reactivity fuel is n-heptane.

Table 2.3 summarizes independent parameters varied in the test. Parameter of interest is in-cylinder pressure trace as a function of engine crank angle. At every steady state operating point 100 cycles of data is collected.

Table 2.3
Test conditions of engine data

Engine Speed (rpm)	Fuel Quantity (mg/st)	Pre- mixed ratio (%)	SOI (bTDC)	Intake manifold temperature (°C)
800	10- 30	20 40 60	15-40	40-110
1000	10 - 40	20 40 60	20-100	40-110
1100	30	60	60-80	70-80
1200	10-40	20 40 60	28-80	40-110
1400	10-40	20 40 60	33-60	40-110
1600	20-40	20 40 60	40-60	40-110
1800	20-40	20 40 60	47-70	60-110
1900	20	20 40	53-60	80-90
2000	20-30	20 40 60	53-80	80-100
2100	20-30	20 40	53-70	80-100
2300	20	20	65	80

2.3.1 Uncertainty Analysis

Level of confidence in the results comes based on the amount of uncertainty associated with the measurement of data. Uncertainty arises in measured data due to numerous factors like instrumentation and operating conditions. Uncertainty associated with various engine parameters are documented in Table 2.4 from [2]. The uncertainties

Table 2.4
Table of measured parameters and associated uncertainties

Parameter[Units]	**Value**	**Uncertainty(+/-)**
Bore [m]	0.086	0.001
Stroke [m]	0.086	0.001
Cylinder Pressure [kPa]	95-4000	1%
Crank Angle [CAD]	0-720	1
T_{in}[$^\circ$ C]	4-100	2%
$P_{in}[kPa]$	95-105	0.5%
$m_{fuel}[mg/st]$	11.0-40.0	0.1%
N [rpm]	800-2300	10

of the derived parameters are tabulated in Table 2.5 from [2]

Table 2.5
Derived parameters and associated uncertainties

Parameter[Units]	**Value +/- Uncertainty**
CA_5_0 [CAD aTDC]	-1 +/- 1
IMEP [kPa]	540.7 +/- 28.1
MPRR [bar/CAD]	12 +/- 0.6

2.4 Heat release rate calculation

In-cylinder pressure trace is collected on engine. The pressure transducers are capable of measuring in range of 0-35000 psi and have sensitivity of 1.442 pC/psi. The pressure transducers measure relative pressure and process of referencing it to intake manifold pressure is called pegging. Pressure signal is obtained as a function of crank angle at an interval of 1 crank angle degree (CAD). In pressure trace, the noise associated with it, has to be cleared off [53] before analysis for heat release rate. Based on the work carried out by [3], a Butterworth low pass filter with a cut off frequency of 0.5 and order 1 was identified to filter pressure trace.

Further calculation of heat release rate is carried out by using first law of thermodynamics and is given by Eq. (2.1).

$$\frac{dQ}{d\theta} = \frac{\gamma}{\gamma - 1}.P\frac{dV}{d\theta} + \frac{1}{\gamma - 1}V\frac{dP}{d\theta} + \frac{dQ_{ht}}{d\theta} + \frac{dQ_{crevice}}{d\theta} \tag{2.1}$$

Where γ is a polytropic compression coefficient calculated from the compression region. Instantaneous volume (V) at each crank angle is calculated by Eq. (2.2). dQ_{ht} refers to heat loss to the walls. $dQ_{crevice}$ refers to crevice loss and is neglected.

$$V(\theta) = V_c + \frac{\pi.B^2}{4}.P(l + a - acos\theta - \sqrt{l^2 - (asin\theta^2)} \tag{2.2}$$

Where B is the diameter of the bore, l is length of the connecting rod, V_c is the clearance volume and a is the crank radius.

The phenomenon for the heat loss to the surrounding is attributed to the convective heat transfer, represented by Eq. (2.3).

$$\frac{dQ_{ht}}{d\theta} = h_c(T(\theta) - T_w) \tag{2.3}$$

Where T is the instantaneous temperature of charge inside the cylinder and T_w is the temperature of the cylinder wall. T is calculated by using the the ideal gas equation. h_c, heat transfer coefficient is calculated by using the Woshini model which was later modified by Chang [54] has been used in LTC combustion regimes.

With heat release rate calculated for each combustion trace, in Chapter 3, classification of heat release type is carried out. Classification of heat release rate traces, helps interpret and optimise combustion efficiency. Rule based and machine learning based approaches are evaluated to identify the best approach to effectively classify heat release trace.

Chapter 3

Classification of heat release rate traces

Machine learning provides a wide range of algorithms for classification. With reference to classification, a multi-class classification problem is being addressed here as the heat release rate traces are intended to be grouped in three predominant combustion phases and the fourth and fifth bins are accounted for the transition. On a classification problem the main goal addressed is that the model should be capable of predicting appropriate class for the given heat release trace. Classification model, is trained to identify heat release rate traces by using either supervised or unsupervised learning techniques of machine learning. Clusters of heat release types of a multi-dimensional engine data is reduced to two dimensional space to identify critical parameter for classification. To start with classification algorithm problem, below are the terminologies used in machine learning for defining the classification model:

- † Feature, refer to measurable/ identifiable parameter of input.
- † Classifier is the learning algorithm that assigns the class to the data based on its learning of the model from the training data. Classifier and Classification model are used interchangeably in most of the cases.

Below is the procedure followed, for building a classification model:

- † Algorithm for classification is identified
- † Training of the classifier for the given input (X) against the label (Y)
- † Predict label (Y) for the input (X), from test data using trained model
- † Evaluate prediction accuracy

The data has to be labelled for classification using supervised learning approach, where X refers to the heat release rate trace and Y refers to the labels of classification. To avoid the impact of bias introduced by the use of threshold, unsupervised learning approach is also evaluated by using k-means approach, in the later sections of this chapter.

3.1 Rule based Classification

Rule based classification of heat release rate trace is carried out based on the subject knowledge. The classified data form basis for developing a supervised machine learning model subsequently. In order to classify the data, the crank angle at the start and end of main heat release are identified for each of the HRR traces manually and then logged into the data files.

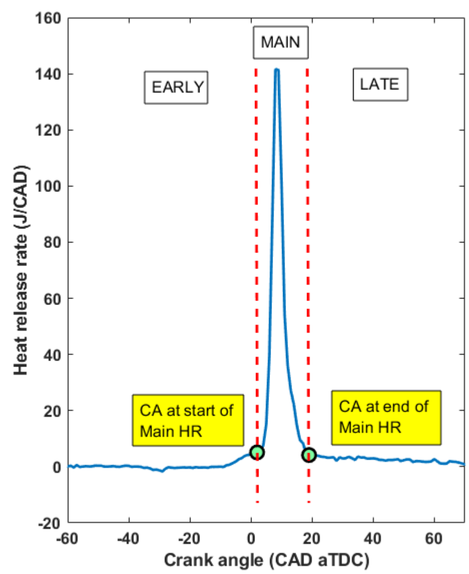

Figure 3.1: Heat release rate trace with Start and End of Main HR depicted

From the crank angle associated with start and end of main heat release by using below relation, the percentage of heat release which happens before main is calculated using Eq. (3.1)) termed as Fraction of Early Heat Release.

$$\text{Fraction of Early Heat Release} = \frac{\text{Cumulative HR from the SOI to Start of main}}{\text{Energy in the fuel quantity injected}} \tag{3.1}$$

The percentage of heat release that happens after the main heat release until CA_{90} is termed as Fraction of Late Heat Release and, is calculated by :

$$\text{Fraction of Late Heat release} = \frac{\text{Cumulative HR from the end of main HR to CA}_{90}}{\text{Energy in the fuel quantity injected}} \tag{3.2}$$

The HRR traces are classified based on the fraction of early and late heat release value. Based on the decision tree in Figure 3.2 , the complete classification is arrived. The threshold value for classification to denote different types of heat release rate is obtained by analysis of the engine experimental data.

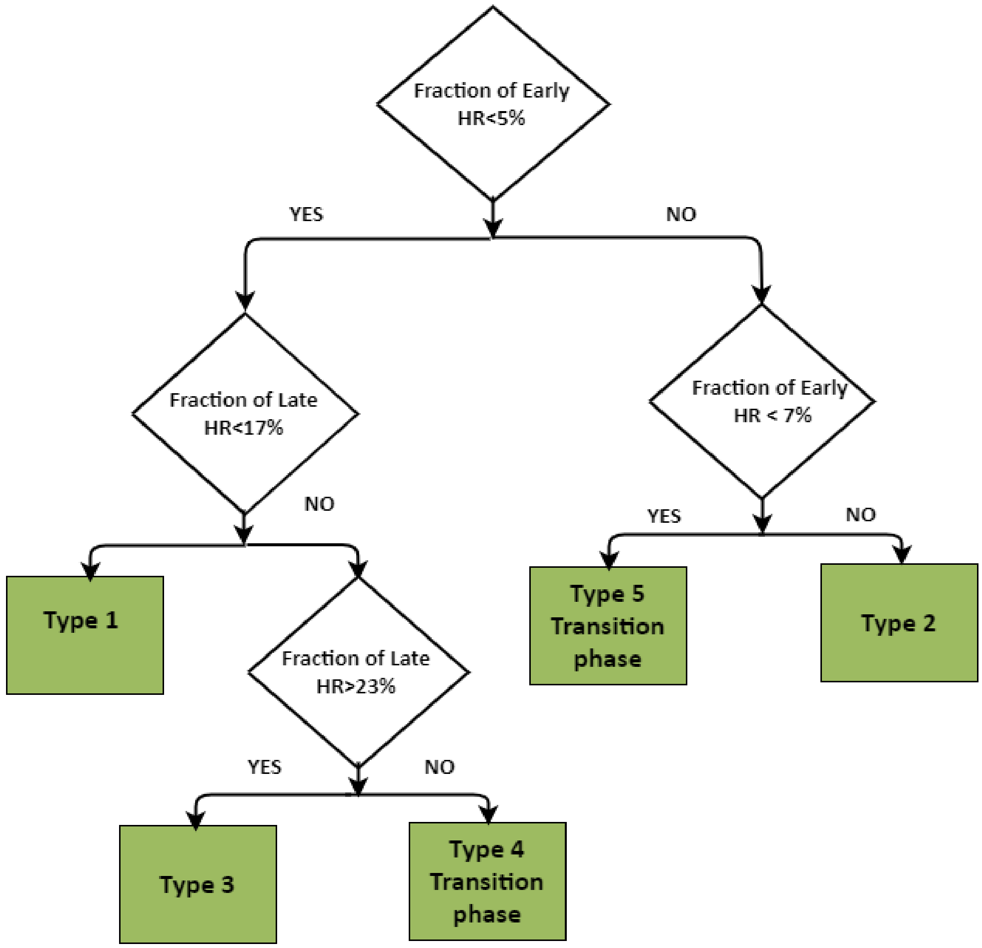

Figure 3.2: Flowchart of Classification Algorithm

Summarized are few traces from each of the classification type in Figure 3.3, depicting 3 classification bins. Between Type 1, Type 2 and Type 3, separate classification Type-4 and Type-5 are identified, to represent the combustion phase transition between the types. Filtered and normalised traces grouped in specific bins are depicted in Figure 3.3.

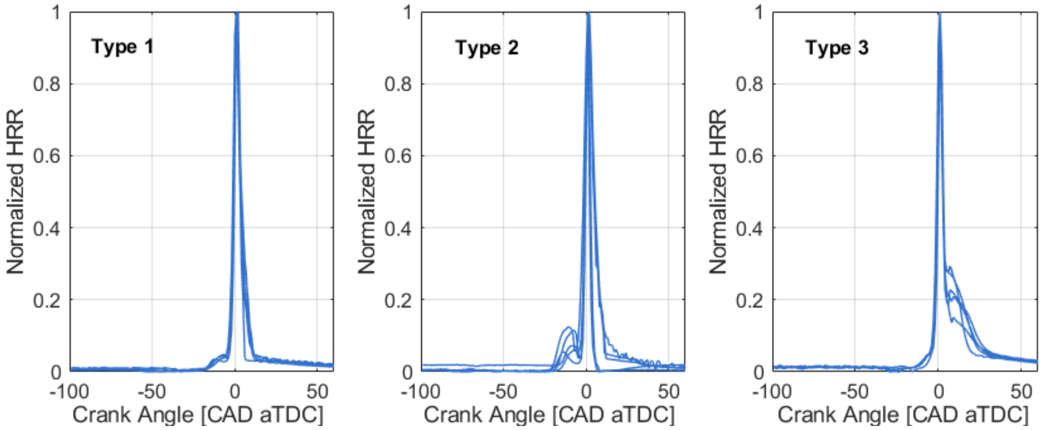

Figure 3.3: Sample heat release rate traces for three main HRR patterns

Each classified type of HRR, group traces which show a unique pattern of combustion.

† ***Type 1 :*** Refers to a type of combustion observed in the HRR where it neither has a significant premixed combustion nor a diffusion combustion. It is similar to the combustion pattern observed in HCCI.

† ***Type 2 :*** Refers to a type of combustion with HRR where it has a significant premixed combustion. It is similar to PCCI type of combustion pattern.

† ***Type 3 :*** Refers to a type of combustion with HRR where it has a significant diffusion combustion. It is similar to combustion HRR pattern observed in RCCI.

Summary of the count of HRR traces identified into each type is listed in Table 3.1

Table 3.1
Summary of the classified HRR traces

Type of HRR traces	**Count of traces**
Type 1	131
Type 2	71
Type 3	373

Distribution of COV_{IMEP} across the data points in Figure 3.4 is analyzed before evaluating other combustion characteristics.

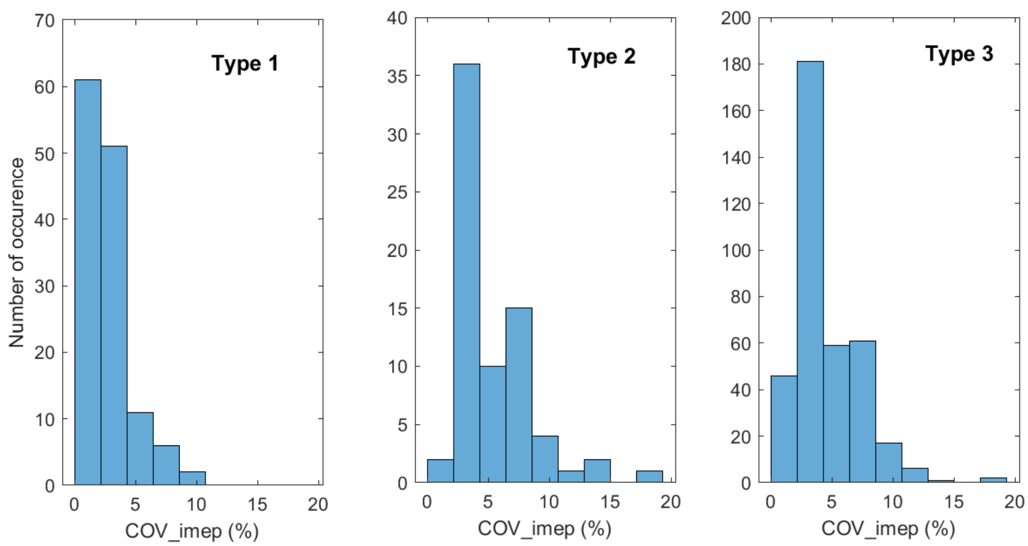

Figure 3.4: Distribution of COV_{IMEP}

Majority of the traces are below the limit of 5% as shown in Table 3.2 and Figure 3.4.

Table 3.2
Table of COV_{IMEP} distribution

	Median %	Mean %	Standard deviation %	Skewness (-)	Kurtosis (-)
Type 1	2.24	2.71	1.74	1.75	6.10
Type 2	4.19	5.36	3.09	1.8	7.13
Type 3	3.94	4.63	2.50	1.42	6.48

3.1.1 Characteristics of combustion type

Characteristics of classified combustion HRR traces are evaluated by looking into multiple combustion parameters and its statistical distribution across the traces grouped into each type.

3.1.1.1 Peak Cylinder Pressure

In Figure 3.5, the spread of peak cylinder pressure across 3 types of heat release is plotted and in Table 3.3 statistical parameters of the each of the distribution are summarized.

Table 3.3
Table of peak cylinder pressure distribution

	Median kPa	Mean kPa	Standard deviation kPa	Skewness (-)	Kurtosis (-)
Type 1	4329	4204	714.2	-0.72	2.73
Type 2	3924	3998	618.2	0.22	2.12
Type 3	3530	3561	417.7	0.31	2.73

Peak cylinder pressure is observed the highest in Type 1, followed by Type 2 and least

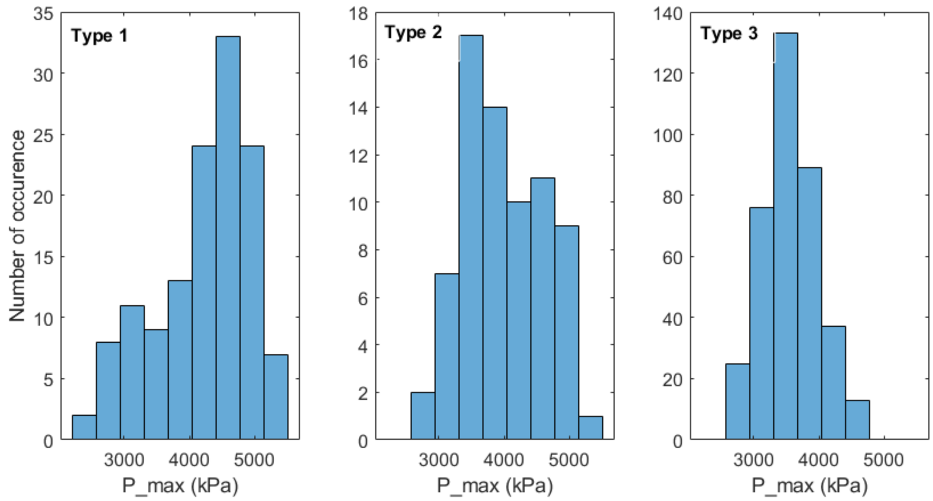

Figure 3.5: Peak cylinder pressure distribution

in Type 3. It is the highest in Type 1, as the most of the fuel heat release happens in the main heat release and least in Type 3 as significant amount of fuel burns after the end of main heat release. Higher peak cylinder pressure is predominantly caused by early combustion which can result in excessive noise and damage to the engine. Type 1 depicts traces with rapid heat release rate which is due to the rapid pressure rise of the combustion mixture. A HRR trace of Type 1 at higher loads can potentially lead to higher peak cylinder pressure. Since, Type2 and Type 3 depict controlled heat release spread over a wider crank angle window, it results in lower peak cylinder pressures.

3.1.1.2 Maximum pressure rise rate

In Figure 3.6, the spread of maximum pressure rise rate across 3 types of heat release is plotted and in Table 3.4 statistical parameters of the each of the distribution are summarized.

Table 3.4
Table of maximum pressure rise rate distribution

	Median bar/CAD	**Mean bar/CAD**	**Standard deviation bar/CAD**	**Skewness (-)**	**Kurtosis (-)**
Type 1	5.77	5.65	2.47	27	2.44
Type 2	4.34	5.23	2.70	0.72	2.42
Type 3	3.93	4.05	1.14	0.53	3.11

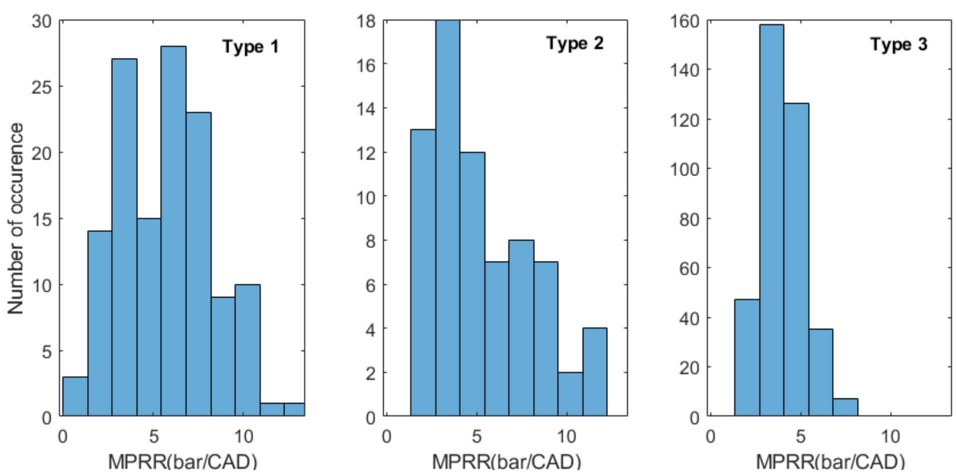

Figure 3.6: Maximum pressure rise rate distribution

Maximum pressure rise rate is observed the highest in Type 1, followed by Type 2 and least in Type 3. Pressure rise rate is significantly governed by mixture reactivity at the start of combustion. It is the highest in Type 1 as it depicts combustion kinetics on a homogeneous mixture resulting in rapid heat release rate and pressure rise rate.

In Type 2 and Type 3, as the flame front propagates, due to in-homogeneity of the mixture a combustion pattern resulting in significant early and late heat release is observed.

3.1.1.3 CA_{10}

In Figure 3.7, the spread of crank angle at 10 percentage of total heat released in an engine cycle across 3 types of heat release is plotted and in Table 3.5 statistical parameters of the each of the distribution are summarized.

Table 3.5
Table of CA_{10} distribution

	Median CAD	**Mean CAD**	**Standard deviation CAD**	**Skewness (-)**	**Kurtosis (-)**
Type 1	5	4.58	5.58	-0.07	2.60
Type 2	-1	-1.88	5.66	-0.50	2.68
Type 3	4	4.03	2.00	-1.27	8.39

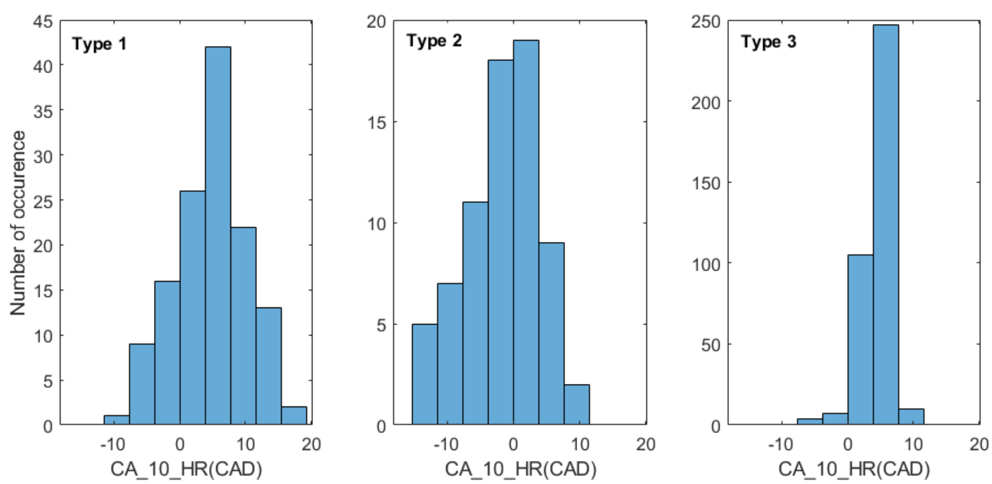

Figure 3.7: CA_{10} distribution

CA_{10} is observed earliest in Type 2, followed by Type 1 and Type 3. It can be justified from the HRR trace of Type 2 from Figure 3.3 due to the significant heat release before the main heat release, it has the earliest CA_{10}. CA_{10} is significantly affected by the ignition delay of the in-cylinder fuel and charge. All these three types of HRR data points had iso-octane injected in the intake port and n- heptane direct injected in cylinder. Based on the homogeneity of the mixture, the ignition delay varied. HRR with least ignition delay resulted in Type 2, followed by Type 1 and Type 3.

3.1.1.4 CA_{90}

In Figure 3.8, the spread of crank angle at 90 percentage of total heat released in an engine cycle across 3 types of heat release is plotted and Table 3.6 statistical parameters of the each of the distribution are summarized.

Table 3.6
Table of CA_{90} distribution

	Median CAD	**Mean CAD**	**Standard deviation CAD**	**Skewness (-)**	**Kurtosis (-)**
Type 1	34	32.41	11.53	-0.76	3.28
Type 2	29	22.4	17.86	-0.18	1.38
Type 3	48	46.59	6.07	-0.42	3.11

CA_{90} is the earliest with Type 2, followed by Type 1 and the last with Type 3. It is directly connected to the the pattern of heat release type and since type 3 has

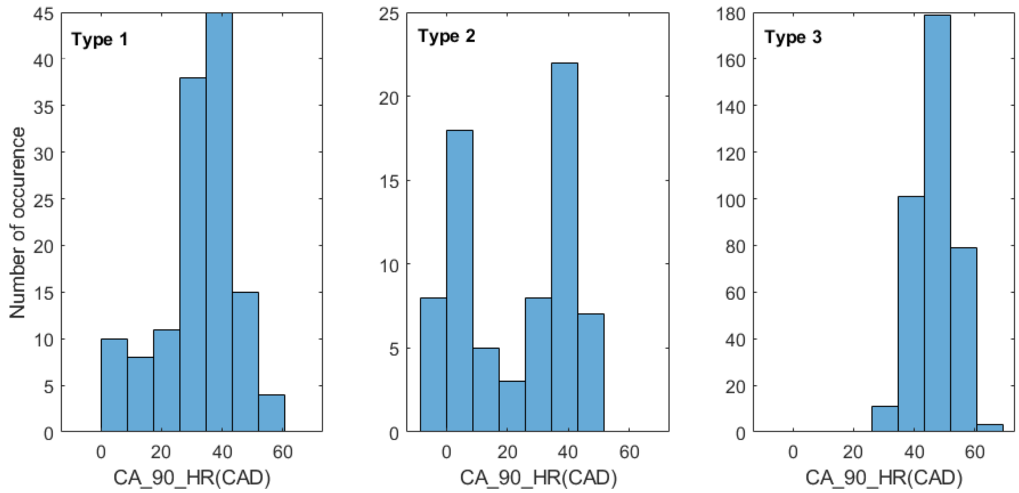

Figure 3.8: CA_{90} distribution

significant late heat release, hence the value of CA_{90} is significantly higher than other types. Homogeneity and ignition delay of the in-cylinder mixture plays a critical role in CA_{90}. Combination of these two parameters result in Type 2 having the least CA_{90} and with Type 3 which predominantly showed diffusion heat release pattern having the highest CA_{90}.

3.1.1.5 Maximum in-cylinder temperature

In Figure 3.9, the spread of maximum in-cylinder temperature across 3 types of heat release is plotted and Table 3.7 statistical parameters of the each of the distribution are summarized.

Higher in-cylinder temperature is observed in Type 1 as the rate of fuel burnt through the main heat release is highest. It is followed by Type 2 and Type 3. Rapid pressure

Table 3.7
Table of Maximum in-cylinder temperature distribution

	Median K	Mean K	Standard deviation K	Skewness (-)	Kurtosis (-)
Type 1	1812	1780	334	-0.35	2.60
Type 2	1494	1508	225	0.09	2.78
Type 3	1508	1536	241	0.36	2.95

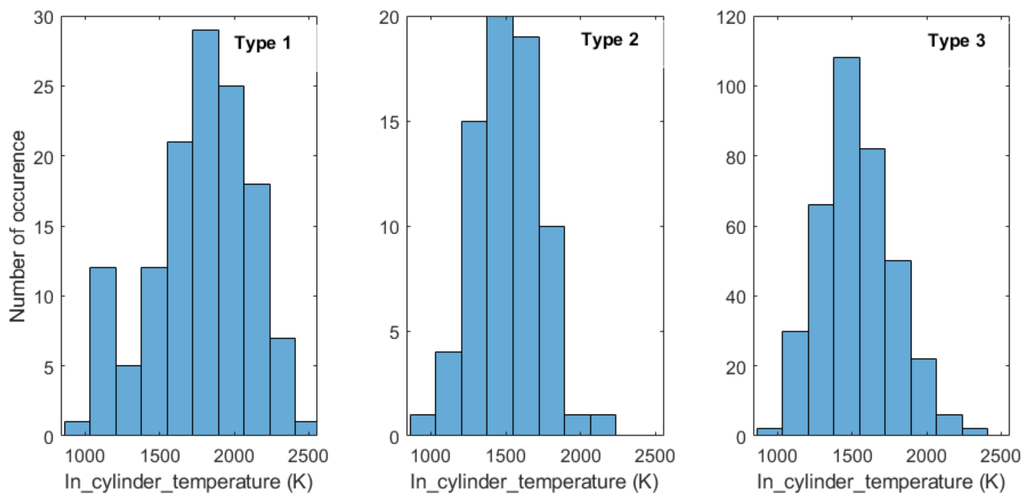

Figure 3.9: Maximum in-cylinder temperature distribution

rise observed in the Type 1 HRR pattern resulted in higher in-cylinder temperature observed. In case of Type 2 and Type 3, they depict similar range of in-cylinder temperature as both of these HRR patterns have comparatively slower heat release rates and wider burn duration.

3.1.1.6 In-cylinder temperature at Start of main heat release

In Figure 3.10, the spread of in-cylinder temperature at the start of main heat release across 3 types of heat release is plotted and Table 3.8 statistical parameters of the of the distribution are summarized.

Table 3.8
Table of in-cylinder temperature distribution at start of main heat release

	Median K	Mean K	Standard deviation K	Skewness (-)	Kurtosis (-)
Type 1	703	702	62.8	-0.07	2.74
Type 2	741	725	59.7	-0.06	2.39
Type 3	698	712	91.5	2.67	21.99

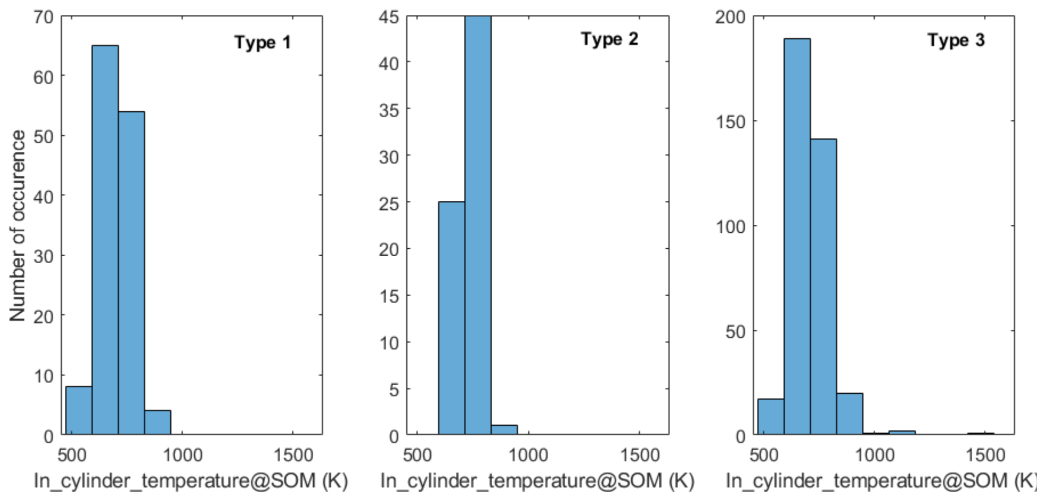

Figure 3.10: In-cylinder temperature at Start of Main distribution

With Type 2 having early heat release, it is the highest while comparing in-cylinder temperatures across start of main, followed by Type 1 and Type 3 together, as both of them don't depict any significant early heat release. In case of Type 1, the in-cylinder temperature arrived at start of main is due to the impact of compression process on the mixture. Similar, is the case with Type 3 pattern as well. Hence both of them show lower in-cylinder temperature at start of main. But, in case of Type 2, some of portion of the combustible mixture is already burnt, resulting in higher in-cylinder temperature at the start of main heat release.

3.1.1.7 In-cylinder temperature at End of main heat release

In Figure 3.11, the spread of in-cylinder temperature at the end of main heat release across 3 types of heat release is plotted and Table 3.9 statistical parameters of the of the distribution are summarized.

Table 3.9
Table of in-cylinder temperature distribution at end of main heat release

	Median K	Mean K	Standard deviation K	Skewness (-)	Kurtosis (-)
Type 1	1781	1758	323	-0.32	2.62
Type 2	1478	1495	220	0.04	2.55
Type 3	1447	1448	189	0.33	3.30

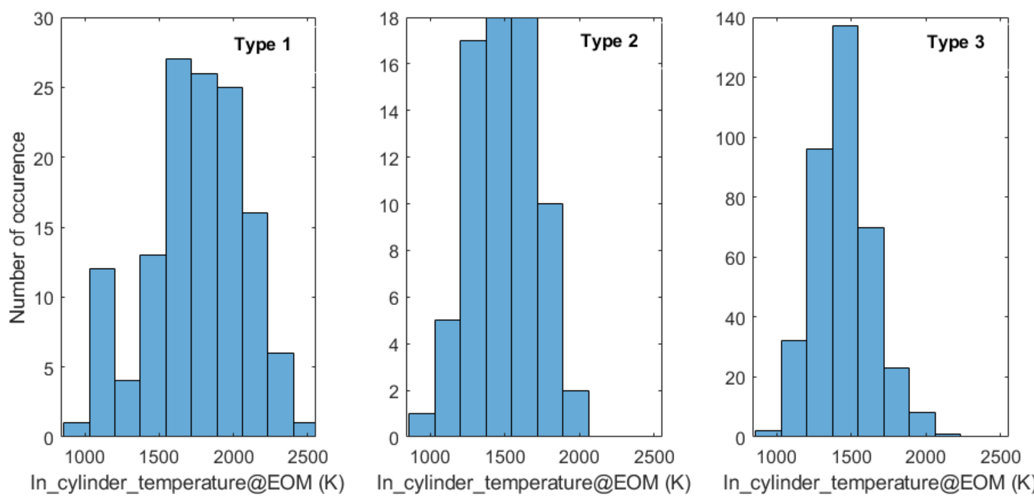

Figure 3.11: In-cylinder temperature at end of Main distribution

With Type 1, most of the fuel is burnt in the main heat release, which results in it being the highest of all 3 types while comparing in-cylinder temperatures across end of main. It is followed by Type 2 and Type 3 in close range.At the end of main heat release, the complete mixture has undergone a constant volume heat release over a smaller burn duration in Type 1. It has resulted in higher in-cylinder temperature at the end of main heat release. Even in case of Type 2, most of the fuel is burnt by end of main heat release, but since the burn duration is wide the heat losses associated resulted in lower in-cylinder temperature. In Type 3, CA_{90} values also indicate that comparatively less percentage of fuel is burnt by end of main heat release. Hence, it also resulted in lower in-cylinder temperature.

3.1.1.8 Exhaust gas temperature

As Type 3 traces have significant late heat release and lower heat loss to coolant, the exhaust gas temperature of these traces will be the highest in comparison with the other two types. It is followed by Type 1 and Type 2 as neither of them have higher late heat release percentage.

3.1.1.9 Engine out emissions

Engine exhaust emission data was not available to compare the three combustion types in this thesis. Here, the expected emission trend is explained by looking at the data available from the literature. In [55] it is clearly documented that change in heat release shapes critically impact the engine out emissions. Inferences from the articles are discussed below, where comparison is being made between HCCI, PCCI and RCCI combustion type.

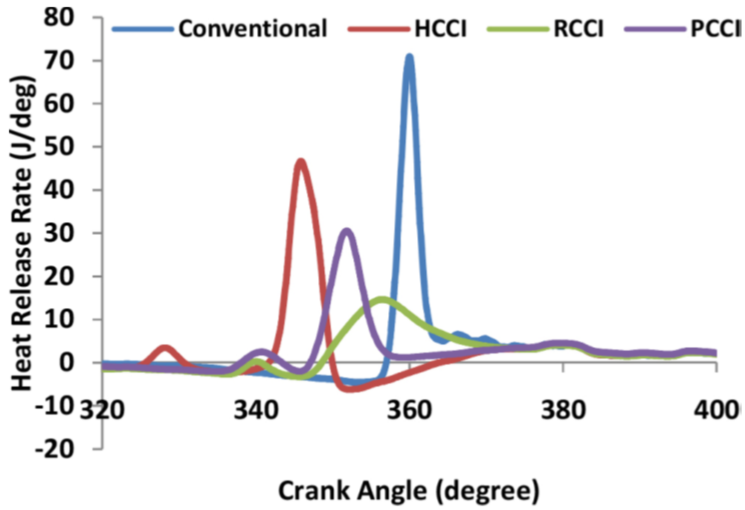

Figure 3.12: Heat release types comparison [55]

The fuel type used for comparison is diesel and gasoline. The classified heat release rates in the article, HCCI, PCCI and RCCI are similar in nature to the heat release types being targeted in the major classification HRR types 1, 2 and 3.

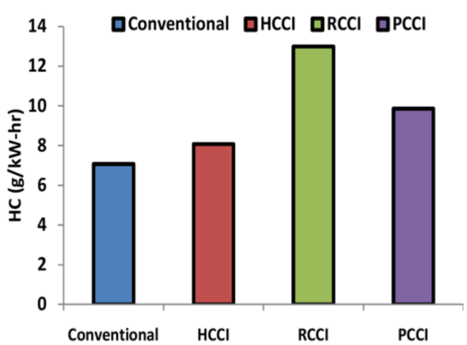

Figure 3.13: HC emission [55]

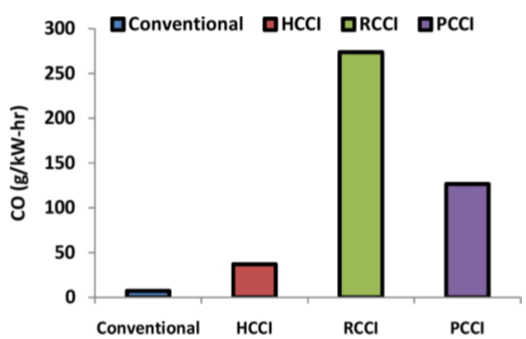

Figure 3.14: CO emission [55]

The data in Figure 3.13 and 3.14, shows that unburned HC and CO emissions are significantly higher in RCCI owing to crevice flow of low reactive gasoline fuel and lower combustion temperatures resulting in lower rate of oxidation of HC and CO.

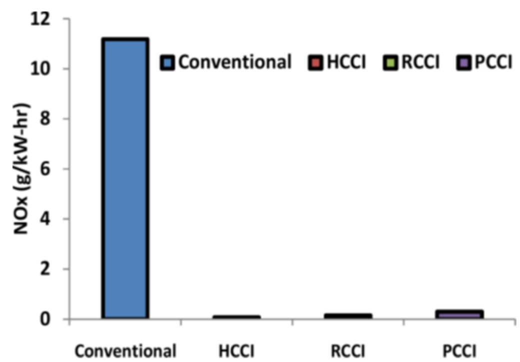

Figure 3.15: NO_x emission [55]

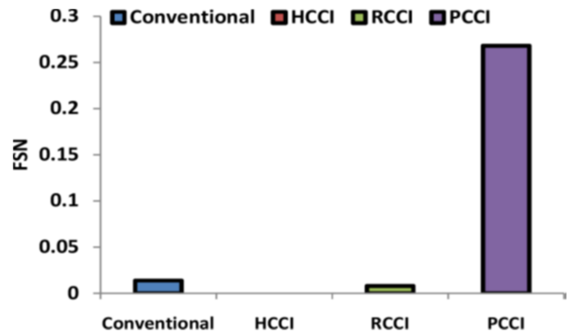

Figure 3.16: Smoke (FSN) [55]

The data in Figure 3.15, NO_x emissions depend strongly upon in-cylinder gas temperatures, oxygen availability and residence time available for high temperature gases. Lower NO_x is achieved due to low combustion temperature. In Figure 3.16, HCCI combustion results in near zero smoke due to higher degree of homogeneity of fuel-air mixture. The smoke emissions are higher in PCCI. This could be due to fuel wall wetting because of early direct injection.

Based on the analysis of various combustion parameters in Section 3.1.1, it was evident that the classification of heat release traces is helpful since it allows for identifying combustion types that have distinct P_{max}, MPRR, CA_{10}, CA_{90}, maximum in-cylinder temperature, in-cylinder temperature at start and end of main heat release T_{exh} and emission characteristics. This information can be used for properly controlling engine combustion. Next, it is desired if the classification can be done automatically. To this end, different machine learning methods were applied and investigated by evaluating their accuracy in classifications. On the classified traces, machine learning technique of supervised learning approach (Convolutional neural network and decision tree) was evaluated and the classifier prediction accuracy was compared. Unsupervised learning was also evaluated on the raw data to evaluate the classification.

3.2 Supervised learning - Convolutional Neural Network

In Supervised learning approach, convolutional neural network is a subset of artificial neural networks. Convolutional neural network has been proved effective for image recognition. In [56] the authors designed CNN, for identifying hand written numbers and it revolutionised application of CNN for image recognition. 1D CNN is used for identifying heat release rate traces is also built as a combination of series of layers to extract the prominent feature of the input and assign it to corresponding output label.

3.2.1 CNN Theory

The CNN takes the 1D vector of HRR trace and passes it across a multiple layers of convolutional, pooling and a fully connected layer to obtain output. Output here is the probability of five different classification bins which could best represent the HRR trace. First layer of 1D CNN is a convolutional layer with an activation function, in which elements from the data, as per kernel dimension is taken and multiplied with the filter weights. Its summed up as a single element in the feature vector. The kernel slides all through the input data and elements of the the feature vector are arrived. Number of filters depicts multiple combinations of weights of the filter, to extract features from input data. Each of theses combination results in a feature vector. All the feature vectors together constitute the convolutional layer. An activation function introduces non linearity in the output and helps in making decisions as depicted in the Figure 3.17. The change in dimension of input data is depicted in Figure 3.18.

Pooling is used to reduce the spatial dimension of the feature vector, in order to reduce the computation involved. Since, pooling operates individually on each of the feature vectors, though maps dimension reduce, the number of maps still remain same. In the final layer global average pooling is used, where it reduces the complete dimension of the feature vector in to a single value. A dense layer is a fully connected neural network layer where in each node on the input is connected to a node on the

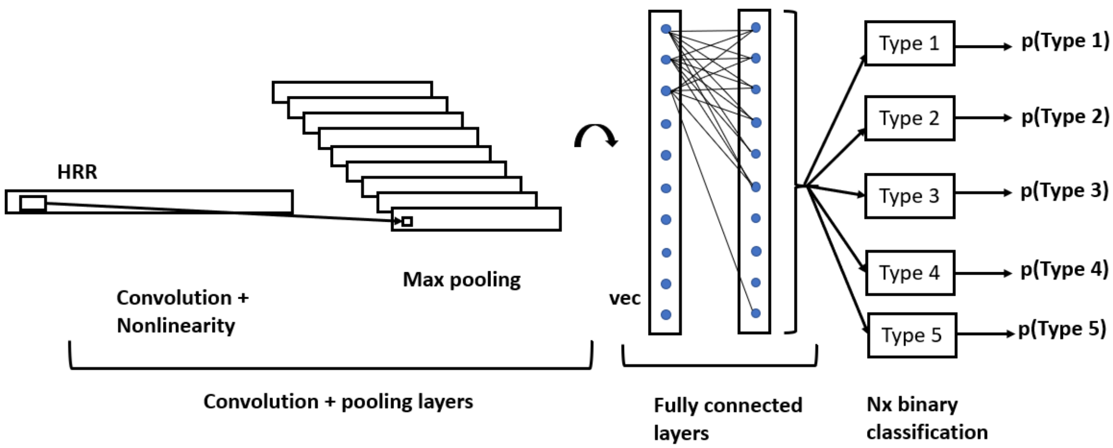

Figure 3.17: Representation of CNN structure

output. A dropout layer is very similar to dense layer except that when the layer is used, the activation is set to zero for some random nodes, by using this approach over fitting is being avoided.

Training of neural network is achieved by adjusting the filter values through back propagation process. During the training process, initially the weights of the filter are randomly assigned and so the output probabilities also end up as random values in the forward pass. The error of the output layer is calculated based on Eq. (3.3), referred to as loss or total error (L). In order to have the predicted and actual label to be same, the loss has to minimum.

$$\text{Total error (L)} = \sum \frac{1}{2}(T - O)^2 \tag{3.3}$$

Where T refers to target probability and O refers to output probability. By using back propagation method, the gradients of the error to weights in the network are adjusted to minimize error. By using gradient descent, the filter weights are adjusted in order to minimize. Weight update is carried out based on Eq. (3.4).

$$\mathrm{W} = W_i - \eta \frac{dL}{dW} \tag{3.4}$$

Where, W is the weight, W_i is the initial weight and η is the learning rate of the network. If the learning rate is set too high it results in large jumps and makes it difficult to reach the optimised point. The process of forward pass, followed by loss calculation and backward pass is carried out for 500 iterations predefined in the coding to get a trained model.

When the same image is fed as input into the trained model, the probability results of the predicted label would more align with the actual label. Thus, the model has learnt to process the particular heat release trace to the corresponding label. Through the process of training only the weights of the filter and connection weights get updated. The structure of the network in terms of number of filters and filter size, remains the same. The heat release rate traces are classified into bins with the rule based algorithm. For supervised learning approach part of the data is fed for training the model and rest is used to evaluate. Thus, 65% of the data is used for training and the rest 35% of the data is used for testing the model.

3.2.2 Application of CNN in HRR shaping

1D CNN model was built and tested using *keras*.It is a python package. In CNN approach for classifying the heat release rate traces, filter of length 9 with 32 features is used and the activation function used is exponential linear unit (ELU). Max pooling is used in the CNN structure built for heat release trace identification. It helps to reduce dimension of feature map in patches. The layer at end is connected completely to its earlier activation layers. Depiction of CNN with convolution and pooling layers, followed by vectored fully interconnected layer resulting in final classification is shown in Figure 3.17. The dimensions of data as it is processed through multiple layers of CNN is detailed in Figure 3.18

Layers on convolution and max pooling extract information from the image with the final dense and dropout layer leading to the classification bins by avoiding overfitting of model to training data.

3.2.2.1 Prediction Accuracy of CNN model

By evaluating with the testing data, model prediction accuracy is observed to be 70%. The prediction accuracy of the model is documented by using a confusion matrix, which compares between the actual and prediction. Diagonal elements of the

```
_________________________________________________________________
Layer (type)                 Output Shape              Param #
=================================================================
conv1d_1 (Conv1D)            (None, 292, 32)           320
_________________________________________________________________
max_pooling1d_1 (MaxPooling1 (None, 97, 32)            0
_________________________________________________________________
conv1d_2 (Conv1D)            (None, 91, 64)            14400
_________________________________________________________________
max_pooling1d_2 (MaxPooling1 (None, 30, 64)            0
_________________________________________________________________
conv1d_3 (Conv1D)            (None, 26, 128)           41088
_________________________________________________________________
global_average_pooling1d_1 ( (None, 128)               0
_________________________________________________________________
dropout_1 (Dropout)          (None, 128)               0
_________________________________________________________________
dense_1 (Dense)              (None, 5)                 645
_________________________________________________________________
lambda_1 (Lambda)            (None, 5)                 0
=================================================================
Total params: 56,453
Trainable params: 56,453
Non-trainable params: 0
```

Figure 3.18: Data dimensions through layers of CNN

matrix depict The traces, in which true label from data and predicted label by model are the same. The higher the diagonal elements, the better is the prediction accuracy of the model.

3.3 Supervised learning - Decision tree

Decision tree is used as a powerful supervised learning model for classification problem. It is capable of achieving higher accuracy and is highly interpretable. Decision tree involves sequential hierarchical decisions which lead to final classification. The model is created by 2 steps including, induction and pruning. Induction is a process

CNN		Predicted Label				
		1	2	3	4	5
True Label	1	36	0	0	2	1
	2	1	16	0	0	18
	3	3	0	97	29	5
	4	9	1	6	38	1
	5	5	2	0	1	9

Figure 3.19: Prediction summary of CNN

in which a decision tree is built, but the nature of training process results in overfitting issue. Through the process of pruning, unnecessary structures from the decision tree are removed to prevent overfitting.

3.3.1 Decision tree theory

Decision tree consists of node, an evaluation condition of a certain feature. Edges/Branch, refers to the outcome of a node, which connects with another node. And, finally leaf nodes, refer to the final outcome resulting in the class labels. Moving into details of the decision tree used for classification of heat release rate traces, recursive binary splitting is used at every node. It splits into two at decision making node. To calculate accuracy of the split at each node, cost of split is evaluated. For a classification problem, cost function (Gini Index Function) gives a perspective of the the goodness of split by the Eq. (3.7).

$$\mathrm{G} = 1 - \Sigma_k({p_k}^2) \tag{3.5}$$

Where p_k is the proportion of class inputs belonging to a particular group. High level of purity i.e higher value of p_k is achieved when the the value of G is lower. The concept of having a single class segregated out is measured by another parameter, information gain. So at every split decision tree algorithm evaluates all the features for the highest value of information gain. Then, it is chosen as a condition for node. It is depicted by the equation (3.8) below.

$$\mathrm{G}ain(S, A) = Entropy(S) - \Sigma_{veValues(A)}\frac{|S_v|}{|S|}.Entropy(S_v) \tag{3.6}$$

Where S refers to set of occurrence, A refers to the feature, S_v is the subset of S when A equals to a particular classification value and *Values(A)* refer to all the possible values of A in the training data. Entropy refers to measure of uncertainty in the random variable, it also depicts the impurity of the collection. At each node the same step step is evaluated till all the classes are achieved as leaf node. But, the issue associated would be overfitting of the model on the training data.

3.3.2 Application of decision tree in HRR shaping

To apply the decision tree method on HRR data, MATLAB predefined function *fitctree* with binary recursive approach is used. The function takes 2 major inputs, with one being the features and other being labels of classification. So in HRR classification, the features considered are the engine control input parameters (engine speed,start of injection of DI fuel, total fuel quantity, pre-mixed ratio and intake manifold temperature. The output is the true labels for traces identified initially for training the model. The Figure 3.20 shows the binary recursive classification arrived at by the decision tree algorithm based on the features of the data. The decision tree approach is prone to overfitting issue, hence the number of leaf nodes were restricted to a maximum of 12, to avoid overfitting issue.

3.3.2.1 Prediction Accuracy of decision tree model

Once the decision tree model is determined, testing data is evaluated. The summary of the true label and predicted is shown in Figure 3.21. The prediction accuracy of the model is 74.5%, with diagonal elements signifying the predictions tallying with the true label.

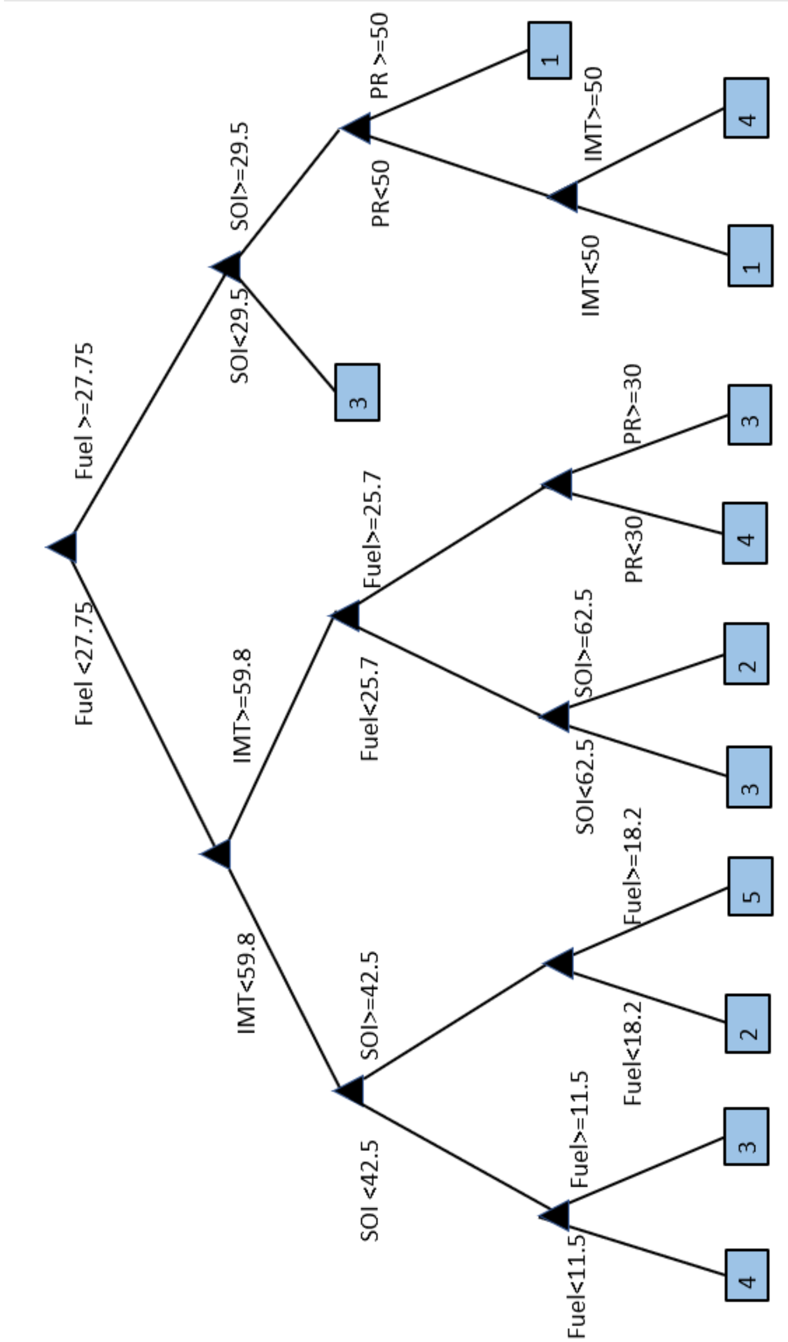

Figure 3.20: Decision tree for the engine HRR classification

Decision Tree		Predicted Label				
		1	2	3	4	5
True Label	1	16	1	4	0	4
	2	0	23	6	2	4
	3	0	2	146	5	3
	4	2	0	11	12	1
	5	0	2	21	3	11

Figure 3.21: Prediction summary of Decision tree

3.4 Unsupervised learning - k-means clustering

In unsupervised learning approach, k-means clustering is used to solve a classification problem. The parent algorithm used for classification of HRR traces is discussed in Section 3.2. It is based on multiple thresholds. In order to eliminate bias introduced by thresholds in training data, an unsupervised approach is being evaluated.

3.4.1 k-means theory

k-means clustering is a popular technique for clustering problem, where centroid would represent data point in a 2-dimensional data frame. In order to classify the centroid would represent a complete HRR trace. k-means clustering starts with random initialisation of centroids, c_1,c_2,...c_k, of heat release rate data. Since, traces are intended to be segregated into five bins, k is initialised to 5. Iteration of following two steps is done, till the centroids converge.

1. In this step each data point based on them minimum euclidean distance is assigned to the nearest center.

$$argmin_{c_i \epsilon C} \; dist(x - c_i)^2 \tag{3.7}$$

   c_i is the centroid belonging to the the collection of Centroids C and each data point x is being assigned to the cluster based on euclidean distance calculated by dist().

2. In the second step of the sequence, centroid is recalculated as the mean of data points assigned to its cluster. The set of data points assigned to i^{th} cluster is S_i.

$$c_i = \frac{1}{|S_i|} * \Sigma_{x_i \epsilon S_i} x_i \tag{3.8}$$

Algorithm is iterated until the sum of euclidean distance has become minimum and no data points switch between clusters. A similar approach is carried out through the complete length of the heat release rate vector to identify the centroid for the cluster of traces.

3.4.2 Application of k-means in HRR shaping

k-means clustering approach was used to classify data into 5 bins. Since, each trace is observed to have different magnitude peak heat release rate it affected the clustering pattern. The traces were normalised individually to range from 0 to 1, so that traces could be clustered on its pattern of heat release rate rather than magnitude of peak.

Centroids are chosen randomly at the beginning of the classification and the euclidean distance of each trace from the centroid is calculated. Traces with the least distance from the centroid are clustered in a bin. From the clustered traces, centroid is recalculated. The process is repeated until the centroid and clustered traces remain same after consecutive iterations.

Figure 3.22 depicts the clustered traces, arrived by K-means in 4 different bins.

3.4.2.1 Drawbacks of k-means classification

With k-means clustering approach, two major drawbacks were observed. With multiple iterations of the clustering, alignment of clustered traces and the centroid of

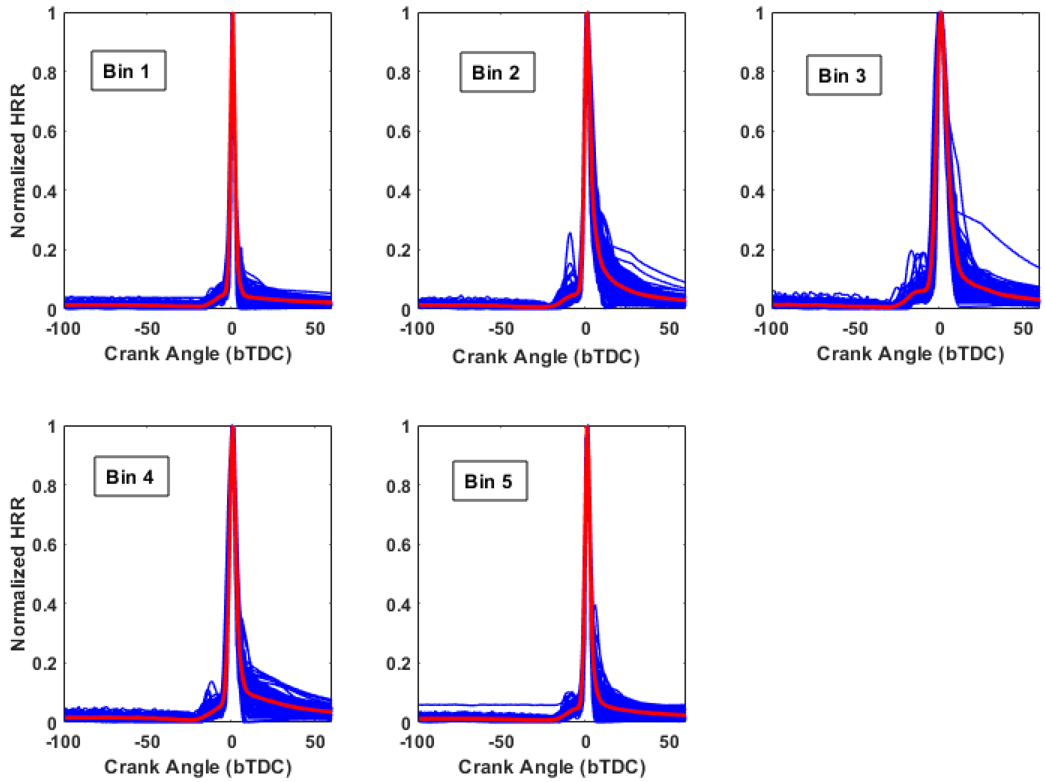

Figure 3.22: k-means classification of traces

the bins changed. Due to this, it became difficult to assign a bin to a specific pattern of heat release rate. Second drawback was that, between the clustered traces in bins, it was difficult to identify distinct differences in heat release rate pattern. This apparently made the classification difficult to justify unique characteristics of each bin.

Due to these drawbacks of k-means, supervised learning approach is preferred. First preference is Decision tree approach leads to a prediction accuracy of 74.5%. Decision tree is built as a function of key operating conditions of engine and its control inputs.

The CNN model leads to an prediction accuracy of 70%. CNN model is built as a function of heat release rate traces from the engine. Use of Machine learning based approach also facilitates in means to learn from the engine in actual operation scenario as well. It is discussed further in the future work section on an idea for implementation of control structure of the above discussed machine learning based models.

Rule based technique, was used to classify HRR traces and classified traces were used in supervised learning approach to train and evaluate the model. With rule based classification, distinct characteristics of grouped traces are also observed in Section 3.1.1. Rule based classified traces are used for identification of scheduling parameters Chapter 4.

Chapter 4

Identification of combustion classifiers

LTC engines heat release rate pattern changes with change in the operating conditions i.e engine speed, intake manifold pressure and temperature) and manipulated variables (fuel quantity, SOI and PR). Hence, it is evident that heat release pattern variation is in a multi dimensional data frame. To control complex combustion heat release in LTC engines, one can use linear parameter varying (LPV) representation to capture non-linear LTC engine behavior in LPV state space model that can be used for combustion control. Building up the result in Chapter 3, an LPV model is developed for LTC engine control. Thus, we need to identify a scheduling parameters of LPV matrices that can represent the non-linearity of the LTC engine as a function of engine conditions and manipulated variables. With proper selection of a scheduling variables details of change in HRR pattern of the engine can be decoded.

4.1 Scheduling parameter identification

The multi dimensional heat release data frame has to be reduced to a one or two dimensional space so that identified parameter can be used as a scheduling variable in the LS-SVM code for building LPV matrices. To this end, principal component analysis (PCA) and multi variable linear regression approach are evaluated to reduce higher dimensions of the data and parameterize the equation with identified dimensions .

4.1.1 Principal Component Analysis (PCA)

Principal component analysis is the procedure of dimension reduction of the large data set into a small one which still holds most of the information from the original data. It is achieved by translating the information from correlated input variables to principal components.

The first principle component is identified such that it accounts for the maximum variability contained in the data; thus the subsequent principle components are chosen such that it could account for rest of the variability in the data set. The principal components are arrived as a linear combination of observed variables weighted by the corresponding eigen values. Values are represented in rotational matrix, which can be interpreted as the rotation of data in order to achieve projection with greatest variance along the axis of first principal component. Subsequent principal axes are chosen such that its geometrically orthogonal.Principal axis identification could be confused with linear regression. The difference is, PCA works to minimize the perpendicular distance between the principal component axis and the data point. But, in linear regression the distance between the predicted and actual value of the data point is minimized.

Looking into the mathematics behind PCA, data is centered by calculating the mean. The covariance matrix of the data is calculated as the sum of the product of the co-ordinate based on the Equation 4.1, with n as the number of observations and X and Y are set of 2 data columns.

$$cov(X,Y) = \frac{1}{n-1} x \Sigma_{i=1}^{n} (X_i - \bar{x})(Y_i - \bar{y}) \tag{4.1}$$

Where X refers to data representing operating conditions i.e engine speed, intake manifold pressure and temperature) and manipulated variables (fuel quantity, SOI and PR) and Y refers to the classified HRR traces. PCA is evaluated in R Studio, a statistical software using *prcomp* function and the rotational matrix with eigen values and the variability associated with each of the principle axes is shown in Table 4.1

Table 4.1
Output of PCA on HRR classifier identification

Principal axis	Parameter name	Proportion of variance (%)
PC1	Start of Injection	26.4
PC2	Premixed ratio	23.5
PC3	Fuel quantity	20.3
PC4	Engine speed	16.5
PC5	Intake manifold temperature	9.4
PC6	Intake manifold pressure	3.9

Even though PCA is a powerful tool, it comes with the limitation of missing on non-linear data patterns. Since, engine data is widely known for its non linear behaviour, the tool is applied on an evaluation basis to look at the outcome and understand the variability explained by the technique across different principal axis.

Based on the results of PCA, its evident that start of injection, premixed ratio, fuel quantity and engine speed have a significant impact in the change of heat release pattern in data. The variability is potentially spread across, more than 2 axis parameters. Hence, a method of multivariable linear regression is also looked into as a potential option for grouping the significant engine inputs arrived through PCA into regression equation.

4.1.2 Multivariable linear regression

Multivariable linear regression is a technique to build a model as a function of two or more explanatory variables and a response variable, by fitting a linear equation on test data. For a model with p explanatory variables, x_1, x_2, x_3, ...,x_p and y as response variable, the model equation could be represented as

$$y_i = \beta_0 + \beta_1.x_{i1} + \beta_2.x_{i2} + ... + \beta_p.x_{ip} + \epsilon_i \qquad \text{for i=1,2,3,..n} \tag{4.2}$$

Where n is the number of observations in data. The fit of the model is governed by the coefficients (β_0, β_1, β_2,.., β_p) of the explanatory variables and ϵ depicts the residual term. The residual term accounts for the deviation of the fitted value to the actual observed value of the response variable.

Most of the occasions the coefficients are computed by statistical software. In theory, the best line fitting data is evaluated by using a cost function. Cost function is a sum of squares of vertical distance from each data point to the predicted value by the fitted line divided by number of observations. These deviations are squared, so that the positive and negative differences don't cancel out each other. The cost function is described in Equation 4.3.

$$\text{Mean Square Error (MSE)} = \frac{1}{n}\Sigma_{i=1}^{n}(y - y_i)^2 \tag{4.3}$$

Where y is observed value and y_i is the predicted value. With the minimisation of cost function, the coefficients of the best fit line are arrived. With this approach, significant engine input parameters could be formulated into a single equation.

4.1.2.1 Application of multi variable linear regression

The classification of heat release traces is based on fraction of early HR and fraction of late HR. With PCA, the parameters with greater influence on the heat release classification is identified as start of injection, premixed ratio,fuel quantity and engine speed. As a combination of these parameters, by using regression approach the fraction of early HR and fraction of late HR are modelled using the identified engine parameters.

Multiple combinations were evaluated to model fraction of early HR and fraction of late HR. By using the R- square value the quality of the model is evaluated. In the Table 4.2, different combinations evaluated are listed.

Table 4.2
Table of iteration of engine parameters to model fraction of early HR and fraction of late HR

Serial Number	Engine Parameters	Number of parameters in Equation	R- square Fraction of Early HR	R- square Fraction of Late HR
1	Start of Injection Premixed ratio	6 (Quadratic terms)	61.9	36.7
2	Start of Injection Premixed ratio Engine Speed	10 (Quadratic terms)	64.5	65.2
3	Start of Injection Premixed ratio Engine Speed Fuel quantity	5 (Linear terms)	59.0	67.4
4	Start of Injection Premixed ratio Engine Speed Fuel quantity	15 (Quadratic terms)	69.1	78.3
5	Start of Injection Premixed ratio Engine Speed Fuel quantity	19 (Cubic terms)	69.6	80.4
6	Start of Injection Premixed ratio Engine Speed Fuel quantity Intake manifold pressure and temperature	19 (Cubic terms)	71.6	79.8

For all the combinations after modelling, the modelled fraction of early HR and fraction of late HR are compared with the experimental data and classification. The accuracy of classification is also evaluated by calculating the prediction accuracy. Upon evaluating all the above mentioned combinations, it was observed that the fifth combination with start of injection, premixed ratio, engine speed and fuel quantity was observed to have significant R^2 value and also resulted in better prediction accuracy in the LPV - Support Vector Machine based system identification discussed in Chapter 5.

Fraction of early HR is formulated as

$-13.2 + 0.012 \times SOI - 0.47 \times PR + 0.03 \times Speed + 0.2 \times FQ + 0.0026 \times SOI^2 +$
$0.013 \times PR^2 - 2.2 \times 10^{-5} \times Speed^2 - 7.2 \times 10^{-3} \times FQ^2 - 2.4 \times 10^{-3} \times SOI \times PR +$
$1.8 \times 10^{-4} \times SOI \times Speed - 3.8 \times 10^{-3} \times SOI \times FQ - 1.2 \times 10^{-4} \times Speed \times FQ$
$-1.1 \times 10^{-5} \times Speed \times PR + 4.5 \times 10^{-3} \times FQ \times PR - 1.9 \times 10^{-5} \times SOI^3$
$-1.2 \times 10^{-4} \times PR^3 + 3.6 \times 10^{-9} \times Speed^3 + 1.0 \times 10^{-4} \times FQ^3$

Fraction of late HR is formulated as

$-16.5 + 0.04 \times SOI + 0.08 \times PR - 0.04 \times Speed + 4.5 \times FQ - 0.025 \times SOI^2$
$-3.2 \times 10^{-03} \times PR^2 + 4.9 \times 10^{-05} \times Speed^2 - 1.6 \times 10^{-01} \times FQ^2 +$
$1.0 \times 10^{-05} \times SOI \times PR + 5.0 \times 10^{-04} \times SOI \times Speed - 1.5 \times 10^{-02} \times SOI \times FQ +$
$2.7 \times 10^{-04} \times Speed \times FQ - 3.6 \times 10^{-04} \times Speed \times PR - 7.3 \times 10^{-03} \times FQ \times PR +$

$1.6 \times 10^{-04} \times SOI^3 + 4.5 \times 10^{-05} \times PR^3 - 1.6 \times 10^{-08} \times Speed^3 + 1.7 \times 10^{-03} \times FQ^3$

The classification of heat release types with experimental values of fraction of early HR and fraction of late HR is shown in Figure 4.1.

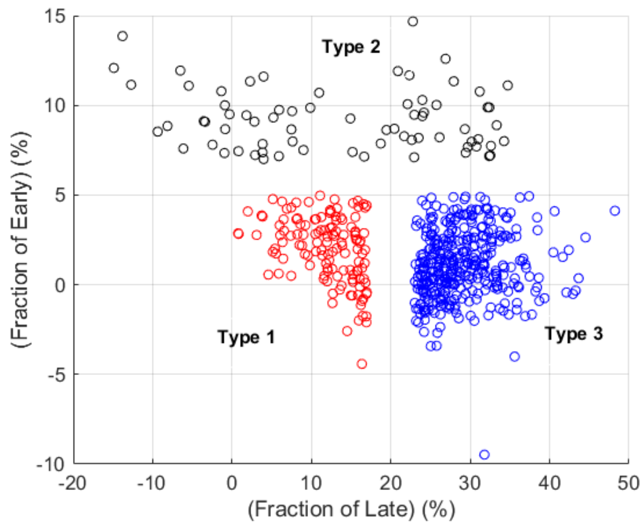

Figure 4.1: Plot of experimental data

With modelled fraction of early HR and fraction of late HR as the scheduling parameter, the identification of LPV matrices for LTC engine is covered in Chapter 5.

Chapter 5

LPV model Identification with combustion classifiers

Combustion classifiers identified in Chapter 4 is used as scheduling parameter to build a LPV model of the LTC engine. By using combustion classifiers as scheduling variable of LPV model, the information of combustion type is inbuilt into LTC engine model. Support Vector Machine is used for identification of LPV matrices and is discussed in Section 5.1

5.1 Support Vector Machine (SVM)

Support vector machine(SVM) is a supervised machine learning approach. It is used both as a classification and regression algorithm. SVM for classification, identify parameters of a hyper plane (line on a 2-dimensional frame) that result in classification of data. In case of regression, it retains all the features in the data and comes up with a system equation from training data with maximum margin and minimum error.

Approach of support vector machine is used to build LPV state space matrix as a function of combustion classifier as scheduling parameter to model the RCCI engine.

5.1.1 LS-SVM system identification

SVM regression approach is used to identify the state space matrices of the engine model. LS SVM state space matrix at discrete instant of time k, can be represented as [50]

$$\begin{aligned} X_{k+1} &= A(p_k)X_k + B(p_k)U_k + K(p_k)e_k \\ Y_k &= C(p_k)X_k + D(p_k)U_k + e_k \end{aligned} \tag{5.1}$$

where X represents states of the system, Y is measurable output of the system and U refers to the manipulated variable for controlling the system. p represents the scheduling parameter and e represents stochastic white noise associated. $A(p_k)$,$B(p_k)$,$C(p_k)$,$D(p_k)$ and $K(p_k)$ represent the the state space matrices of the system and vary as a function of the parameter p_k. Equation 5.1 is restructured as

$$e_k = Y_k - C(p_k)X_k - D(p_k)U_k \tag{5.2}$$

Substituting back into Equation 5.1

$$\begin{aligned} X_{k+1} &= A(p_k)X_k + B(p_k)U_k + K(p_k)Y_k - K(p_k)C(p_k)X_k - K(p_k)D(p_k)U_k \\ X_{k+1} &= (A(p_k) - K(p_k)C(p_k))X_k + (B(p_k) - K(p_k)D(p_k))U_k + K(p_k)Y_k \end{aligned} \tag{5.3}$$

$$\begin{aligned} \bar{A} &= A(p_k) - K(p_k)C(p_k) \\ \bar{B} &= B(p_k) - K(p_k)D(p_k) \end{aligned} \tag{5.4}$$

So, Equation 5.1 can be rewritten as

$$\begin{aligned} X_{k+1} &= \bar{A}(p_k)X_k + \bar{B}(p_k)U_k + K(p_k)Y_k \\ Y_k &= C(p_k)X_k + D(p_k)U_k + e_k \end{aligned} \tag{5.5}$$

The plant matrices $\bar{A}(p_k)$,$\bar{B}(p_k)$,$C(p_k)$,$D(p_k)$ and $K(p_k)$ are computed using support vector machine approach. By taking the training data into SVM framework, the plant matrices are transformed using weighing matrices(W), regression vectors or features of the data (ϕ) as shown in Equation 5.6

$$\begin{aligned} X_{k+1} &= W_1\phi_1(p_k) + W_2\phi_2(p_k) + W_3\phi_3(p_k) + \epsilon_k \\ Y_k &= W_4\phi_4(p_k) + W_5\phi_5(p_k) + \zeta_k \end{aligned} \tag{5.6}$$

where ϵ and ζ represent the residual error at the instant k. Equation 5.6 is deduced further by representing the regression vector(ϕ) as a function of basis function (Φ)

$$\begin{aligned} X_{k+1} &= W_1\Phi_1(p_k)X_k + W_2\Phi_2(p_k)U_k + W_3\Phi_3(p_k)Y_k + \epsilon_k \\ Y_k &= W_4\Phi_4(p_k)X_k + W_5\Phi_5(p_k)U_k + \zeta_k \end{aligned} \tag{5.7}$$

In order to identify the state space matrices the weighting matrices have to be determined. To optimise the estimation,least square optimisation method is chosen and the cost function(J) in shown in Equation (5.8)

$$J = \frac{1}{2}\Sigma_{i=1}^{5}||W_i||_F^2 + \frac{1}{2}\Sigma_{k=1}^{N}(\epsilon_k^T\Gamma\epsilon_k + \zeta_k^T\psi\zeta_k) \tag{5.8}$$

where Γ and ζ represent the diagonal regularisation parameters used on the the residual errors to avoid overfitting of the training data. $||x||_F$ is the Forbenius norm. Cost function is optimised by using Lagrange optima identification. The equation with Lagrangian multipliers are shown

$$
\begin{aligned}
L(W_1, W_2, W_3, W_4, W_5, \epsilon, \zeta, \alpha, \beta) = J - (\Sigma_{j=1}^{N} \alpha_j^T (W_1 \Phi_1(p_j) X_j + W_2 \Phi_2(p_j) U_j + \\
W_3 \Phi_3(p_j) Y_j) + \epsilon_j - X_{j+1}) - \Sigma_{j=1}^{N} \beta_j^T (W_4 \Phi_4(p_j) X_j + \\
W_5 \Phi_5(p_j) U_j + \zeta_j - Y_j)
\end{aligned}
\tag{5.9}
$$

α_j and β_j are Lagrange multipliers at the instant j. Optimum solution is arrived by taking partial derivative of the Equation 5.9

$$
\begin{aligned}
\frac{\partial L}{\partial W_1} = 0, \implies W_1 = \Sigma_{j=1}^{N} \alpha_j \Phi_1^T(p_j) X_j^T \\
\frac{\partial L}{\partial W_2} = 0, \implies W_2 = \Sigma_{j=1}^{N} \alpha_j \Phi_2^T(p_j) U_j^T \\
\frac{\partial L}{\partial W_3} = 0, \implies W_3 = \Sigma_{j=1}^{N} \alpha_j \Phi_3^T(p_j) Y_j^T \\
\frac{\partial L}{\partial W_4} = 0, \implies W_4 = \Sigma_{j=1}^{N} \beta_j \Phi_4^T(p_j) X_j^T \\
\frac{\partial L}{\partial W_5} = 0, \implies W_5 = \Sigma_{j=1}^{N} \beta_j \Phi_5^T(p_j) U_j^T \\
\frac{\partial L}{\partial \alpha_j} = 0, \implies \epsilon_j = X_{j+1} - W_1 \Phi_1^T(p_j) X_j^T - W_2 \Phi_2^T(p_j) U_j^T - W_3 \Phi_3^T(p_j) Y_j^T \\
\frac{\partial L}{\partial \beta_j} = 0, \implies \zeta_j = Y_j - W_4 \Phi_4^T(p_j) X_j^T - W_5 \Phi_5^T(p_j) U_j^T \\
\frac{\partial L}{\partial \epsilon_j} = 0, \implies \alpha_j = \Gamma \epsilon_j \\
\frac{\partial L}{\partial \zeta_j} = 0, \implies \beta_j = \psi \zeta_j
\end{aligned}
\tag{5.10}
$$

Substituting back in Equation 5.7

$$X_{k+1} = \Sigma_{j=1}^{N}\alpha_j X_j^T(\Phi_1(p_j)^T)(\Phi_1(p_k))X_k + \Sigma_{j=1}^{N}\alpha_j X_j^T(\Phi_2(p_j)^T)(\Phi_2(p_k))U_k +$$
$$\Sigma_{j=1}^{N}\alpha_j X_j^T(\Phi_3(p_j)^T)Y_k(\Phi_3(p_k)) + \Gamma^{-1}\alpha_k$$
$$Y_k = \Sigma_{j=1}^{N}\beta_j X_j^T(\Phi_4(p_j)^T)X_k(\Phi_4(p_k)) + \Sigma_{j=1}^{N}\beta_j X_j^T(\Phi_5(p_j)^T)U_k(\Phi_5(p_k)) + \psi^{-1}\beta_k \tag{5.11}$$

By applying the kernel trick to reduce $(\Phi_1(p_j)^T).(\Phi_1(p_k))$ with $K^{-1}(p_j, p_k)$. By substituting results from Equation 5.10 in Equation 5.11, it can be rewritten as

$$\begin{aligned} X_{k+1} &= \alpha\Omega + \Gamma^{-1}\alpha \\ Y_k &= \beta\Xi + +\psi^{-1}\beta \end{aligned} \tag{5.12}$$

Ω and Ξ represent an array of kernel or grammian matrices. Deriving from the Equation 5.12

$$\begin{aligned} vec(\alpha) &= (I_N \otimes \Gamma_{-1} + \Omega^T I_{nx})^{-1} vec(X_{k+1}) \\ vec(\beta) &= (I_N \otimes \Psi_{-1} + \Xi^T I_{ny})^{-1} vec(Y_k) \end{aligned} \tag{5.13}$$

where $\otimes$ represent the Kronecker product, I_{nx},I_{ny},I_N all represent the identity matrices and vec refers to vectorization function.

By applying kernel trick and α and β identified, Equation 5.11 is restructured as

$$X_{k+1} = \Sigma_{j=1}^{N} \alpha_j X_j^T k^{-1}(p_j, p_k) X_k + \Sigma_{j=1}^{N} \alpha_j U_j^T k^{-2}(p_j, p_k) U_k + \\ \Sigma_{j=1}^{N} \alpha_j Y_j^T () k^{-3}(p_j, p_k) Y_k + \Gamma^{-1}\alpha_k \tag{5.14}$$

$$Y_k = \Sigma_{j=1}^{N} \beta_j X_j^T (k^{-4}(p_j, p_k)) X_k + \Sigma_{j=1}^{N} \beta_j U_j^T k^{-5}(p_j, p_k) U_k + \psi^{-1}\beta_k$$

From the Equation 5.15, the state space matrices could be deduced

$$\begin{aligned} \bar{A}(p_k) &= \Sigma_{k=1}^{N} \alpha_k X_k^T k^{-1}(p_k, .) \\ \bar{B}(p_k) &= \Sigma_{k=1}^{N} \alpha_k U_k^T k^{-2}(p_k, .) \\ K(p_k) &= \Sigma_{k=1}^{N} \alpha_k Y_k^T k^{-3}(p_k, .) \\ C(p_k) &= \Sigma_{k=1}^{N} \beta_k X_k^T k^{-3}(p_k, .) \\ D(p_k) &= \Sigma_{k=1}^{N} \beta_k U_k^T k^{-3}(p_k, .) \end{aligned} \tag{5.15}$$

5.1.2 Test data

To identify LPV state space model for the lTC engine, transient engine data is required. Transient engine data was collected from the experimentally validated LTC engine model [4, 5] by varying operating conditions and the control inputs to the engine. Start of injection (SOI) of the DI fuel, fuel quantity (FQ) and premixed fuel ratio (PR) are the engine manipulated variables changed during the test. Engine speed was kept to constant 1000rpm.

5.1.3 LTC engine modelling

Using the LS-SVM approach mentioned in Section 5.1.1, Combustion parameters prediction by coming up with linear parametric varying system matrices is discussed in this subsection.

States of the system (X) are $\begin{bmatrix} \mathrm{CA}_{50} & \mathrm{MPRR} & \mathrm{T}_{soc} & \mathrm{P}_{soc} & \mathrm{IMEP} \end{bmatrix}^T$

Manipulated Variables of the system (U) are $\begin{bmatrix} \mathrm{SOI} & \mathrm{FQ} & \mathrm{PR} \end{bmatrix}^T$

Scheduling parameter of the system (p) is $\begin{bmatrix} \mathrm{p}_1 & \mathrm{p}_2 \end{bmatrix}^T$,

where p_1 is fraction of early HR and p_2 is fraction of late HR

Output of the system (Y) is $\begin{bmatrix} \mathrm{CA}_{50} & \mathrm{MPRR} & \mathrm{IMEP} \end{bmatrix}^T$

Hyper parameters to be optimized by the LS-SVM algorithm are

† Kernel functions associated with each of the system matrix A, B and C

† Sigma functions associated with each of the system matrix A, B and C

† Multiplier associated with each of the system matrix A, B and C

† Regularisation parameters associated with each of the 5 states of the system

† Regularisation parameter associated with each of the 3 outputs of the system.

5.1.3.1 Model identification results

Identification of hyper parameters associated with LTC engine model with LPV-SVM approach was accomplished by using the Mode Frontier Optimisation Tool. Details on the tool are discussed on Appendix C.

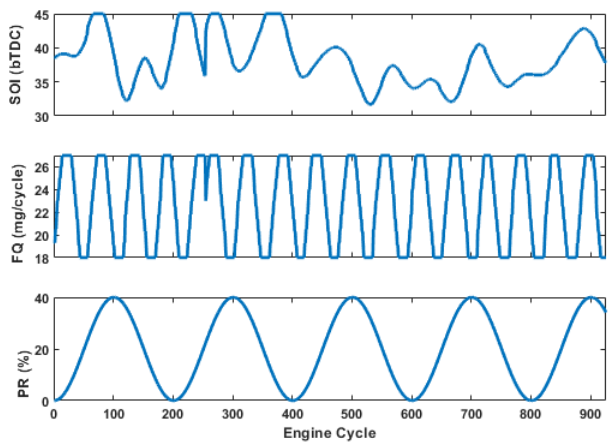

Figure 5.1: Manipulated variables of the LTC engine

In Figure 5.1 the manipulated variables of the LTC engine are shown. The range of manipulated variables also define the training range of manipulated variables of the LTC engine model. Other operating parameters like engine speed at 1000 rpm, intake temperature at 60°C and intake pressure at 96.5 kPa are maintained at a constant value.

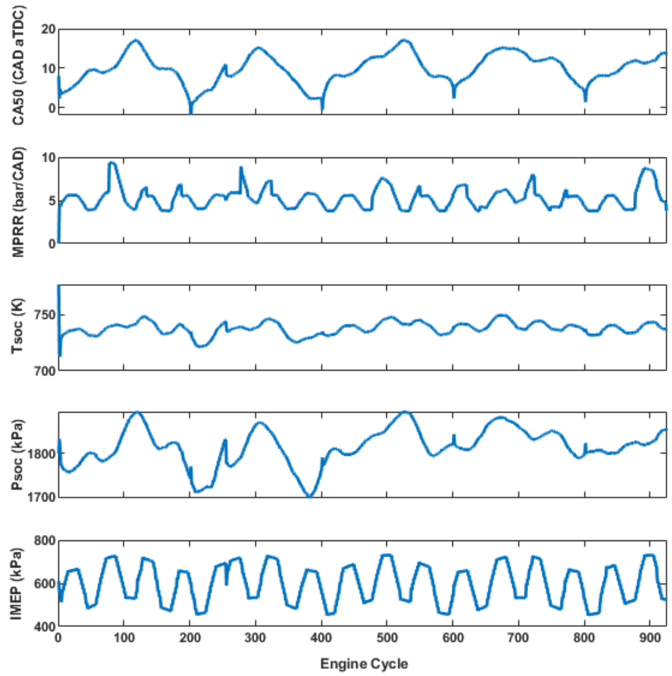

Figure 5.2: States of the LTC engine

In Figure 5.2 the states of the LTC engine are shown. The states are estimated by the experimentally validated LTC engine model.

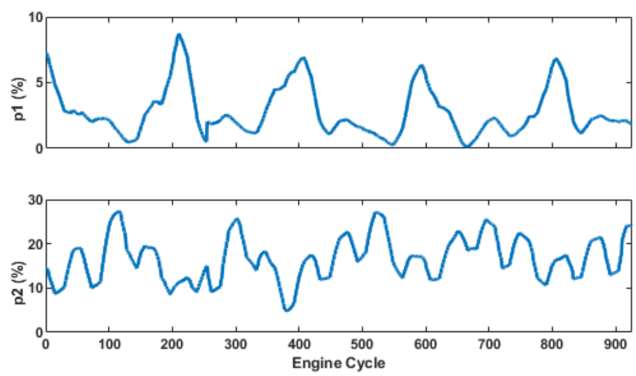

Figure 5.3: Scheduling parameters of the LTC engine

In Figure 5.3 the scheduling parameters of the LTC engine are shown. The range of both the scheduling parameters cover all three combustion types of interest.

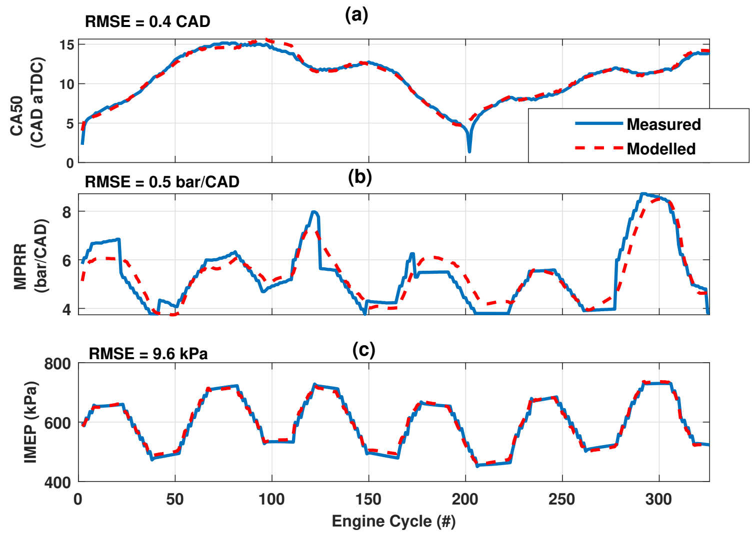

Figure 5.4: Comparison of measured and modelled output of LTC engine

In Figure 5.4 the comparison of prediction and measured values of the LTC engine are shown. 35% of the data used for testing is shown in the plot. The LPV model is able to predict CA_{50}, MPRR and IMEP with a RMSE of 0.4 CAD, 0.5 bar/CAD and 9.6 kPa. Error observed could be associated to the measurement uncertainty associated with experimental data used to build the model and prediction errors of the experimentally validated LTC engine. Additionally, the states P_{soc} and T_{soc} are internally calculated since these parameters are very difficult to be measured in the engine, which can also introduce error int he output.

5.1.3.2 System matrices

With Mode Frontier, the hyper parameters of the state space model are identified. The identified hyper parameters summary is listed in Appendix D. Variation in the coefficients of the the system matrices for the change in the scheduling parameter are depicted in the figures below 5.5, 5.6 and 5.7. The variation in the elements of the matrices depict the non-linearity of the LTC engine captured into the state space model.

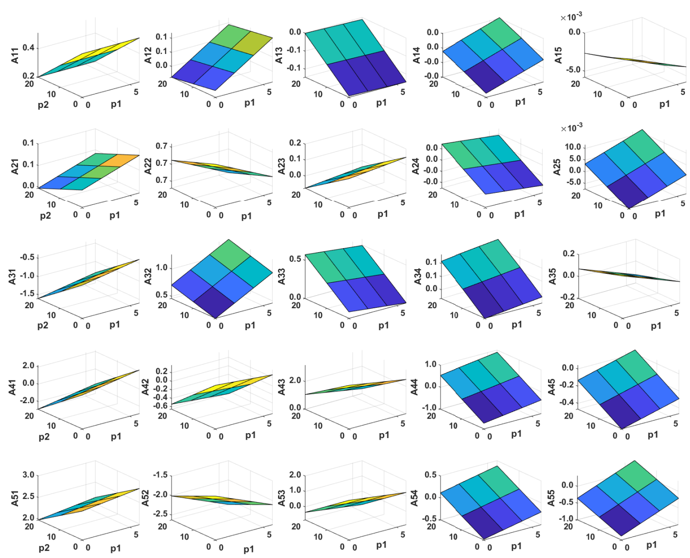

Figure 5.5: $\bar{A}(p_{1k},p_{2k})$ matrix elements as a function of scheduling parameters

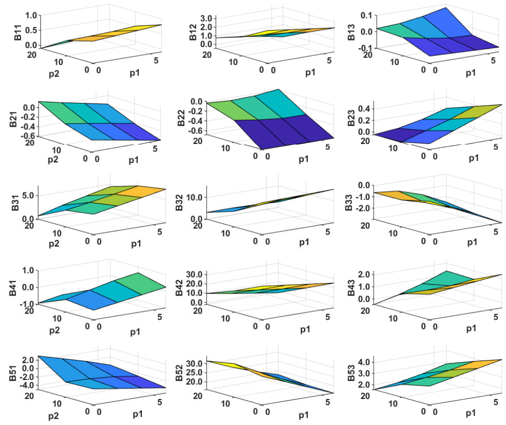

Figure 5.6: $\bar{B}(p_{1k},p_{2k})$ matrix elements as a function of scheduling parameters

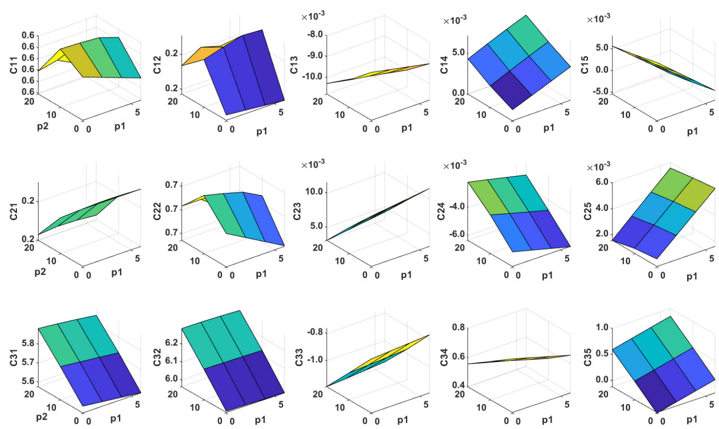

Figure 5.7: C(p_{1k},p_{2k}) matrix elements as a function of scheduling parameters

Chapter 6

Control of combustion phasing and IMEP with MPRR limitation

This chapter centers on system, identification of a multi- input multi- output (MIMO) state space model for the LTC engine and design of an adaptive MPC for control of CA_{50} and IMEP while limiting maximum pressure rise rate.

6.1 LPV identification

System identification by using LPV- SVM approach was discussed in Chapter 5.

6.1.1 Evaluation of model accuracy

To evaluate the validity of model prediction across all combinations of manipulated variables, a comparison is carried out with the parent LTC engine physics based model from the research work [4]. This helped to identify specific zones where the predicted model accuracy is acceptable for the LTC engine control.

All three manipulated variables, SOI is varied from 0 to 80 bTDC, injected fuel quantity is varied from 5 to 55 mg/cycle and PR is varied from 0 to 60 to evaluate prediction accuracy of the LPV-SVM model of LTC engine. The predicted values of LPV-SVM model is compared with the physics based plant model. Since, LPV-SVM model is a data-driven model it is observed to be valid only across the trained region and it is listed in Table 6.2

Table 6.1
Valid operating region of LPV-SVM model of LTC engine

Manipulated Variable	**Range**
Start of Injection	(32 - 45) CAD bTDC
Fuel quantity	(18- 27) mg/cycle
Premixed ratio	(0-40) %

The Figures 6.1 to 6.3 show the comparison between LPV -SVM model of the LTC engine and the physics based plant of the engine as a function of scheduling parameters (modelled values of fraction of early HR and fraction of late HR).

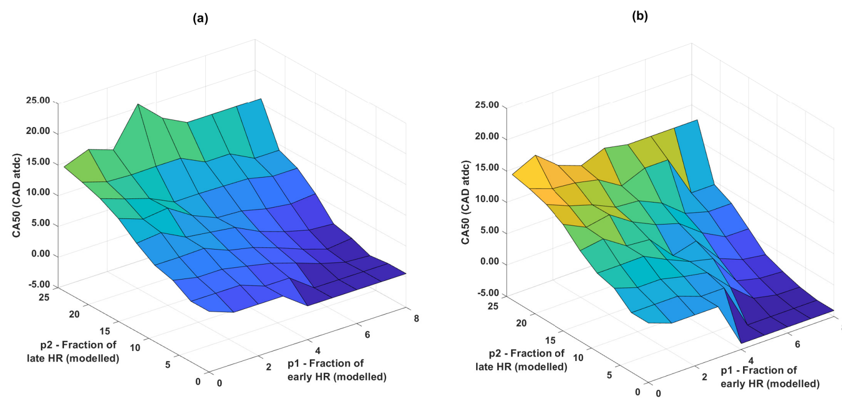

Figure 6.1: Predicted CA_{50} from (a) LPV-SVM model and (b) physics based plant model as function of scheduling parameter p1 and p2

Comparison between figures 6.1(a) and 6.1(b) shows that the same trend is followed though prediction variability is observed in CA_{50} prediction.

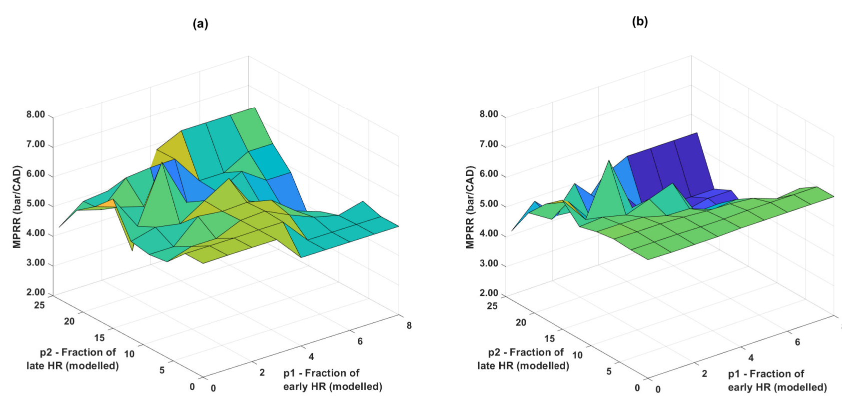

Figure 6.2: Predicted MPRR from (a) LPV-SVM model and (b) physics based plant model as function of scheduling parameter p1 and p2

Comparison between figures 6.2(a) and 6.2(b) shows that the MPRR prediction is in the similar range as that of the RCCI physical model.

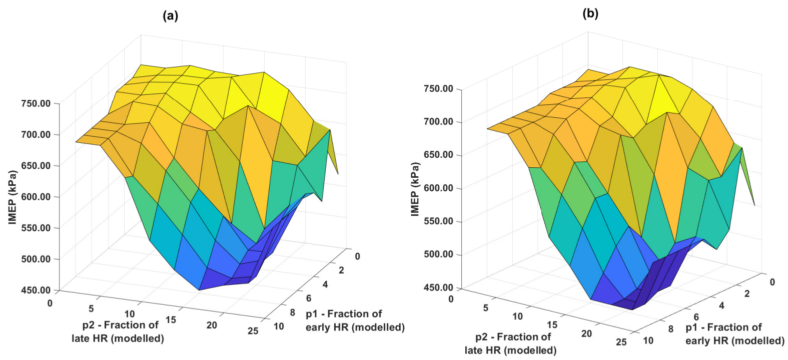

Figure 6.3: Predicted IMEP from (a) LPV-SVM model and (b) physics based plant model as function of scheduling parameter p1 and p2

Comparison between Figures 6.3(a) and 6.3(b) shows that the IMEP prediction is very close between the LPV-SVM model and RCCI physical model as the prediction accuracy of LPV-SVM model was observed high for IMEP.

6.2 Model Predictive Control

An MPC controller is designed for combustion control of the LTC engine. The MPC uses the LPV model from Section 6.2 to predict future outputs of the LTC engine and optimise the manipulated variables based on the optimisation of cost function. MPC Toolbox of Matlab is used as part of the design. In LPV-SVM model of the the LTC engine, at any instant of operation the system matrices are derived as a function of p_1 (fraction of early HR) and p_2 (fraction of late HR).

6.2.1 Design

Prediction of states and solution to optimisation problem is only arrived for certain future time steps. The number of future steps in which the output of the system is predicted is called *prediction horizon* and the manipulated variables of the system are optimised for a certain number of steps called *control horizon*. It is a quadratic optimisation at each of the control step. Hence, control horizon and prediction horizon are selected as 20 and 10 engine cycles, respectively.

The solution of quadratic problem (QP) optimisation results in the identification of manipulated variables of the system. It includes a cost function, whose value is minimised by the controller. Optimisation is constrained by constraints, which are the bounds on the manipulated variables, their rate of change, states and outputs of the system. This results in a realistic and optimal solution. A solution for manipulated variables minimises the cost function and also fulfil the requirements of constraints.

Cost function is built as a sum of three terms in the current design.

$$J(z_k) = J_y(z_k) + J_{\Delta u}(z_k) + J_{\epsilon}(z_k) \tag{6.1}$$

where z_k is the QP decision over the control interval

k is current control interval

J_y refers to output reference tracking

$J_{\Delta u}$ refers to manipulated variable tracking

J_ϵ refers to constraint violation

Output reference tracking is achieved by the controller cost function.

$$J_y(z_k) = \sum_{j=1}^{n_y} \sum_{i=1}^{p} \left\{ \frac{w_{i,j}^y}{s_j^y} \left[r_j(k+i|k) - y_j(k+i|k) \right] \right\}^2 \tag{6.2}$$

In the equation, p represents the prediction horizon,n_y refers to number of plant outputs, z_k is the decision of the QP.

$$z_k^T = \begin{bmatrix} u(k|k)^T & u(k+1|k)^T & u(k+p-1|k)^T & \epsilon_k \end{bmatrix} \tag{6.3}$$

$r_j(k+i|k)$ and $y_j(k+i|k)$ refers to the reference and predicted value of the j^{th} plant output at the i^{th} step of the prediction horizon. s_j^y refers to the scale factor for the j^{th} plant output and $w_{i,j}^y$ is the tuning weight for the j^{th} plant output at the i^{th} step of the prediction horizon.

The second scalar parameter used by the controller in the cost function to keep the rate of change of manipulated variables of the system is

$$J_{\Delta u}(z_k) = \sum_{j=1}^{n_u} \sum_{i=0}^{p-1} \left\{ \frac{w^{\Delta u}_{i,j}}{s^u_j} \left[u_j(k+i|k) - u_{jtarget}(k+i|k)) \right] \right\}^2 \tag{6.4}$$

Where, n_u refers to the number of manipulated variables. s^u_j refers to the scale factor for the j^{th} plant output and $w^{\Delta u}_{i,j}$ is the tuning weight for the j^{th} plant manipulated variable rate of change at the i^{th} step of the prediction horizon.

The designed controller employs the parameter J_ϵ to measure the violation of constraints.

$$J_\epsilon(z_k) = \rho_\epsilon \epsilon_k^2 \tag{6.5}$$

Where, ϵ_k is the slack variable at control interval k and ρ represents the penalty weight associated to it. The maximum and minimum limit set on the plant outputs, manipulated variables and the rate of change of manipulated variables, predominantly constitute the explicit constraints associated with the MPC,

$$\begin{gathered} \frac{y_{j,min}(i)}{s^y_j} - \epsilon_k V^y_{j,min}(i) \leq \frac{y_j(k+i|k)}{s^y_j} \leq \frac{y_{j,max}(i))}{s^y_j} + \epsilon_k V^y_{j,max}(i), \\ i = 1:p, \quad j = 1:n_y z \end{gathered} \tag{6.6}$$

$$\frac{u_{j,min}(i)}{s_j^u} - \epsilon_k V_{j,min}^u(i) \le \frac{u_j(k+i-I|k)}{s_j^u} \le \frac{u_{j,max}(i))}{s_j^u} + \epsilon_k V_{j,max}^u(i),$$
$$i = 1:p, \quad j = 1:n_u \tag{6.7}$$

$$\frac{\Delta u_{j,min}(i)}{s_j^u} - \epsilon_k V^{\Delta u}{}_{j,min}(i) \le \frac{\Delta u_j(k+i-I|k)}{s_j^u} \le \frac{\Delta u_{j,max}(i))}{s_j^u} + \epsilon_k V^{\Delta u}{}_{j,max}(i),$$
$$i = 1:p, \quad j = 1:n_u \tag{6.8}$$

Where, $y_{j,min}(i)$ and $y_{j,max}(i)$ refer to the min and max bounds set on the j^{ih} outputs of the system at the ith step of the prediction horizon. Similarly, $u_{j,min}(i)$ and $u_{j,max}(i)$ refer to themin and max bounds set on the manipulated variables and $\Delta u_{j,min}(i)$ and $\Delta u_{j,max}(i)$ refer to the min and max bounds set on the rate of change of the manipulated variable.

6.2.2 Application

Adaptive MPC is used to track the output, CA_{50} and IMEP of the system and limit MPRR by using SOI, fuel quantity and PR as manipulated variables. The control time step is set to 1 engine cycle. The prediction horizon and control horizon are set to 20 and 10 engine cycles.

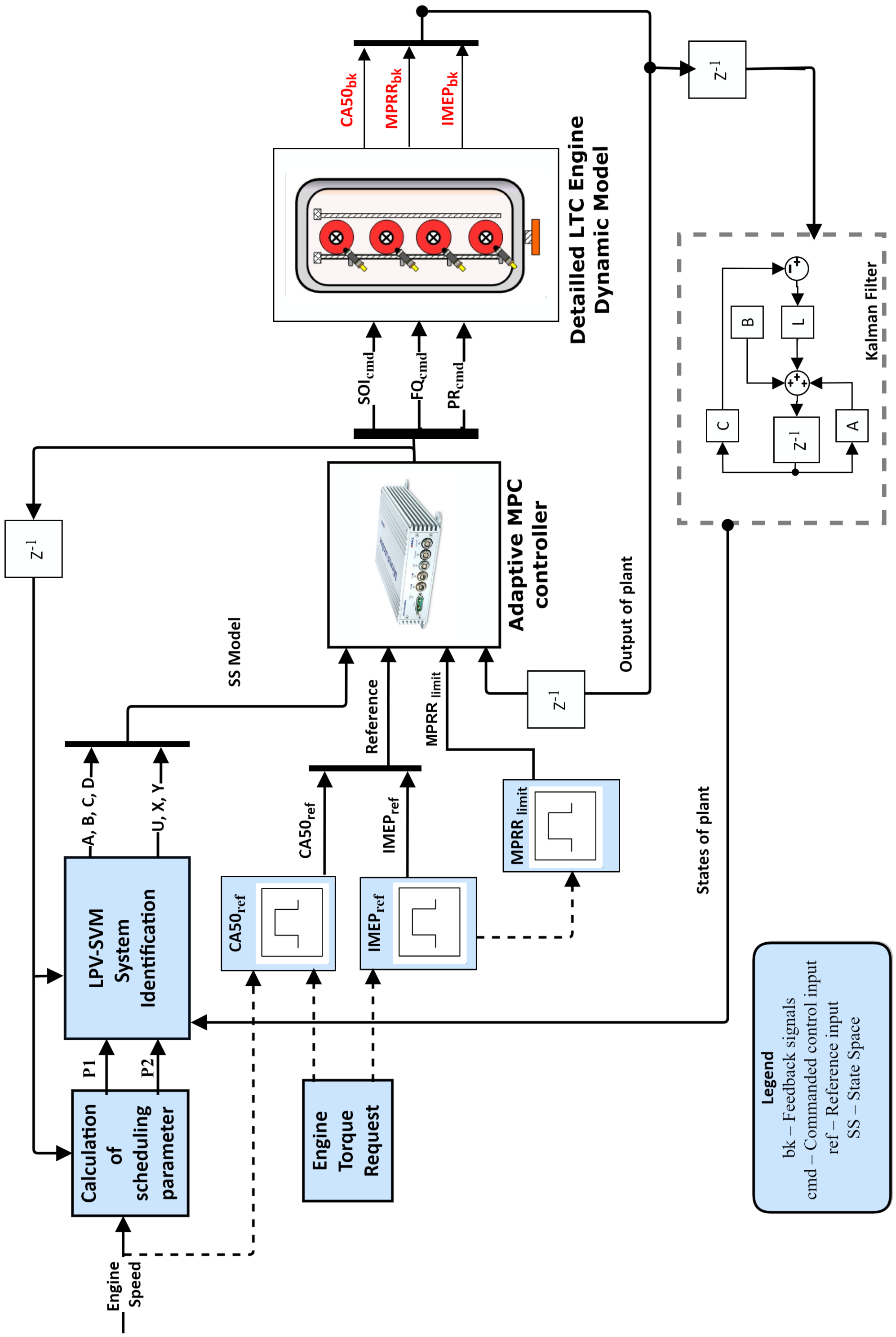

Figure 6.4: Schematic of the designed LPV-MPC controller for the LTC engine

6.2.2.1 Control structure

Control structure of the desired adaptive MPC controller is shown in Figure-6.4. Scheduling parameters (p1, p2) are calculated from engine speed, start of injection, fuel quantity injected and premixed ratio. Based on the scheduling parameters, LPV matrices of the LTC engine can be identified. These matrices are used by MPC to predict performance of the LTC engine. CA_{50}, IMEP and MPRR constraint are fed to the MPC controller. The LTC physics based plant is fed with manipulated variables (start of injection, fuel quantity injected and premixed ratio) at each engine cycle. Kalman filter is used in the schematic to predict the unmeasured states of the physics based plant. The CA_50 and IMEP reference on implementation in an engine, is derived from the engine speed and torque request to the electronic control module based on driver operation. The connection of engine speed and torque request are depicted in dotted line as its not set up in the current model, but are depicted in the control structure to show model's relevance to real life operation of engine.

The weights of the allowed rate of change of manipulated variables and output are tuned to achieve required tracking performance. The weights of the rate of change of SOI is 0.3, fueling quantity is 0.5 and PR is 0.05. With the setting, PR is the quickest lever to be changed followed by SOI and fueling quantity.

Table 6.2
Summary of constraints applied on manipulated variables and outputs of the adaptive MPC

Variable	Minimum constraint	Maximum constraint
Start of Injection	32 CAD bTDC	45 CAD bTDC
Fuel quantity	18 mg/cycle	27 mg/cycle
Premixed ratio	0%	40%
CA_{50}	-10 CAD aTDC%	30 CAD aTDC%
IMEP	500 kPa%	1000 kPa%
MPRR	0%	6%

6.2.2.2 Tracking Performance

The tracking performance of the designed controller to follow the desired change of CA_{50} from 5 to 12 CAD aTDC and IMEP from 525 kPa to 650 kPa. As the system tracks the change in output by holding MPRR less than 6bar/CAD. The change in manipulated variables and scheduling parameter of the LPV system is also evaluated in the various cases depicted in Figures from 6.5 to 6.9.

In Figure 6.5, the tracking ability of designed controller to follow the desired change in both CA_{50} and IMEP is evaluated. Tracking with RMSE of 1.2 CAD for CA_{50}, IMEP with a RMSE of 6.2 kPa and MPRR is limited to 6.1 bar/CAD.

In Figure 6.6, the tracking ability of designed controller of a LTC engine for a change in both IMEP and CA_{50} while the restrictions on MPRR being relaxed to 8bar/CAD. Tracking with RMSE of 1 CAD for CA_{50}, IMEP with RMSE of 10.3 kPa and the maximum pressure rise rate is limited to 6.3 bar/CAD. Also, with relaxed MPRR, CA_{50} tracking performance improved significantly but the error associated with IMEP tracking increased.

In Figure 6.7, the tracking ability of the designed controller to follow a change in outputs of LTC engine with measurement uncertainty is evaluated. The measurement uncertainty from Table 2.5 are added to the outputs of the LTC engine physics based plant, to simulate measurement uncertainty. Tracking with RMSE of 2.2 CAD for CA_{50}, RMSE of 17.3 kPa for IMEP and the maximum pressure rise rate is observed to be 6.5 bar/CAD. Error in tracking had gone up due to uncertainty in the outputs. In 83^{rd} engine cycle, as all the manipulated variables saturate a violation in the MPRR is observed. The controller comes into action to bring the MPRR within limit in subsequent cycles.

To compare the effect of selecting proper scheduling variables, the results from this thesis are compared with those in [5]. To this end, Figure 6.8 is added in which LTC engine tracking capability achieved is achieved by using only PR as scheduling parameter. Tracking was achieved only by using SOI and fueling quantity as the manipulated variables of the LTC engine. It is evident that the maximum tracking capability for IMEP was limited due to CA_{50} tracking errors when IMEP $\geq$ 650kPa. In Figure 6.9, the tracking ability of LTC engine to follow the change in IMEP set to 690 kPa with constraints on MPRR set at 6bar/CAD using new scheduling variables and also, using PR as the additional manipulated variable. Tracking with RMSE of 1.1 deg for CA_{50}, IMEP with RMSE of 8.6 kPa and MPRR limited to 6 bar/CAD was achieved. SOI and PR have almost saturated to its maximum in order to achieve the target. Reduction in RMSE of CA_{50} and IMEP is seen on comparison of Figure 6.8 and Figure 6.9.

In Figure 6.10, the tracking ability of the designed controller of LTC engine with CA_{50} target raised to 14 CAD aTDC while constraints on MPRR set to 6bar/CAD is shown. Tracking is achieved with RMSE of 1.7 CAD for CA_{50}, IMEP with RMSE of 5.8 kPa and the maximum pressure rise rate is limited to 6.2 bar/CAD. PR has saturated to 40 in order to achieve the target. The motivation for evaluating controller ability in tracking delayed CA50, comes from the result of work carried out in [57]. It shows that retarded combustion phasing shows benefit of smooth heat release rate and reduced MPRR.

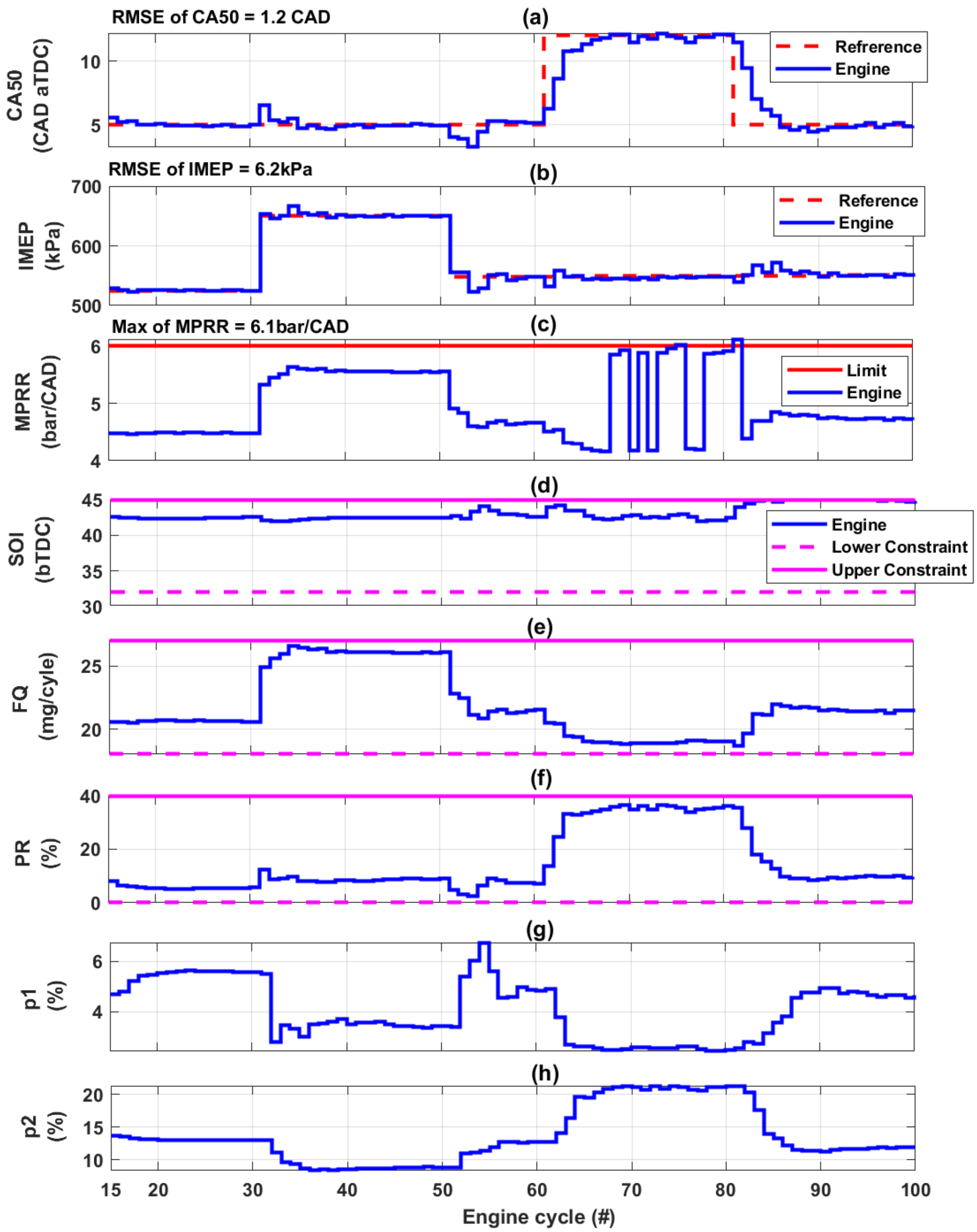

Figure 6.5: Tracking capability of designed controller to follow desired CA_{50} and IMEP with MPRR limit is 6 bar/CAD

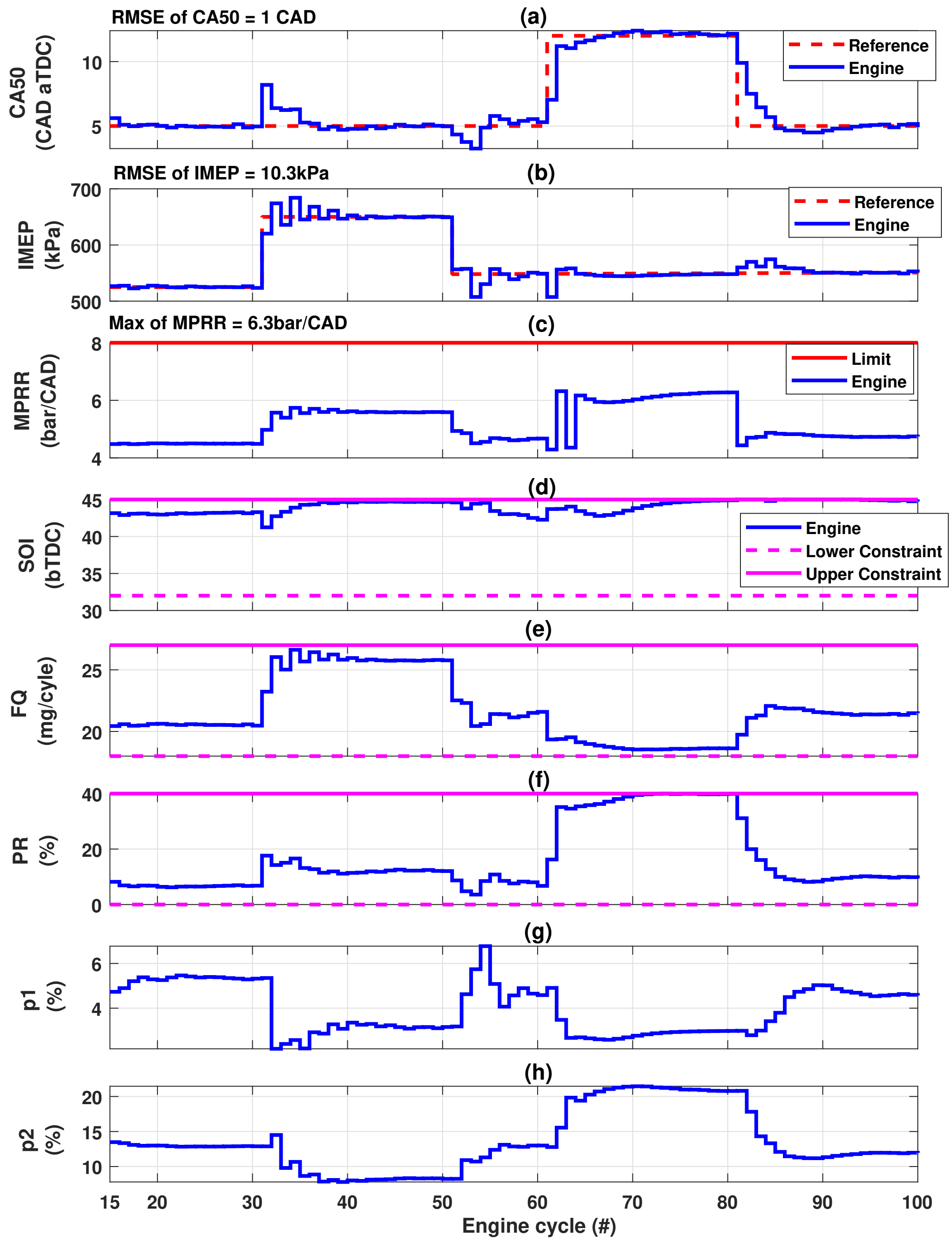

Figure 6.6: Tracking capability of designed controller to follow desired CA_{50} and IMEP. The MPRR limit is 8 bar/CAD

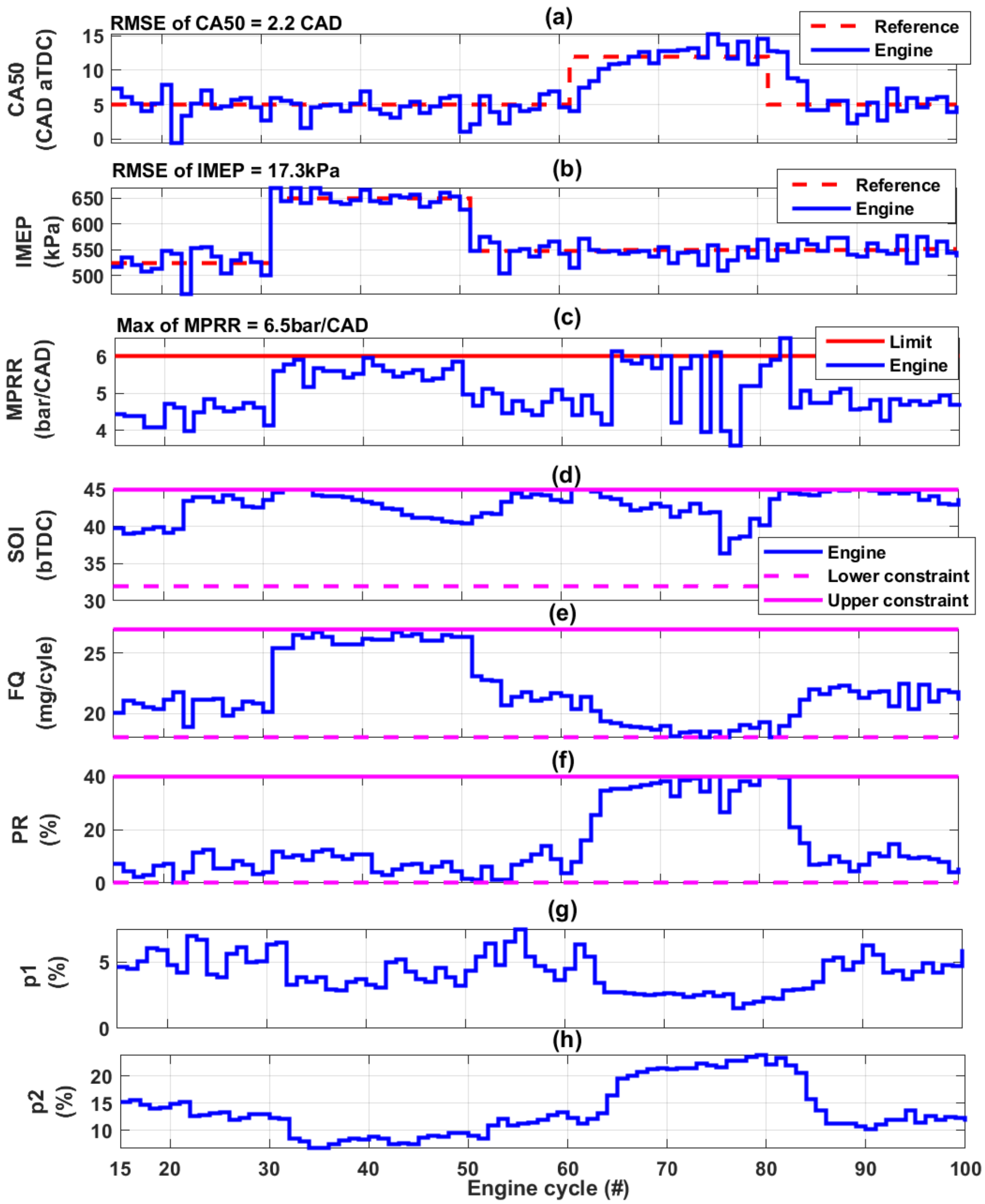

Figure 6.7: Tracking capability of designed controller to follow desired CA_{50} and IMEP along with measurement uncertainty added in measured outputs of LTC engine. The MPRR limit is 6 bar/CAD

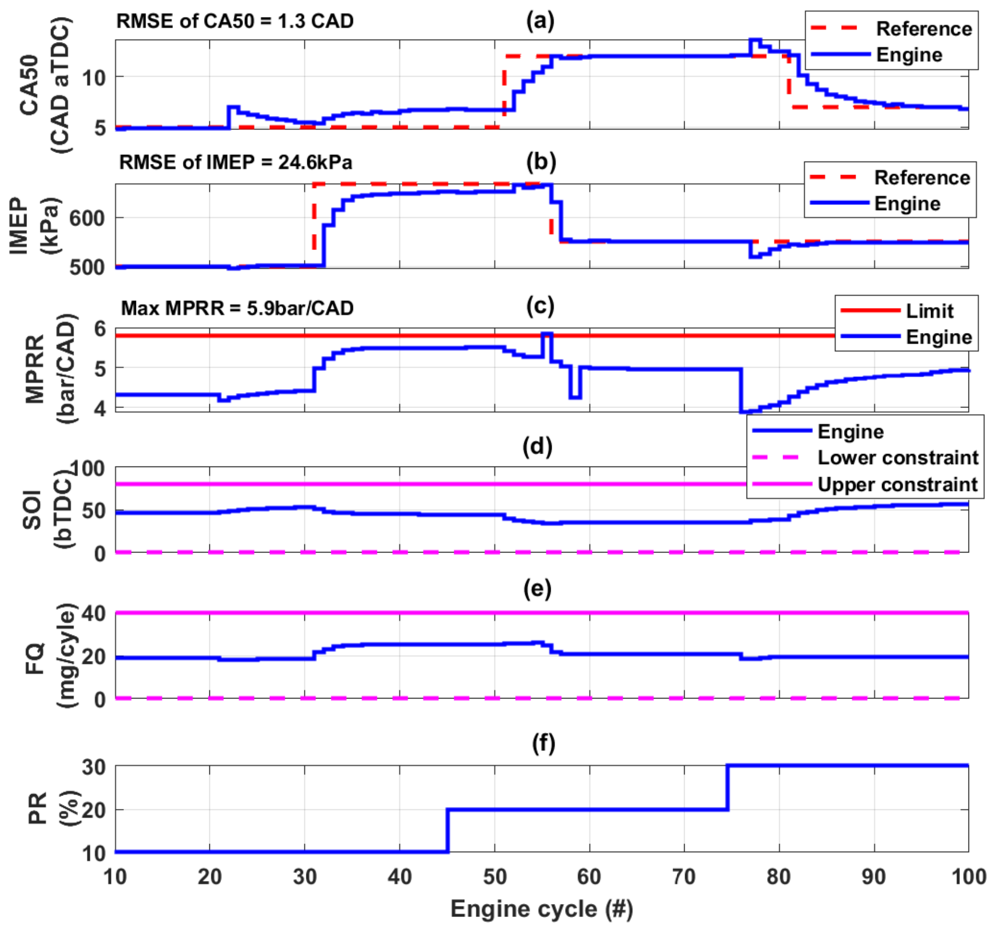

Figure 6.8: Tracking capability achieved for CA_{50} and IMEP with PR as scheduling parameter [49]. MPRR limit is 5.8 bar/CAD

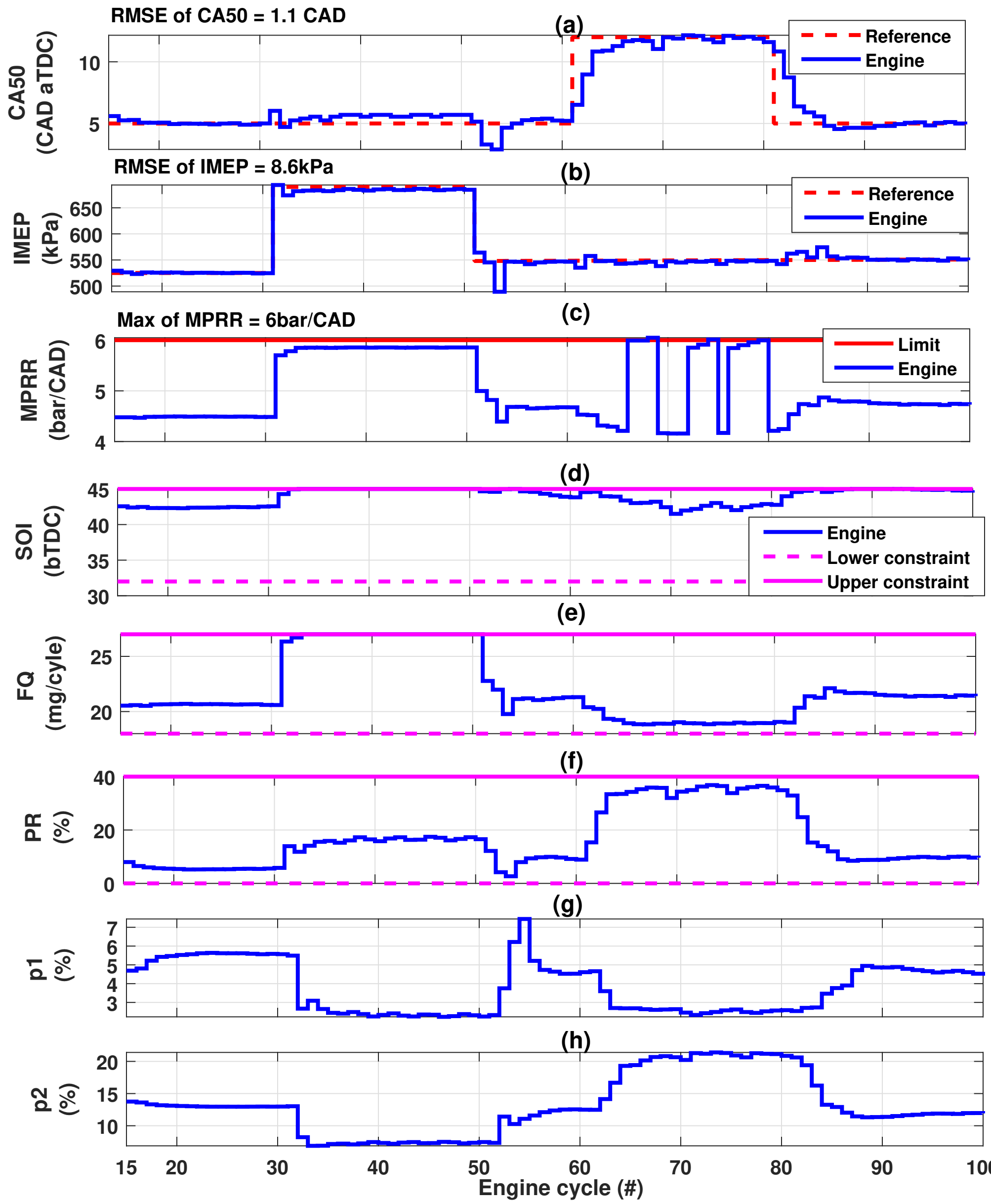

Figure 6.9: Maximum tracking capability achieved for IMEP, when increased to 690kPa and MPRR limit is 6 bar/CAD

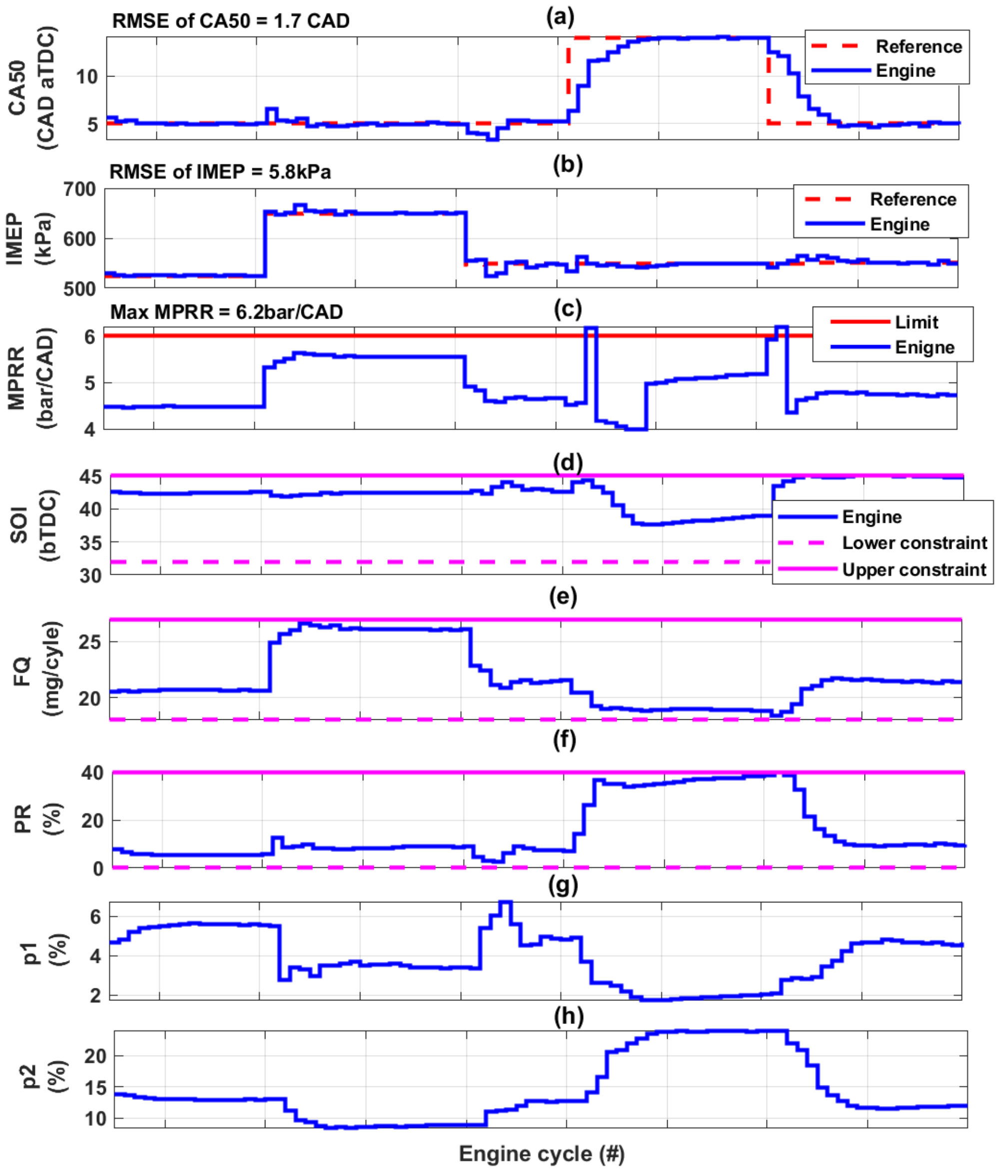

Figure 6.10: Maximum tracking capability achieved for CA_{50},when increased to 14 CAD aTDC and MPRR limit is 6 bar/CAD

Chapter 7

Conclusions and Future Work

7.1 Summary and Conclusions

In this research work, classification of heat release rate traces of LTC engine was developed. Significant engine inputs leading to different HR shapes were identified. The parameters fraction of early HR and fraction of late HR used for classification were modelled using significant engine inputs. The modelled fraction of early HR and fraction of late HR were used as scheduling variables into the LPV-SVM matrices of the LTC engine model. This model was used to build MPC to control LTC engine. Major contributions/ findings from this research work are presented below.

† Heat release rate data from the experimental study conducted on the LTC engine were analysed. A rule based classification was developed to classify HRR traces into three significant combustion pattern similar to HCCI, PCCI and RCCI. Two transition bins were also identified to create accommodate traces transitioning between the significant combustion pattern.

† Characteristics of the distribution of classified traces were studied. Distribution of combustion parameters like, peak cylinder pressure, maximum pressure rise rate, CA_{10}, CA_{90}, maximum in-cylinder temperature at start and end of main heat release were analysed. It was observed that combustion parameters had a distinct characteristics across three significant classification bins and the information from these parameters could be further used for controlling the engine.

† As a next step to classify the HRR traces automatically, supervised and unsupervised techniques of machine techniques were applied. With unsupervised approach, it was evident that the classified clusters didn't clearly represent different combustion patterns. On comparison between CNN and decision tree, it was observed that decision tree prediction with higher accuracy of 74.5%.

† In order to model a LPV matrices of the LTC engine, scheduling parameter of LPV matrices were identified. PCA was used to identify the significant LTC engine inputs. SOI, PR ,fuel quantity and engine speed are the significant inputs of engine combustion. Linear regression was used to model, fraction of early

HR and fraction of late HR as a function of these significant engine inputs. The combination of modelled fraction of early HR and fraction of late HR which resulted in highest R^2 value was selected as scheduling parameters.

† Using Support Vector Machine(SVM) approach, a data driven LPV control model of the LTC engine was developed. The LPV model used modelled fraction of early HR and fraction of late HR as the scheduling parameters. The model was validated with the data generated by the detailed LTC engine dynamic model. It was able to predict CA_{50}, IMEP and MPRR with RMSE of 0.4 CAD, 16.6 kPa and 0.4 bar/CAD.

† MPC was built to control the LPV model of the LTC engine. It was developed with the prediction horizon of 20 engine cycles and control horizon of 10 engine cycles. The controller was able to track CA_{50} and IMEP with MPRR constraint of 6bar/CAD with SOI, PR and Fuel quantity as manipulated variables. It was able to track CA_{50} and IMEP with RMSE of 1.2 CAD and 6.2 kPa. MPC performance on CA_{50} tracking improved with MPRR constraint of 8 bar/CAD. But, the tracking error of IMEP increased.It was able to track CA_{50} and IMEP with RMSE of 1 CAD and 10.3 kPa.

† Disturbance rejection capability of the MPC was also evaluated by addition of measurement uncertainty into the outputs of the detailed LTC physics based dynamic plant. The MPC controller was able to track CA_{50} and IMEP of 690 kPa with RMSE of 1.1CAD and 8.6 kPa on MPRR constraint of 6 bar/CAD.

The controller was also able to track IMEP and CA_{50} of 14CAD with RMSE of 5.6 kPa and 1.7CAD on MPRR constraint of 6 bar/CAD.

7.2 Future work

Based on the findings of this work, a few areas can be explored further. They are listed below.

7.2.1 Control architecture for a multi-mode engine using HRR classification

In order to control the heat release type of the engine real time, an idea of the control architecture depicted in Figure (7.1) can be pursued. The proposed architecture may consist of multiple blocks:

Architecture consists of multiple blocks.

† Prediction models including

1. model to predict as a function of control inputs of LTC engine
2. model to predict as a function of HRR trace

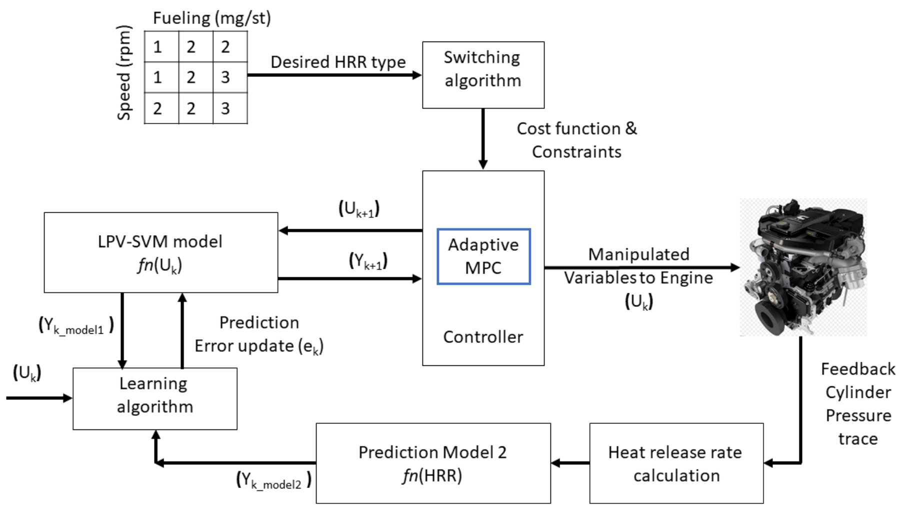

Figure 7.1: Proposed control architecture for a multi-mode engine using HRR classification

† Algorithm for desired HRR type input

† Learning algorithm

† MPC controller

In the following the main blocks in Figure 7.1 are briefly explained

7.2.1.1 Predictive models

Two predictive models are used in this control structure. One of the predictive model works as a function of manipulated variables of the engine, like LPV-SVM model built in Chapter 5. It is represented as LPV-SVM as a function of inputs in Figure 7.1 .The model based on inputs, calculates the scheduling parameters. Based on scheduling parameters, can predict the HRR type. It can also calculate the output of the LTC engine, as a function of LPV matrices identified with the scheduling parameters. The second model, works as the function of HRR trace, like CNN model built in Section 3.2. It is represented as Prediction model 2 in Figure 7.1.

7.2.1.2 Algorithm for desired HRR type input

A map based logic is set to identify desired heat release rate type as a function of engine speed and fuel quantity injected. Also, based on the HRR type is chosen corresponding cost function and constraints also are fed to the controller. Cost function associated with heat release type 1 is to maximise main heat release, with type 2 is to maximise fraction of early heat release and with type 3 is to maximise fraction of late heat release. Constraints are rate of change of control inputs to engine and limiting constraints combustion parameters. Limiting constraints are on MPRR, CA_{50}, co-efficient of variation of IMEP and emissions. Desired heat release rate type is fed to the Adaptive model predictive controller(MPC).

7.2.1.3 MPC controller

Controller block interacts with the LPV-SVM model in order to optimise future control inputs to the engine plant. Its depicted in the control architecture with the nomenclature of (k+1). The finalised control input is fed to the engine plant. With the help of in cylinder pressure transducer on the engine, the feedback cylinder pressure trace is collected and converted to heat release rate as a function of engine crank angle. By using Prediction model 2, the heat release rate type is identified.

7.2.1.4 Learning Algorithm

Learning algorithm is the final block in the architecture which will ensure that LPV-SVM model is updated based on real time observations and prediction based on engine in-cylinder pressure data. This block could consist of three elements.

- † Operating conditions to learn
- † Error calculation
- † Learning summary table and update of LPV-SVM model

Engine operating with $COV_{IMEP} \leq 3\%$ to ensure stability of operation and with no occurrence of engine combustion related error are some of the conditions to be considered for the learning algorithm to learn. An update summary table is setup inside the learning algorithm, it has the count of region of fueling and engine speed updated in real life operation. The prediction error(e_k) shown in Figure 7.1 is calculated as a weighted sum of current prediction by LPV-SVM model and the difference in prediction between LPV-SVM model and Model 2. Once e_k is calculated, the learning algorithm updates the value for future reference in both the summary table and prediction LPV-SVM model. The learning process will help the model to update the prediction as the function of control inputs to reflect real time operating condition of the engine.Complete operational model with the architecture shown in 7.1 is still in the concept phase, it is yet to be built and verified.

7.2.2 Other future works

Here is the list of other ideas to advance the outcomes from this thesis

† Experimental implementation and validation of the designed controllers from Chapter 6.

† Design of LPV data driven models from Chapter 5 using the engine experimental data, including COV_{IMEP}, emissions and combustion noise constraints and on board learning based on real time engine data

References

[1] K. Sadabadi. "Modelling and control of combustion of an RCCI engine". Master's thesis, Michigan technological University, 2015.

[2] K. Kannan. "An experimental investigation of Low temperature Combustion regimes in a light duty". Master's thesis, Michigan technological University, 2016.

[3] N Kondipati. "Experimental Study , Modelling and Controller for an RCCI Engine". Master's thesis, Michigan technological University, 2017.

[4] A. Raut. "Model based control of RCCI Engine". Master's thesis, Michigan technological University, 2017.

[5] A. Basina. "Modelling and control of Maximum Pressure rise rate in RCCI Engine". Master's thesis, Michigan technological University, 2019.

[6] S. Rizvi, J. Velni, R. Toth, and N. Meskin. "A Kernel based Approach to MIMO LPV State Space Identification and Application to a Nonlinear Process System".

IFAC-PapersOnLine, 48:85 – 90, 2015. 1st IFAC Workshop on Linear Parameter Varying Systems LPVS 2015.

[7] United States Environmental Protection Agency. "Fast Facts US transportation sector greenhouse gas emission 1990-2017" . Technical Report EPA-420-F-19-047, 2019.

[8] J. Dec. "A Conceptual Model of DI Diesel Combustion Based on Laser-Sheet Imaging". In *SAE Technical Paper*. SAE International, 1997. 970873.

[9] A. Agarwal, A. Singh, and R. Maurya. "Evolution, challenges and path forward for Low temperature combustion". *Progress in Energy and Combustion Science*, 61:1–56, 2017.

[10] A. Dempsey, R. Walker, E. Gingrich, and R. Reitz. "Comparison of Low temperature Combustion Strategies for Advanced Compression Ignition Engines with a focus on Controllability". *Combustion Science and Technology*, 186:210–241, 2014.

[11] D. Foster and Phil. "Low Temperature Combustion-A Thermodynamic pathway to high efficiency engines". 2012.

[12] M. Nazemi. "Modelling and analysis of reactivity controlled compression ignition (RCCI) Combustion". Master's thesis, Michigan technological University, 2015.

[13] G. Neely, S. Sasaki, S. and, Y. Huang, J. Leet, and D. Stewart. "New diesel emission control strategy to meet US tier 2 emission regulations". In *SAE Technical Paper*. SAE International, 2005. 2005-01-1091.

[14] R. Hasegawa and H. Yanagihara. "HCCI Combustion in Di Diesel Engine". In *SAE Technical Paper*, 2003. 2003-01-0745.

[15] G. Shibata, K. Oyama, T. Urushihara, and T. Nakano. "Correlation of low temperature heat release with Fuel composition and HCCI engine Combustion". In *SAE Technical Paper*. SAE International, 2005. 2005-01-0138.

[16] S. Kokjohn, R. Hanson, D. Splitter, and R. Reitz. "Experiments and Modeling of Dual-Fuel HCCI and PCCI Combustion Using In-Cylinder Fuel Blending". *SAE Int. J. Engines*, 2:24–39, 2009.

[17] K. Inagaki, T. Fuyuto, K. Nishikawa, K. Nakakita, and I. Sakata. "Dual Fuel PCI Combustion Controlled by In- Cylinder Stratification of Ignitability". In *SAE Technical Paper*. SAE International, 2006. 2006-01-0028.

[18] K. Okude, K. Mori, S. Shiino, and T. Moriya. "Premixed compression Ignition (PCI) combustion in simultaneous reduction of NO_x and soot in diesel engine". In *SAE Technical Paper*. SAE International, 2004. 2004-01-1907.

[19] A. Dempsey. *"Dual Fuel Reactivity Controlled Compression Ignition(RCCI) with Alternative Fuels"*. PhD thesis, University of Wisconsin-Madison, 2013.

[20] S. Kokjohn, R. Hanson, D. Splitter, and R. Reitz. "Fuel reactivity Controlled Compression Ignition (RCCI):A pathway to Controlled High Efficiency Clean Combustion". *International Journal of Engine Research*, 12:209–226, 2011.

[21] A. Paykani, A. Kakaee, P. Rahnama, and R. Reitz. "Progress and recent trends in Reactivity controlled compression Ignition Engines". *International Journal of Engine Research*, 17:481–524, 2016.

[22] R. Stone. *"Engine Modelling In Introduction to internal combustion engines"*. Palgrave,London, 1992.

[23] J. Powell. "A review of IC engine Models for control system design". *IFAC Proceedings Volumes*, 20:235 – 240, 1987. 10th Triennial IFAC Congress on Automatic Control - 1987 Volume III, Munich, Germany, 27-31 July.

[24] D. Solomatine, L. See, and R. Abrahart. *"Data-Driven Modelling: Concepts, Approaches and Experiences"*, pages 17–30. Springer Berlin Heidelberg, Berlin, Heidelberg, 2008.

[25] D. Solomatine and A. Ostfeld. "Data-driven modelling: some past experiences and new approaches". *Journal of Hydroinformatics*, 10:3–22, 2008.

[26] A. Sharma, V. Sugumaran, and S. Devasenapati. "Misfire detection in an IC engine using vibration signal and decision tree algorithms". *Measurement*, 50:370 – 380, 2014.

[27] G. Bhadane, A. Jadhav, V. Bhong, S. Inamdhar, and D. Narsale. *"Misfire detection in Automotive engines with convolutional neural network"*, pages 121–131. 2020.

[28] T. Gangopadhyay, A. Locurto, J. Michael, and S. Sarkar. *"Deep learning Algorithms for detection of Combustion Instabilities"*. Springer, Singapore, 2020.

[29] S. Salam and T. Verma. "Analysis of significance of variables in IC engine operation:an empirical methodology". *Energy Conversion and Management*, 207:112520, 2020.

[30] B. Bahri, A. Aziz, M. Shahbakhti, and M. Said. "Understanding and detecting misfire in an HCCI engine fuelled with ethanol". *Applied Energy*, 108:24 – 33, 2013.

[31] B. Bahri, A. Aziz, M. Shahbakhti, and M. Said. "Misfire Detection Based on Statistical Analysis for an Ethanol Fueled HCCI Engine". *International Review of Mechanical Engineering*, 6:1276–1282, 2012.

[32] A. Ghazimirsaied, M. Shahbakhti, and C. Koch. "HCCI Engine Combustion Phasing Prediction Using a Symbolic-Statistics Approach". *Journal of Engineering for Gas Turbines and Power*, 132, 2010.

[33] B. Bahri, M. Shahbakhti, K. Kannan, and A. Aziz. "Identification of ringing operation for low temperature combustion engines". *Applied Energy*, 171:142 – 152, 2016.

[34] B. Bahri, M. Shahbakhti, and A. Aziz. "Real-time modeling of ringing in HCCI engines using artificial neural networks". *Energy*, 125:509 – 518, 2017.

[35] G. Huang, Q. Zhu, and C. Siew. "Extreme learning machine: Theory and applications". *Neurocomputing*, 70:489 – 501, 2006. Neural Networks.

[36] K. Wong, P. Wong, C. Cheung, and C. Vong. "Modelling and optimisation of biodiesel engine performance using advanced machine learning methods". *Energy*, 55:519 – 528, 2013.

[37] C. Vong and P. Wong. "Engine ignition signal diagnosis with wavelet packet transform and multi-class least squares support vector machines". *Expert Systems with Applications*, 38:8563 – 8570, 2011.

[38] M. Pacella. "Unsupervised classification of multi channel profile data using PCA: An application to an emission control system". *Computers Industrial Engineering*, 122:161 – 169, 2018.

[39] R. Ahmed, M. Sayed, S. Gadsen, J. Tjong, and S. Habibi. "Automotive Internal Combustion Engine Fault Detection and Classification using Artificial Neural Network Techniques". *IEEE Transactions on Vehicular Technology*, 64:21–33, 2015.

[40] J. Rezaei, M. Shahbakhti, B. Bahri, and A. Aziz. "Performance prediction of HCCI engines with oxygenated fuels using artificial neural networks". *Applied Energy*, 138:460 – 473, 2015.

[41] M. Bidarvatan and M. Shahbakhti. "Gray-box modeling for performance control of an HCCI engine with blended fuels". *Journal of Engineering for Gas Turbines and Power*, 136, 2014.

[42] A. Cranmer, M. Shahbakhti, and J. Hedrick. "Grey-box modeling architectures for rotational dynamic control in automotive engines". In *2012 American Control Conference (ACC)*, pages 1278–1283, 2012.

[43] M. Bidarvatan and M. Shahbakhti. Grey-box modeling for hcci engine control. In *ASME 2013 Internal Combustion Engine Division Fall Technical Conference, ICEF 2013*, volume 1, 10 2013.

[44] P. Wong, K. Wong, C. Vong, and C. Cheung. "Modeling and optimization of bio-diesel engine performance using kernel-based extreme learning machine and cuckoo search". *Renewable Energy*, 74:640 – 647, 2015.

[45] S. Roy, R. Banerjee, and P. Bose. "Performance and exhaust emissions prediction of a CRDI assisted single cylinder diesel engine coupled with EGR using artificial neural network". *Applied Energy*, 119:330 – 340, 2014.

[46] A. Malikopoulos, D. Assanis, and P. Papalambros. "Real-time self-learning optimization of diesel engine calibration". *Journal of Engineering for Gas Turbines and Power*, 131, 2008.

[47] K. Ebrahimi, M. Aliramezani, and C. Koch. "An HCCI Control Oriented Model

that Includes Combustion Efficiency". *IFAC-PapersOnLine*, 49:327 – 332, 2016. 8th IFAC Symposium on Advances in Automotive Control AAC 2016.

[48] A. Norouzi, K. Ebrahimi, and C. Koch. "Integral Discrete-time Sliding Mode Control of Homogeneous Charge Compression Ignition (HCCI) Engine Load and Combustion Timing". *IFAC-PapersOnLine*, 52:153 – 158, 2019. 9th IFAC Symposium on Advances in Automotive Control AAC 2019.

[49] G. Najafi, B. Ghobadian, and H. Rahimi. "Combustion analysis of a CI engine performance using waste cooking bio-diesel fuel with an artificial neural network aid". *American Journal of Applied Sciences*, 4, 2007.

[50] B Irdmousa, S. Rizvi, J. Velni, J. Naber, and M. Shahbakhti. "Data Driven Modelling and Predictive Control of Combustion Phasing for RCCI Engines". In *2019 American Control Conference (ACC)*, pages 1617–1622, 2019.

[51] M. Bidarvatan, V. Thakkar, and M. Shahbakhti. "Grey-box Modeling and Control of HCCI Engine Emissions". In *2014 American Control Conference*, pages 837–842, 2014.

[52] M. Howell and M. Best. "On-line PID tuning for engine idle-speed control using continuous action reinforcement learning automata". *Control Engineering Practice*, 8:147 – 154, 2000.

[53] F. Payri, A. Broatch, B. Tormas, and V. Marant. "New methodology for In-

Cylinder Pressure Analysis in Direct Injection Diesel Engines Application to Combustion Noise". *Measurement Science and Technology*, 16:540, 2005.

[54] J. Chang, O. Guralp, Z. Filipi, D. Assanis, T. Kuo, P. Najt, and R. Rask. "New Heat Transfer Correlation for an HCCI Engine Derived from Measurements of Instantaneous Surface Heat Flux". *SAE Technical Paper*, 2004. 2004-01-2996.

[55] M. Pandian and A. Krishnasamy. "A Comparison of Different Low Temperature Combustion Strategies in a Small Single Cylinder Diesel Engine under Low Load Conditions" . In *SAE Technical Paper*. SAE International, 2017. 2017-01-2363.

[56] Y. Lecunn, L. Bottou, Y. Bengio, and P. Haffner. "Gradient-Based Learning Applied to document Recognition". *Proceedings of the IEEE*, 86:2278–2324, 1998.

[57] M. Sjöberg, J. Dec, A. Babajimopoulos, and D. Assanis. "Comparing Enhanced Natural Thermal Stratification Against Retarded Combustion Phasing for Smoothing of HCCI Heat-Release". In *SAE Technical Paper*. SAE International, 2004. 2004-01-2994.

Appendix A

LTC engine data used for identification of scheduling parameter

Data tabulated are collected from the LTC engine in APSRC lab for the research work by references [3],LTC-04

SOI (bTDC)	PR (%)	Total Fuel mass (mg/cycle)	Engine Speed (rpm)	Intake air temperature (Deg c)	Intake air Pressure (kPa)	CA_Start of Main HR (aTDC)	CA_End of Main HR (aTDC)	Heat release type	Fraction of early (%)	Fraction of Late (%)
25	20	19	800	40	112	1	12	3	0.9	24.2
25	20	27	800	40	114	2	14	4	0.1	17.6
35	20	10	1000	39	111	3	20	5	6.6	16.6
35	20	14	1000	39	111	2	16	3	4.4	24.4
35	20	19	1000	40	112	2	14	3	3.0	24.5
35	20	28	1000	40	111	3	17	1	1.3	16.0
50	20	12	1200	40	109	3	17	2	10.0	25.7
50	20	15	1200	40	109	3	17	2	8.2	23.5
50	20	19	1200	40	108	0	12	3	4.8	25.1
50	20	28	1200	40	110	1	14	4	2.5	17.1
60	20	12.5	1400	39	115	3	20	2	11.7	22.3
60	20	14.8	1400	40	114	3	15	2	10.3	24.0
60	20	16.5	1400	40	115	1	13	2	8.1	22.6
60	20	18.5	1400	40	115	0	11	5	6.3	21.3
35	40	14	800	41	112	2	17	4	4.2	21.1
35	40	17	800	40	113	1	15	3	3.2	24.5
35	40	20	800	40	113	-1	20	1	1.7	16.4
35	40	23	800	40	114	0	11	3	1.3	24.2
35	40	28	800	40	113	1	17	1	0.9	12.6
40	40	14	1000	40	111	2	19	5	6.5	21.1
40	40	17	1000	40	110	1	14	5	5.2	26.8
40	40	20	1000	40	111	0	21	1	4.3	16.8
40	40	24	1000	40	110	0	17	1	2.9	15.5
40	40	28	1000	40	109	2	19	1	2.7	12.0
50	40	16	1200	40	107	3	21	2	8.7	20.4
50	40	19	1200	40	109	2	17	5	6.9	20.7
50	40	22	1200	40	107	1	16	5	5.5	18.5

SOI (bTDC)	PR (%)	Total Fuel mass (mg/cycle)	Engine Speed (rpm)	Intake air temperature (Deg c)	Intake air Pressure (kPa)	CA_Start of Main HR (aTDC)	CA_End of Main HR (aTDC)	Heat release type	Fraction of early (%)	Fraction of Late (%)
50	40	26	1200	40	108	2	17	1	4.6	15.2
50	40	31	1200	40	107	6	22	1	3.7	10.6
60	40	16.3	1400	40	113	3	26	2	9.3	14.9
60	40	19	1400	40	114	3	18	2	7.9	18.7
60	40	22	1400	40	115	2	13	5	6.7	18.0
60	40	19	1600	40	113	7	26	2	8.6	19.4
60	40	22	1600	40	113	7	28	2	7.1	16.6
60	40	25	1600	40	113	6	14	5	5.5	52.2
40	60	19.5	800	40	113	3	14	3	3.5	32.6
40	60	22	800	40	114	2	11	3	3.0	33.7
40	60	29	800	40	112	6	19	1	2.4	10.7
45	60	19	1000	39	109	2	12	5	5.4	30.8
45	60	22	1000	40	108	3	18	1	4.7	15.8
45	60	25	1000	40	108	3	17	1	4.3	13.2
45	60	28	1000	40	108	4	17	1	3.8	11.2
45	60	33	1000	40	109	10	30	1	3.0	6.5
20	20	9	800	59	112	-2	15	4	2.8	19.0
20	20	10.1	800	60	112	-1	14	4	2.8	19.7
20	20	13	800	60	112	-2	14	3	1.3	27.9
20	20	18.5	800	60	112	2	14	3	1.5	26.2
20	20	22	800	60	112	-3	14	3	0.0	24.9
20	20	27	800	60	112	-2	17	4	-0.4	19.3
25	20	9	1000	60	110	1	13	2	7.1	22.9
25	20	10	1000	59	110	1	14	5	6.1	21.8

SOI (bTDC)	PR (%)	Total Fuel mass (mg/cycle)	Engine Speed (rpm)	Intake air temperature (Deg c)	Intake air Pressure (kPa)	CA_Start of Main HR (aTDC)	CA_End of Main HR (aTDC)	Heat release type	Fraction of early (%)	Fraction of Late (%)
25	20	13	1000	60	110	0	16	3	3.3	27.5
25	20	18	1000	60	110	0	17	3	2.0	24.8
25	20	22	1000	60	110	2	15	3	1.8	25.4
25	20	27	1000	60	110	-2	19	4	0.2	19.2
35	20	10	1200	59	109	1	14	2	10.1	22.1
35	20	13	1200	60	108	1	15	5	6.6	29.2
35	20	17	1200	60	108	-1	14	3	3.9	28.7
35	20	22	1200	60	108	0	15	3	2.8	25.2
35	20	27	1200	60	108	0	16	4	1.9	21.2
45	20	11	1400	59	115	1	15	2	9.5	23.0
45	20	12	1400	60	115	0	13	2	8.1	31.0
45	20	14	1400	60	114	0	12	5	7.0	29.7
45	20	18	1400	60	114	-1	11	3	4.2	32.1
45	20	22	1400	60	114	-1	13	3	3.0	27.6
45	20	27	1400	60	115	-1	12	3	2.0	25.4
50	20	12	1600	60	111	3	17	2	9.9	32.2
50	20	14	1600	60	112	2	14	2	7.7	32.6
50	20	18	1600	60	113	1	16	3	4.9	29.4
50	20	22	1600	60	112	2	15	3	3.9	29.2
50	20	28	1600	60	112	3	18	4	2.8	21.5
60	20	12.5	1800	59	114	0	11	2	11.1	34.7
60	20	14	1800	59	114	0	10	2	9.9	32.4
60	20	18	1800	60	114	-1	9	2	7.2	32.5
60	20	21	1800	58	117	0	11	5	5.3	30.5
60	20	27	1800	59	116	2	13	3	3.6	26.9
70	20	15.5	2000	56	102	1	13	2	14.7	22.8
70	20	18.5	2000	51	102	0	11	2	11.9	20.9
25	40	12.5	800	58	112	-2	15	3	1.2	25.1

SOI (bTDC)	PR (%)	Total Fuel mass (mg/cycle)	Engine Speed (rpm)	Intake air temperature (Deg c)	Intake air Pressure (kPa)	CA_Start of Main HR (aTDC)	CA_End of Main HR (aTDC)	Heat release type	Fraction of early (%)	Fraction of Late (%)
25	40	14	800	59	113	-2	14	3	0.5	25.8
25	40	18	800	60	113	-1	12	3	0.7	31.6
25	40	23	800	60	114	0	15	3	0.0	27.8
25	40	28	800	60	113	2	15	3	0.2	23.0
30	40	13	1000	59	110	1	15	3	4.4	25.7
30	40	15	1000	60	110	0	16	3	3.1	25.5
30	40	18.5	1000	60	110	0	14	3	2.5	29.5
30	40	23	1000	60	110	-1	12	3	1.2	29.6
30	40	28	1000	60	110	1	13	3	1.2	24.7
40	40	16	1200	60	108	1	13	5	5.6	32.7
40	40	19	1200	60	109	0	13	3	3.9	32.4
40	40	23.5	1200	60	108	1	14	3	3.0	28.2
40	40	27.5	1200	60	108	3	19	4	2.7	18.7
47	40	16.5	1400	59	115	1	12	5	5.2	36.7
47	40	19.5	1400	60	114	1	11	3	4.9	36.3
47	40	24	1400	61	114	1	17	3	3.2	25.2
47	40	29	1400	60	115	3	18	4	2.3	21.5
60	40	16	1600	59	115	2	14	2	7.7	29.7
60	40	19	1600	60	114	1	13	5	5.9	26.9
60	40	21	1600	60	112	2	11	5	6.5	29.7
65	40	17	1800	59	115	2	13	2	8.7	29.3
65	40	20	1800	59	114	1	13	5	6.9	24.9
30	60	19.5	800	59	114	0	14	3	1.1	37.0
30	60	21	800	60	114	0	13	3	1.3	36.5
30	60	24	800	60	115	1	13	3	0.5	33.3

SOI (bTDC)	PR (%)	Total Fuel mass (mg/cycle)	Engine Speed (rpm)	Intake air temperature (Deg c)	Intake air Pressure (kPa)	CA_Start of Main HR (aTDC)	CA_End of Main HR (aTDC)	Heat release type	Fraction of early (%)	Fraction of Late (%)
30	60	24	800	60	115	1	13	3	0.5	33.3
30	60	29	800	60	112	3	17	1	0.5	13.3
35	60	19.8	1000	59	110	0	13	3	3.1	35.8
35	60	22	1000	60	109	0	12	3	2.7	35.8
35	60	25	1000	60	110	1	12	3	2.1	30.4
35	60	29	1000	60	110	3	20	1	1.6	11.4
50	60	20.5	1200	60	107	3	18	5	5.5	24.5
50	60	23	1200	60	106	3	20	4	4.9	17.3
50	60	27	1200	60	107	5	23	1	4.2	12.4
50	60	31	1200	60	107	8	28	1	3.7	8.2
55	60	21.5	1400	59	113	6	22	5	5.5	29.7
55	60	24	1400	60	113	5	23	4	4.8	19.2
55	60	28	1400	60	113	7	30	1	4.1	12.5
55	60	33	1400	61	113	13	40	1	4.3	7.4
23	20	9.2	800	80	114	-1	12	4	0.2	21.1
23	20	10.2	800	80	113	-3	12	4	-0.2	18.6
23	20	12.7	800	80	114	-3	7	3	-0.5	31.0
23	20	18	800	80	112	-5	7	3	-1.2	27.0
23	20	22	800	80	112	-2	8	4	-0.3	21.9
23	20	26.5	800	80	111	-2	6	4	-0.8	22.9
25	20	10	1000	80	114	-1	12	3	1.4	25.0
25	20	12.5	1000	80	112	-2	12	3	-0.1	33.5
25	20	18	1000	80	113	-1	13	3	-0.5	29.4
25	20	22	1000	80	113	1	15	3	-0.4	25.4
25	20	26	1000	80	113	-4	16	4	-1.5	22.4
30	20	9.5	1200	80	110	-2	12	3	3.7	27.5
30	20	12	1200	80	110	-1	13	3	2.1	32.6
30	20	18	1200	80	109	-1	14	3	0.4	30.2

SOI (bTDC)	PR (%)	Total Fuel mass (mg/cycle)	Engine Speed (rpm)	Intake air temperature (Deg c)	Intake air Pressure (kPa)	CA_Start of Main HR (aTDC)	CA_End of Main HR (aTDC)	Heat release type	Fraction of early (%)	Fraction of Late (%)
30	20	22	1200	80	110	0	15	3	0.1	26.9
30	20	26	1200	80	109	2	18	4	0.3	22.8
37	20	10	1400	79	116	-2	10	3	3.9	29.2
37	20	13	1400	80	116	-2	10	3	1.5	36.7
37	20	18	1400	80	115	-1	12	3	0.8	33.2
37	20	22	1400	80	115	-2	15	3	0.0	28.0
37	20	25.5	1400	80	115	-1	17	3	0.0	24.4
42	20	11	1600	80	114	-1	12	3	4.1	30.1
42	20	13	1600	80	114	0	13	3	2.7	34.4
42	20	18	1600	80	113	0	16	3	1.3	29.7
42	20	22	1600	80	113	1	16	3	0.9	28.0
42	20	25.5	1600	80	111	2	19	3	0.9	24.1
53	20	12	1800	80	118	-1	13	3	4.0	34.1
53	20	13	1800	80	117	0	13	3	3.7	34.7
53	20	18	1800	80	117	-1	13	3	1.8	32.6
53	20	22	1800	80	118	0	16	3	1.1	27.6
53	20	26	1800	80	118	0	17	3	0.5	23.9
57	20	12	2000	80	108	0	11	2	8.9	33.3
57	20	13	2000	80	108	0	15	2	8.0	30.2
57	20	18	2000	80	109	0	13	3	4.9	31.3
57	20	22	2000	80	108	-1	15	3	3.1	27.7
57	20	26	2000	80	109	3	18	4	3.1	22.7
65	20	12	2200	79	100	2	16	2	12.6	26.9
65	20	13	2200	80	100	1	14	2	10.8	31.2
65	20	17	2200	79	102	1	11	2	8.0	34.3

SOI (bTDC)	PR (%)	Total Fuel mass (mg/cycle)	Engine Speed (rpm)	Intake air temperature (Deg c)	Intake air Pressure (kPa)	CA_Start of Main HR (aTDC)	CA_End of Main HR (aTDC)	Heat release type	Fraction of early (%)	Fraction of Late (%)
16	40	10.2	800	80	112	-2	13	3	-1.7	30.1
16	40	14	800	80	112	-1	13	3	-1.3	28.0
16	40	18	800	80	113	-3	14	3	-2.0	30.5
16	40	22	800	80	99	0	12	3	1.1	30.2
16	40	27	800	80	113	2	14	3	-1.4	24.4
25	40	11.5	1000	80	113	0	13	3	0.6	31.8
25	40	18	1000	80	113	1	14	3	-0.2	33.4
25	40	22	1000	80	112	0	15	3	-0.8	30.8
25	40	26.5	1000	80	106	2	16	3	0.3	26.3
20	20	10.3	1000	100	113	-2	13	3	2.5	24.9
20	20	13	1000	100	112	-2	16	3	0.7	28.6
20	20	18	1000	100	112	0	17	3	0.1	26.0
20	20	22	1000	100	112	4	19	4	0.1	22.8
20	20	26	1000	100	114	5	22	4	-0.2	19.3
28	20	10.7	1200	99	108	-3	13	3	4.7	23.9
28	20	12.7	1200	100	109	-1	14	3	3.6	30.1
28	20	18	1200	100	107	0	15	3	2.3	27.2
28	20	22	1200	100	108	1	23	4	1.6	19.5
28	20	26	1200	99	109	2	19	4	0.9	21.4
33	20	13	1400	100	115	-1	14	3	2.9	30.5
33	20	18	1400	100	116	0	14	3	1.5	30.4
33	20	22	1400	100	115	1	16	3	1.4	27.0
40	20	22	1600	100	112	0	16	3	1.6	27.4
40	20	26	1600	100	81	2	17	5	7.0	22.3
47	20	12	1800	99	115	-2	10	5	5.7	34.7
47	20	18	1800	100	116	0	12	3	2.7	33.8
47	20	22	1800	99	116	0	16	3	1.7	27.2
47	20	26	1800	100	116	1	15	3	1.3	26.8

SOI (bTDC)	PR (%)	Total Fuel mass (mg/cycle)	Engine Speed (rpm)	Intake air temperature (Deg c)	Intake air Pressure (kPa)	CA_Start of Main HR (aTDC)	CA_End of Main HR (aTDC)	Heat release type	Fraction of early (%)	Fraction of Late (%)
53	20	13.5	2000	98	109	-1	14	2	8.2	26.1
53	20	18	2000	99	109	0	12	5	6.0	31.6
53	20	22	2000	98	109	0	14	3	4.2	27.9
53	20	26	2000	99	109	-1	16	3	2.7	24.4
17	40	11	800	100	110	-2	12	3	0.5	28.7
17	40	13.5	800	100	111	-1	11	3	0.0	29.7
17	40	18	800	100	112	-1	11	3	-0.4	34.8
17	40	22	800	100	110	-2	11	3	-0.6	28.3
17	40	26	800	100	110	1	12	3	-0.4	26.9
24	40	11.2	1000	99	111	0	14	3	2.7	29.7
24	40	13.6	1000	99	112	1	14	3	1.7	30.6
24	40	18	1000	100	112	0	14	3	0.2	33.3
24	40	26	1000	100	112	2	18	3	0.2	24.6
32	40	11.7	1200	99	107	0	14	5	5.9	29.5
32	40	13.8	1200	100	107	0	14	3	4.8	29.3
32	40	18	1200	100	107	-1	13	3	2.7	34.1
32	40	22	1200	100	107	0	14	3	2.0	32.0
32	40	26	1200	100	108	0	15	3	1.4	27.9
39	40	12	1400	99	114	0	14	5	5.6	30.0
39	40	14	1400	100	115	0	12	3	4.7	31.9
39	40	18	1400	100	114	-1	13	3	2.4	33.7
39	40	22	1400	100	115	-1	14	3	1.7	31.9
39	40	26	1400	100	115	0	13	3	1.1	30.7
49	40	12.7	1600	99	112	0	12	5	6.5	33.1
49	40	14	1600	100	111	0	15	5	5.7	29.5

SOI (bTDC)	PR (%)	Total Fuel mass (mg/cycle)	Engine Speed (rpm)	Intake air temperature (Deg c)	Intake air Pressure (kPa)	CA_Start of Main HR (aTDC)	CA_End of Main HR (aTDC)	Heat release type	Fraction of early (%)	Fraction of Late (%)
49	40	18	1600	100	113	0	13	3	4.1	33.1
49	40	22	1600	100	110	2	14	3	3.6	32.3
49	40	26	1600	100	110	3	18	3	2.5	25.8
58	40	14	1800	99	115	0	12	5	5.7	35.5
58	40	18	1800	100	115	0	13	3	4.3	32.0
58	40	22	1800	100	114	0	11	3	3.1	32.8
58	40	24	1800	101	115	1	11	3	3.2	31.4
65	40	16	2000	98	109	0	14	2	7.7	30.8
65	40	18	2000	99	108	0	11	2	7.2	32.4
15	60	17	800	102	111	-2	12	3	-0.4	42.1
15	60	17.7	800	99	111	-4	12	3	-0.5	42.9
15	60	20	800	99	112	-4	11	3	-0.3	43.3
15	60	24	800	100	110	-3	11	3	-0.8	39.3
29	60	18	1000	99	111	-2	10	3	1.9	42.4
29	60	20.5	1000	99	112	-2	10	3	1.5	41.7
29	60	24	1000	100	112	-1	11	3	0.9	37.0
29	60	27.5	1000	100	111	-1	12	3	0.4	28.3
40	60	19	1200	99	108	-2	11	3	3.7	38.4
40	60	21	1200	100	108	-2	10	3	3.0	38.5
40	60	24	1200	100	108	-1	11	3	2.6	35.1
40	60	27.4	1200	100	109	1	12	3	2.2	27.7
52	60	19.8	1400	99	115	-2	12	3	3.2	31.5
52	60	21.5	1400	100	114	-2	11	3	3.2	29.2
52	60	24.5	1400	100	114	-1	10	3	2.6	30.1
52	60	28	1400	99	115	0	14	1	2.3	16.1
58	60	21	1600	99	110	3	19	3	4.3	32.2
58	60	24.5	1600	100	110	4	21	3	3.8	25.3
58	60	30	1600	100	109	8	25	1	3.6	13.9

SOI (bTDC)	PR (%)	Total Fuel mass (mg/cycle)	Engine Speed (rpm)	Intake air temperature (Deg c)	Intake air Pressure (kPa)	CA_Start of Main HR (aTDC)	CA_End of Main HR (aTDC)	Heat release type	Fraction of early (%)	Fraction of Late (%)
70	60	21	1800	100	114	5	21	3	3.8	28.4
70	60	24	1800	100	116	6	27	1	3.0	15.5
70	60	28	1800	100	114	7	24	1	3.2	15.0
80	60	23	2000	99	109	6	30	5	5.3	13.5
80	60	27	2000	99	109	6	26	1	5.0	11.1
35	40	11.7	1200	79	109	0	14	5	6.1	28.7
35	40	13.5	1200	80	109	0	14	5	5.0	28.5
35	40	18	1200	80	109	-1	14	3	2.6	32.0
35	40	22	1200	80	109	-1	15	3	1.8	29.0
35	40	26.5	1200	80	109	1	16	3	1.5	24.0
40	40	12	1400	79	114	1	15	5	6.1	29.3
40	40	14.3	1400	80	116	1	14	3	4.2	30.1
40	40	18	1400	80	116	0	13	3	2.7	34.6
40	40	22	1400	80	117	0	14	3	1.6	32.2
40	40	26	1400	80	116	1	15	3	1.5	28.5
52	40	13	1600	80	113	0	15	5	6.2	30.4
52	40	14.8	1600	80	114	1	14	5	5.4	33.0
52	40	18	1600	80	112	0	11	3	4.9	37.4
52	40	22	1600	80	111	2	14	3	4.2	30.8
52	40	26	1600	80	111	4	15	3	3.5	30.2
60	40	13.5	1800	80	115	0	15	2	7.4	29.4
60	40	15	1800	79	116	1	14	5	6.7	32.6
60	40	20	1800	80	116	0	12	3	4.2	31.1
60	40	22	1800	80	116	0	11	3	3.9	30.3
70	40	16	2000	80	107	2	17	2	9.6	24.2

SOI (bTDC)	PR (%)	Total Fuel mass (mg/cycle)	Engine Speed (rpm)	Intake air temperature (Deg c)	Intake air Pressure (kPa)	CA_Start of Main HR (aTDC)	CA_End of Main HR (aTDC)	Heat release type	Fraction of early (%)	Fraction of Late (%)
70	40	17	2000	80	105	1	14	2	9.4	24.0
16	60	17.5	800	80	112	-2	13	3	-0.1	38.4
16	60	20	800	80	110	-3	10	3	0.4	43.6
16	60	24	800	80	109	-2	11	3	-0.1	36.0
16	60	28	800	80	110	0	13	3	-0.4	26.2
29	60	18.5	1000	80	111	-1	12	3	1.8	40.5
29	60	20	1000	80	101	-1	11	3	4.1	40.6
29	60	24	1000	80	96	-1	12	3	4.0	35.1
29	60	28	1000	80	96	1	14	4	3.2	22.9
42	60	19.2	1200	80	99	-1	11	5	6.2	38.0
42	60	20.5	1200	80	97	-1	10	5	6.0	38.5
42	60	24.5	1200	80	108	0	11	3	2.7	31.7
42	60	28.5	1200	80	108	2	15	4	2.1	18.5
52	60	20	1400	80	84	0	14	2	11.3	27.9
52	60	25	1400	81	115	0	11	3	2.9	27.3
52	60	28.5	1400	80	115	2	17	1	2.8	14.1
60	60	20.5	1600	80	114	2	15	3	4.2	26.7
60	60	23	1600	80	113	2	16	4	3.9	21.1
60	60	26	1600	80	113	3	17	4	3.6	17.1
60	60	31	1600	80	114	5	17	1	3.2	12.6
70	60	22	1800	79	113	5	21	4	4.6	22.8
70	60	24	1800	80	114	4	19	4	3.9	20.9
70	60	28	1800	80	115	5	19	4	3.6	18.0
70	60	31	1800	80	116	7	20	1	3.7	13.7
15	20	10	800	100	112	-2	12	4	0.7	22.2
15	20	13	800	100	112	-4	12	3	0.0	27.8
15	20	18	800	100	111	1	11	3	0.2	27.0
15	20	22	800	101	112	1	14	4	-0.7	22.8

SOI (bTDC)	PR (%)	Total Fuel mass (mg/cycle)	Engine Speed (rpm)	Intake air temperature (Deg c)	Intake air Pressure (kPa)	CA_Start of Main HR (aTDC)	CA_End of Main HR (aTDC)	Heat release type	Fraction of early (%)	Fraction of Late (%)
15	20	26	800	101	112	-2	15	4	-1.1	20.5
30	20	10	800	40	95	-1	11	1	-0.1	16.1
30	20	14	800	40	95	-2	9	3	-0.8	24.7
30	20	17	800	40	95	-4	10	4	-1.0	22.1
30	20	21	800	40	96	-2	8	4	-0.1	20.4
30	20	28	800	40	96	-2	8	1	-1.1	16.2
40	20	12	1000	40	94	-2	11	3	0.6	23.7
25	20	9	800	40	94	1	15	1	-1.7	16.5
25	20	11	800	42	95	1	13	4	-1.0	19.4
25	20	19	800	40	95	1	12	4	-0.3	20.8
25	20	27	800	40	95	2	12	1	-0.5	16.9
35	20	10	1000	39	94	3	20	1	0.6	15.3
35	20	14	1000	39	95	1	14	4	1.0	22.5
35	20	19	1000	40	95	0	14	4	-0.1	21.3
35	20	28	1000	40	95	1	15	1	-0.6	15.1
50	20	12	1200	40	94	3	14	5	5.2	25.3
50	20	15	1200	40	93	2	10	3	3.8	34.5
50	20	19	1200	40	94	0	12	4	1.9	21.4
50	20	28	1200	40	94	1	14	1	0.8	14.0
60	20	12.5	1400	39	93	4	17	2	8.3	21.7
60	20	14.8	1400	40	93	2	15	5	6.1	19.2
60	20	16.5	1400	40	93	1	12	5	5.3	18.9
60	20	18.5	1400	40	94	0	11	4	4.3	17.1
35	40	14	800	41	95	2	14	4	1.1	22.9
35	40	17	800	40	95	1	12	3	0.6	26.2

SOI (bTDC)	PR (%)	Total Fuel mass (mg/cycle)	Engine Speed (rpm)	Intake air temperature (Deg c)	Intake air Pressure (kPa)	CA_Start of Main HR (aTDC)	CA_End of Main HR (aTDC)	Heat release type	Fraction of early (%)	Fraction of Late (%)
35	40	20	800	40	95	0	9	3	1.0	26.7
35	40	23	800	40	95	2	10	3	1.1	23.1
35	40	28	800	40	95	2	15	1	0.3	11.6
40	40	14	1000	40	94	2	16	4	2.3	22.4
40	40	17	1000	40	94	1	12	3	1.2	26.8
40	40	20	1000	40	94	-1	10	3	0.9	25.9
40	40	24	1000	40	95	2	10	4	2.0	21.5
40	40	28	1000	40	95	2	12	1	0.9	16.4
50	40	16	1200	40	93	3	17	3	3.6	23.3
50	40	19	1200	40	94	2	14	4	2.6	21.7
50	40	22	1200	40	94	2	13	4	2.8	18.3
50	40	26	1200	40	94	2	15	1	1.8	14.2
50	40	31	1200	40	93	6	21	1	1.7	9.2
60	40	16.3	1400	40	93	4	19	4	4.9	19.3
60	40	19	1400	40	93	4	18	1	4.4	17.0
60	40	22	1400	40	92	2	13	1	3.8	15.5
60	40	19	1600	40	92	7	21	4	4.4	22.1
60	40	22	1600	40	93	7	23	4	3.9	17.7
60	40	25	1600	40	92	5	14	3	2.6	44.5
40	60	19.5	800	40	94	3	14	3	1.8	29.5
40	60	22	800	40	95	2	12	3	1.8	26.6
40	60	29	800	40	95	7	18	1	2.2	8.5
45	60	19	1000	39	94	3	13	3	3.3	23.2
45	60	22	1000	40	94	3	15	1	1.9	16.7
45	60	25	1000	40	94	3	17	1	1.7	12.1
45	60	28	1000	40	94	3	16	1	1.6	9.6
45	60	33	1000	40	93	10	28	1	1.7	5.5
20	20	9	800	59	95	-2	14	4	-3.7	19.9

SOI (bTDC)	PR (%)	Total Fuel mass (mg/cycle)	Engine Speed (rpm)	Intake air temperature (Deg c)	Intake air Pressure (kPa)	CA_Start of Main HR (aTDC)	CA_End of Main HR (aTDC)	Heat release type	Fraction of early (%)	Fraction of Late (%)
20	20	10.1	800	60	94	-1	14	4	-2.4	19.2
20	20	13	800	60	95	-2	14	3	-2.4	26.2
20	20	18.5	800	60	95	0	14	3	-1.1	23.8
20	20	22	800	60	95	3	14	4	0.1	22.1
20	20	27	800	60	95	2	17	4	-1.3	17.4
25	20	9	1000	60	94	1	14	4	-2.0	22.3
25	20	10	1000	59	94	1	14	4	-1.7	21.8
25	20	13	1000	60	94	0	16	3	-1.0	25.4
25	20	18	1000	60	94	1	15	3	-1.0	24.8
25	20	22	1000	60	94	2	15	4	-0.2	22.6
25	20	27	1000	60	94	2	17	4	-1.1	19.3
35	20	10	1200	59	93	1	14	4	0.7	21.4
35	20	13	1200	60	93	1	15	3	1.1	26.1
35	20	17	1200	60	94	0	13	3	-0.2	27.3
35	20	22	1200	60	93	0	13	3	0.0	24.1
35	20	27	1200	60	93	2	16	4	-0.2	19.4
45	20	11	1400	59	93	1	14	4	2.6	21.9
45	20	12	1400	60	93	0	13	3	2.2	27.2
45	20	14	1400	60	93	0	12	3	1.7	26.2
45	20	18	1400	60	93	-1	11	3	1.2	27.5
45	20	22	1400	60	93	0	13	3	0.7	24.0
45	20	27	1400	60	94	-1	13	4	-0.2	20.8
50	20	12	1600	60	93	3	17	3	3.8	27.5
50	20	14	1600	60	93	3	14	3	3.5	27.1
50	20	18	1600	60	93	2	16	3	2.0	25.0

SOI (bTDC)	PR (%)	Total Fuel mass (mg/cycle)	Engine Speed (rpm)	Intake air temperature (Deg c)	Intake air Pressure (kPa)	CA_Start of Main HR (aTDC)	CA_End of Main HR (aTDC)	Heat release type	Fraction of early (%)	Fraction of Late (%)
50	20	22	1600	60	93	2	15	3	1.3	24.4
50	20	28	1600	60	93	3	18	4	0.9	18.1
60	20	12.5	1800	59	93	1	11	5	5.2	30.6
60	20	14	1800	59	93	1	10	3	4.9	27.9
60	20	18	1800	60	93	-1	9	3	2.5	29.1
60	20	21	1800	58	93	0	10	3	2.5	27.3
60	20	27	1800	59	93	2	13	3	1.2	23.7
70	20	15.5	2000	56	94	1	11	5	5.6	23.5
70	20	18.5	2000	51	93	0	10	4	3.9	20.3
25	40	12.5	800	58	95	0	15	3	-1.3	23.2
25	40	14	800	59	94	0	14	3	-1.6	24.3
25	40	18	800	60	95	-1	12	3	-0.8	29.0
25	40	23	800	60	95	0	15	3	-0.5	24.1
25	40	28	800	60	95	2	15	4	-0.5	20.3
30	40	13	1000	59	94	1	16	4	0.1	23.0
30	40	15	1000	60	94	1	14	3	0.4	24.3
30	40	18.5	1000	60	94	1	13	3	0.1	27.6
30	40	23	1000	60	94	-1	13	3	-0.4	25.0
30	40	28	1000	60	94	0	14	4	-0.3	18.5
40	40	16	1200	60	93	2	13	3	2.4	28.5
40	40	19	1200	60	93	0	12	3	1.1	29.3
40	40	23.5	1200	60	94	2	15	4	1.1	22.3
40	40	27.5	1200	60	93	3	17	4	0.9	17.4
47	40	16.5	1400	59	93	1	12	3	2.3	31.4
47	40	19.5	1400	60	93	1	11	3	1.5	31.6
47	40	24	1400	61	94	3	13	3	2.2	25.9
47	40	29	1400	60	94	3	18	4	1.1	17.2
60	40	16	1600	59	93	2	12	3	4.2	28.4

SOI (bTDC)	PR (%)	Total Fuel mass (mg/cycle)	Engine Speed (rpm)	Intake air temperature (Deg c)	Intake air Pressure (kPa)	CA_Start of Main HR (aTDC)	CA_End of Main HR (aTDC)	Heat release type	Fraction of early (%)	Fraction of Late (%)
60	40	19	1600	60	93	1	13	4	3.3	21.5
60	40	21	1600	60	93	2	11	3	3.7	25.0
65	40	17	1800	59	93	1	11	3	3.8	30.3
65	40	20	1800	59	92	1	13	4	3.1	21.8
30	60	19.5	800	59	95	0	14	3	0.5	32.9
30	60	21	800	60	96	0	13	3	1.1	31.6
30	60	24	800	60	95	1	13	3	0.6	27.6
30	60	29	800	60	95	3	15	1	0.3	16.1
35	60	19.8	1000	59	94	0	13	3	0.8	31.4
35	60	22	1000	60	94	0	12	3	1.1	30.5
35	60	25	1000	60	94	1	12	3	1.4	26.2
35	60	29	1000	60	94	3	15	1	0.8	15.8
50	60	20.5	1200	60	94	3	16	3	2.8	25.1
50	60	23	1200	60	94	3	16	4	2.3	20.3
50	60	27	1200	60	93	5	18	1	2.0	13.2
50	60	31	1200	60	94	8	22	1	2.2	8.8
55	60	21.5	1400	59	93	6	22	3	2.7	25.1
55	60	24	1400	60	93	5	21	4	2.4	18.7
55	60	28	1400	60	93	7	23	1	2.7	15.5
55	60	33	1400	61	93	13	34	1	3.3	9.2
23	20	9.2	800	80	97	-1	12	1	-2.0	16.0
23	20	10.2	800	80	96	-3	12	1	-2.6	14.5
23	20	12.7	800	80	96	-3	7	3	-1.7	26.2
23	20	18	800	80	96	-3	7	4	-1.0	22.3
23	20	22	800	80	96	-4	7	4	-1.8	19.3

SOI (bTDC)	PR (%)	Total Fuel mass (mg/cycle)	Engine Speed (rpm)	Intake air temperature (Deg c)	Intake air Pressure (kPa)	CA_Start of Main HR (aTDC)	CA_End of Main HR (aTDC)	Heat release type	Fraction of early (%)	Fraction of Late (%)
23	20	26.5	800	80	95	-4	6	4	-1.9	18.7
25	20	10	1000	80	96	-1	12	4	-1.8	20.8
25	20	12.5	1000	80	96	-2	12	3	-1.9	28.6
25	20	18	1000	80	96	-1	13	3	-1.4	25.3
25	20	22	1000	80	96	1	15	4	-0.9	21.6
25	20	26	1000	80	95	0	16	4	-1.5	19.0
30	20	9.5	1200	80	96	-2	12	3	-1.4	23.5
30	20	12	1200	80	96	-1	13	3	-0.8	28.0
30	20	18	1200	80	95	-1	14	3	-1.2	26.2
30	20	22	1200	80	96	0	16	4	-1.0	22.9
30	20	26	1200	80	96	2	18	4	-0.6	19.7
37	20	10	1400	79	95	-2	10	3	0.3	25.4
37	20	13	1400	80	94	-2	10	3	-0.3	31.9
37	20	18	1400	80	95	-1	16	3	-0.5	25.7
37	20	22	1400	80	94	0	14	3	-0.2	25.3
37	20	25.5	1400	80	94	0	14	3	-0.2	23.4
42	20	11	1600	80	95	-1	11	3	0.4	27.2
42	20	13	1600	80	95	0	13	3	0.5	29.8
42	20	18	1600	80	94	0	13	3	0.2	28.5
42	20	22	1600	80	95	1	16	3	0.1	24.6
42	20	25.5	1600	80	95	2	16	3	0.0	23.4
53	20	12	1800	80	94	-1	10	3	2.5	32.6
53	20	13	1800	80	94	-1	11	3	2.6	30.5
53	20	18	1800	80	95	-1	11	3	0.9	30.2
53	20	22	1800	80	94	0	13	3	0.6	26.0
53	20	26	1800	80	94	0	14	4	0.2	22.6
57	20	12	2000	80	95	0	11	3	2.7	31.6
57	20	13	2000	80	95	0	11	3	2.9	32.3

SOI (bTDC)	PR (%)	Total Fuel mass (mg/cycle)	Engine Speed (rpm)	Intake air temperature (Deg c)	Intake air Pressure (kPa)	CA_Start of Main HR (aTDC)	CA_End of Main HR (aTDC)	Heat release type	Fraction of early (%)	Fraction of Late (%)
57	20	18	2000	80	95	0	11	3	1.4	30.7
57	20	22	2000	80	95	1	15	3	0.4	25.2
57	20	26	2000	80	95	1	17	4	0.0	21.6
65	20	12	2200	79	95	2	16	3	4.0	25.1
65	20	13	2200	80	95	1	14	3	3.6	28.1
65	20	17	2200	79	95	1	11	3	2.4	32.7
16	40	9.5	800	79	59	-1	13	3	-4.0	35.6
16	40	10.2	800	80	96	-2	13	3	-3.4	25.0
16	40	14	800	80	95	-1	12	3	-2.0	24.3
16	40	18	800	80	96	1	12	3	-1.2	27.4
16	40	22	800	80	82	0	12	3	-1.6	28.3
16	40	27	800	80	96	2	14	4	-0.9	19.5
25	40	11.5	1000	80	96	0	13	3	-1.1	26.6
25	40	13.5	1000	80	96	0	16	3	-1.3	24.2
25	40	18	1000	80	95	0	15	3	-0.9	27.6
25	40	22	1000	80	95	0	15	3	-0.9	26.3
25	40	26.5	1000	80	90	2	16	4	-0.6	22.5
35	40	11.7	1200	79	94	0	14	3	0.2	26.1
35	40	13.5	1200	80	95	0	14	3	0.7	25.3
35	40	18	1200	80	98	0	13	3	0.7	28.7
35	40	22	1200	80	95	-1	15	3	0.2	24.6
35	40	26.5	1200	80	95	1	16	4	0.1	19.9
40	40	12	1400	79	94	1	15	3	1.5	26.3
40	40	14.3	1400	80	94	1	13	3	1.4	27.8
40	40	18	1400	80	95	0	13	3	0.6	31.0

SOI (bTDC)	PR (%)	Total Fuel mass (mg/cycle)	Engine Speed (rpm)	Intake air temperature (Deg c)	Intake air Pressure (kPa)	CA_Start of Main HR (aTDC)	CA_End of Main HR (aTDC)	Heat release type	Fraction of early (%)	Fraction of Late (%)
40	40	22	1400	80	94	0	13	3	0.5	29.4
40	40	26	1400	80	95	1	15	3	0.6	24.4
52	40	13	1600	80	94	0	15	3	2.2	26.6
52	40	14.8	1600	80	94	1	13	3	2.2	30.6
52	40	18	1600	80	95	0	11	3	2.4	32.7
52	40	22	1600	80	94	2	15	3	2.3	25.5
52	40	26	1600	80	95	4	17	4	1.9	22.7
60	40	13.5	1800	80	94	0	13	3	4.0	29.5
60	40	15	1800	79	94	1	16	3	3.6	25.2
60	40	20	1800	80	93	0	13	3	2.3	25.9
60	40	22	1800	80	94	0	11	3	2.5	27.7
70	40	16	2000	80	94	2	17	4	3.6	22.5
70	40	17	2000	80	94	1	14	4	3.7	21.6
16	60	17.5	800	80	95	-4	14	3	-1.7	32.3
16	60	20	800	80	93	-3	12	3	-1.4	35.9
16	60	24	800	80	91	-2	11	3	-1.0	34.4
16	60	28	800	80	95	-2	13	4	-1.2	21.0
29	60	18.5	1000	80	95	-1	12	3	-0.2	36.1
29	60	20	1000	80	82	-1	11	3	-0.4	38.2
29	60	24	1000	80	80	0	12	3	-0.2	34.1
29	60	28	1000	80	80	1	14	3	-0.3	23.8
42	60	19.2	1200	80	84	-1	11	3	1.3	36.3
42	60	20.5	1200	80	84	-1	11	3	1.1	34.1
42	60	24.5	1200	80	94	2	14	4	2.5	18.8
42	60	28.5	1200	80	94	2	16	1	1.4	12.2
52	60	20	1400	80	48	0	14	3	0.6	33.3
52	60	22	1400	80	26	0	13	3	0.4	35.6
52	60	25	1400	81	94	0	12	4	2.0	20.2

SOI (bTDC)	PR (%)	Total Fuel mass (mg/cycle)	Engine Speed (rpm)	Intake air temperature (Deg c)	Intake air Pressure (kPa)	CA_Start of Main HR (aTDC)	CA_End of Main HR (aTDC)	Heat release type	Fraction of early (%)	Fraction of Late (%)
52	60	28.5	1400	80	93	2	14	1	2.2	13.9
60	60	20.5	1600	80	94	1	15	4	2.5	22.9
60	60	23	1600	80	94	2	16	1	2.9	16.6
60	60	26	1600	80	94	2	17	1	2.7	12.9
60	60	31	1600	80	94	5	17	1	2.8	9.0
70	60	22	1800	79	94	5	21	4	3.5	19.4
70	60	24	1800	80	93	4	19	4	3.1	17.3
70	60	28	1800	80	93	5	21	1	3.0	11.2
70	60	31	1800	80	94	7	21	1	3.6	8.1
15	20	10	800	100	96	-2	12	4	-3.9	20.4
15	20	13	800	100	95	-2	12	3	-2.6	24.2
15	20	18	800	100	99	0	11	3	-2.0	23.2
15	20	22	800	101	95	0	14	4	-1.6	18.8
15	20	26	800	101	95	1	15	1	-1.8	16.9
20	20	10.3	1000	100	96	-2	13	4	-2.4	22.2
20	20	13	1000	100	95	1	16	3	-1.6	25.5
20	20	18	1000	100	95	2	17	3	-1.6	23.7
20	20	22	1000	100	95	4	19	4	-1.3	20.6
20	20	26	1000	100	96	5	21	4	-1.2	17.6
28	20	10.7	1200	99	94	-3	12	3	-2.1	23.5
28	20	12.7	1200	100	94	-1	14	3	-1.3	27.3
28	20	18	1200	100	95	0	15	3	-1.4	24.8
28	20	22	1200	100	95	1	16	4	-0.6	22.6
28	20	26	1200	99	95	2	19	4	-0.8	19.0
33	20	11.2	1400	100	81	-2	10	3	-0.9	29.9

SOI (bTDC)	PR (%)	Total Fuel mass (mg/cycle)	Engine Speed (rpm)	Intake air temperature (Deg c)	Intake air Pressure (kPa)	CA_Start of Main HR (aTDC)	CA_End of Main HR (aTDC)	Heat release type	Fraction of early (%)	Fraction of Late (%)
33	20	13	1400	100	92	-1	14	3	-1.2	28.1
33	20	18	1400	100	93	0	14	3	-0.4	26.8
33	20	22	1400	100	93	1	16	3	-0.5	24.5
33	20	26	1400	100	7	3	16	3	0.2	31.8
40	20	26	1600	100	62	2	17	3	-0.7	24.3
47	20	12	1800	99	93	-2	10	3	1.1	31.8
47	20	18	1800	100	93	-1	12	3	0.3	29.9
47	20	22	1800	99	93	0	15	3	0.2	25.0
47	20	26	1800	100	94	1	14	3	0.3	24.2
53	20	13.5	2000	98	94	-1	14	3	1.2	25.1
53	20	18	2000	99	94	-1	11	3	1.2	29.8
53	20	22	2000	98	94	0	13	3	0.2	27.4
53	20	26	2000	99	94	0	16	4	-0.1	22.5
17	40	11	800	100	95	-4	12	3	-3.4	25.8
17	40	13.5	800	100	94	-4	11	3	-2.7	25.9
17	40	18	800	100	95	-1	9	3	-1.3	32.6
17	40	22	800	100	95	-3	11	3	-1.4	24.2
17	40	26	800	100	95	1	12	3	-1.0	23.0
24	40	11.2	1000	99	94	0	14	3	-1.0	25.8
24	40	26	1000	100	94	2	18	4	-0.7	21.3
32	40	11.7	1200	99	94	0	14	3	0.3	26.8
32	40	13.8	1200	100	93	0	14	3	0.8	26.0
32	40	18	1200	100	94	-1	13	3	-0.3	30.3
32	40	22	1200	100	94	0	14	3	0.0	28.0
32	40	26	1200	100	94	0	15	3	0.0	23.9
39	40	12	1400	99	93	0	14	3	0.7	27.5
39	40	14	1400	100	94	0	12	3	1.5	28.3
39	40	18	1400	100	93	-1	12	3	0.4	30.9

SOI (bTDC)	PR (%)	Total Fuel mass (mg/cycle)	Engine Speed (rpm)	Intake air temperature (Deg c)	Intake air Pressure (kPa)	CA_Start of Main HR (aTDC)	CA_End of Main HR (aTDC)	Heat release type	Fraction of early (%)	Fraction of Late (%)
39	40	22	1400	100	93	-1	14	3	0.4	27.5
39	40	26	1400	100	94	1	13	3	0.4	26.8
49	40	12.7	1600	99	94	0	14	3	2.6	26.6
49	40	14	1600	100	93	0	16	3	1.7	25.2
49	40	18	1600	100	94	0	13	3	1.9	29.3
49	40	22	1600	100	94	2	14	3	1.9	28.0
49	40	26	1600	100	94	3	18	4	1.1	22.2
58	40	14	1800	99	93	0	13	3	2.5	29.7
58	40	18	1800	100	93	0	14	3	2.5	26.9
58	40	22	1800	100	93	0	11	3	1.5	29.4
58	40	24	1800	101	93	1	10	3	1.8	29.2
65	40	16	2000	98	93	0	14	3	2.9	27.3
65	40	18	2000	99	94	0	14	4	2.7	22.8
15	60	17	800	102	94	-2	12	3	-1.8	36.9
15	60	17.7	800	99	94	-4	12	3	-1.7	37.8
15	60	20	800	99	95	-4	11	3	-0.9	38.7
15	60	24	800	100	95	-3	11	3	-1.0	35.9
29	60	18	1000	99	95	-2	10	3	0.4	38.6
29	60	20.5	1000	99	95	-2	10	3	0.5	37.5
29	60	24	1000	100	95	-1	10	3	0.5	34.2
29	60	27.5	1000	100	94	0	11	3	0.2	26.4
40	60	19	1200	99	94	-2	11	3	1.0	35.1
40	60	21	1200	100	94	-2	10	3	1.0	34.3
40	60	24	1200	100	94	-1	11	3	1.1	30.4
40	60	27.4	1200	100	94	1	12	3	1.0	24.1

SOI (bTDC)	PR (%)	Total Fuel mass (mg/cycle)	Engine Speed (rpm)	Intake air temperature (Deg c)	Intake air Pressure (kPa)	CA_Start of Main HR (aTDC)	CA_End of Main HR (aTDC)	Heat release type	Fraction of early (%)	Fraction of Late (%)
52	60	19.8	1400	99	93	-2	12	3	1.6	27.7
52	60	21.5	1400	100	94	-2	12	4	2.1	20.9
52	60	24.5	1400	100	93	-1	10	3	1.8	26.2
52	60	28	1400	99	94	0	12	1	2.0	15.8
58	60	21	1600	99	94	3	20	3	2.5	25.6
58	60	24.5	1600	100	94	4	22	4	2.5	18.4
58	60	30	1600	100	94	8	25	1	2.8	10.5
70	60	21	1800	100	93	3	23	4	3.0	19.7
70	60	24	1800	100	93	6	26	1	2.4	13.8
70	60	28	1800	100	93	7	24	1	2.9	10.9
80	60	23	2000	99	94	6	30	1	3.6	10.4
80	60	27	2000	99	94	6	26	1	4.2	6.9
100	20	14	1000	40	101	-2	13	2	11.3	2.3
100	20	15.5	1000	40	100	-3	7	2	11.1	-5.5
100	20	17	1000	40	100	-4	5	2	11.1	-12.7
80	20	13	1000	40	101	-2	15	2	11.6	4.0
80	20	15	1000	40	101	-3	8	2	10.8	-1.3
80	20	17	1000	40	101	-4	6	2	8.8	-8.1
60	20	13	1000	40	101	-3	10	2	8.0	7.6
60	20	15	1000	40	101	-4	7	2	7.0	4.0
60	20	17	1000	40	101	-4	4	5	5.0	3.9
60	20	18	1000	40	102	-3	4	2	7.4	0.8
50	20	13	1000	40	102	-4	8	1	4.8	12.9
50	20	15	1000	40	101	-4	8	1	3.6	13.1
50	20	17	1000	40	102	-5	6	1	2.4	11.9
50	20	19	1000	40	101	-6	6	1	1.9	11.3
50	20	22	1000	40	102	-6	3	1	1.8	12.7
40	20	13.2	1000	40	101	-3	8	4	1.9	20.0

SOI (bTDC)	PR (%)	Total Fuel mass (mg/cycle)	Engine Speed (rpm)	Intake air temperature (Deg c)	Intake air Pressure (kPa)	CA_Start of Main HR (aTDC)	CA_End of Main HR (aTDC)	Heat release type	Fraction of early (%)	Fraction of Late (%)
40	20	15	1000	40	101	-2	8	4	1.3	21.8
40	20	18	1000	40	101	-3	8	4	0.7	21.1
40	20	22	1000	40	102	-3	8	4	0.8	17.8
40	20	29	1000	40	102	-1	10	1	0.5	11.6
30	20	12.5	1000	40	96	0	13	3	-9.5	31.8
30	20	15	1000	40	96	0	13	3	-0.4	24.1
30	20	17	1000	40	97	0	14	4	-0.4	22.6
30	20	19	1000	40	96	-1	13	4	-0.9	22.8
30	20	22	1000	40	96	1	14	4	-0.5	20.7
30	20	29	1000	40	96	2	15	1	-0.6	15.9
20	20	13	1000	40	96	4	23	4	-1.3	21.7
20	20	15	1000	40	96	5	26	4	-1.2	20.4
20	20	17	1000	40	96	6	25	4	-1.1	20.8
20	20	22	1000	40	96	5	27	4	-0.8	17.2
20	20	28	1000	40	96	5	31	1	-1.0	12.6
100	30	16	1000	40	96	0	15	2	9.7	7.6
100	30	18	1000	40	95	0	14	2	8.7	-0.9
80	30	14	1000	40	95	1	30	2	9.7	5.9
80	30	17	1000	40	95	0	12	2	9.1	2.8
80	30	19	1000	40	96	0	10	2	9.1	-3.6
60	30	13.5	1000	40	96	-1	17	5	6.0	11.7
60	30	15	1000	40	95	-1	13	2	7.5	9.0
60	30	17	1000	40	96	-1	9	5	5.9	6.3
60	30	19	1000	40	95	-1	8	5	5.5	3.8
50	30	13	1000	40	96	-1	14	1	4.5	16.5

SOI (bTDC)	PR (%)	Total Fuel mass (mg/cycle)	Engine Speed (rpm)	Intake air temperature (Deg c)	Intake air Pressure (kPa)	CA_Start of Main HR (aTDC)	CA_End of Main HR (aTDC)	Heat release type	Fraction of early (%)	Fraction of Late (%)
50	30	15	1000	40	95	-1	12	1	4.3	15.9
50	30	17	1000	40	95	-2	11	1	3.8	13.0
50	30	19	1000	40	96	-3	7	1	2.5	15.7
50	30	22	1000	40	95	-3	6	1	3.0	13.1
40	30	12.5	1000	40	96	2	14	4	2.5	19.9
40	30	15	1000	40	95	0	12	3	1.7	23.8
40	30	17	1000	40	95	-1	12	4	1.5	21.9
40	30	20	1000	40	95	0	12	4	1.9	19.8
40	30	24	1000	40	95	-2	9	4	0.2	19.9
40	30	28	1000	40	96	-1	10	1	0.2	15.2
30	30	12.5	1000	40	95	2	18	4	-0.8	19.9
30	30	15	1000	40	95	2	16	3	-0.4	25.6
30	30	17	1000	40	95	2	17	3	-0.3	24.0
30	30	20	1000	40	95	2	15	3	0.4	23.4
30	30	24	1000	40	96	1	14	4	-0.2	21.9
30	30	28	1000	40	95	4	15	4	0.5	17.9
20	30	13	1000	40	96	6	29	4	-1.6	19.2
20	30	15	1000	40	95	8	34	1	-0.4	17.0
20	30	17	1000	40	95	7	31	4	-1.0	18.7
100	40	17	1000	40	96	0	13	2	7.8	3.8
100	40	19	1000	40	96	1	9	2	9.1	-3.4
80	40	14	1000	40	96	1	18	2	10.7	11.0
80	40	15	1000	40	95	1	17	2	9.9	9.8
80	40	17	1000	40	96	-1	11	2	9.5	-0.3
60	40	13.5	1000	40	97	0	15	2	7.4	15.2
60	40	18	1000	40	97	-2	9	1	4.8	5.1
40	40	13.3	1000	40	96	2	13	3	3.4	23.7
40	40	20	1000	40	96	-1	8	3	1.9	25.7

SOI (bTDC)	PR (%)	Total Fuel mass (mg/cycle)	Engine Speed (rpm)	Intake air temperature (Deg c)	Intake air Pressure (kPa)	CA_Start of Main HR (aTDC)	CA_End of Main HR (aTDC)	Heat release type	Fraction of early (%)	Fraction of Late (%)
40	40	30	1000	40	96	3	13	1	1.2	11.8
40	40	40	1000	40	97	8	27	1	0.6	4.6
20	40	13	1000	40	96	9	29	4	0.6	19.6
20	40	20	1000	40	96	7	28	4	0.1	20.9
20	40	30	1000	40	96	8	27	4	0.4	19.4
20	40	33	1000	40	96	8	29	1	0.3	15.2
30	40	12.5	1000	40	96	3	18	4	1.4	21.7
30	40	18.5	1000	40	96	1	14	3	1.1	27.9
30	40	24.5	1000	40	96	2	12	3	0.6	27.7
30	40	35.5	1000	40	96	6	22	1	0.5	7.4
30	40	37.5	1000	40	96	9	32	1	0.6	5.9
40	60	20	1000	40	96	1	12	3	1.1	31.8
40	60	22	1000	40	96	1	12	3	1.3	30.7
40	60	24	1000	40	96	2	13	3	1.2	23.7
40	60	26	1000	40	97	2	13	4	1.1	21.7
40	60	28	1000	40	96	3	14	4	0.9	18.0
60	60	19	1000	40	95	1	19	1	3.0	11.7
60	60	20	1000	40	96	2	19	1	3.4	8.6
60	60	22	1000	40	96	3	21	1	3.6	6.5
60	60	25	1000	40	96	3	18	1	2.7	7.4
80	60	20	1000	40	96	2	21	1	4.6	9.7
80	60	22	1000	40	96	2	12	3	4.1	48.2
40	20	11	1000	60	97	2	17	1	-0.5	12.7
40	20	12	1000	60	96	-1	12	1	-0.1	13.8
40	20	14	1000	60	98	-2	8	1	0.3	16.6

SOI (bTDC)	PR (%)	Total Fuel mass (mg/cycle)	Engine Speed (rpm)	Intake air temperature (Deg c)	Intake air Pressure (kPa)	CA_Start of Main HR (aTDC)	CA_End of Main HR (aTDC)	Heat release type	Fraction of early (%)	Fraction of Late (%)
40	20	16	1000	60	99	-3	7	4	0.8	18.6
40	20	19	1000	60	102	-5	8	1	1.2	16.7
40	20	23	1000	60	102	-4	6	1	0.8	15.7
40	20	28	1000	60	101	-3	6	1	0.9	12.0
60	20	11.7	1000	60	96	-4	13	5	5.1	10.8
60	20	12	1000	60	96	-5	10	5	6.0	10.7
60	20	13.5	1000	60	97	-6	8	5	5.6	8.6
60	20	17	1000	60	102	-7	1	2	7.8	-2.5
80	20	12.8	1000	60	97	-5	13	2	8.7	7.5
80	20	14	1000	60	97	-5	9	2	9.3	5.2
80	20	15	1000	60	97	-7	4	2	10.0	-0.9
80	20	16	1000	60	101	-7	1	2	13.9	-13.8
30	40	13.5	1000	60	97	-2	10	4	-1.4	22.7
30	40	15.5	1000	60	97	0	9	3	-0.2	23.4
30	40	17	1000	60	97	-2	10	4	-0.6	22.8
30	40	20	1000	60	97	-2	9	3	-0.8	26.4
30	40	23	1000	60	97	-2	9	3	-0.7	26.6
30	40	28	1000	60	100	-1	11	4	-0.6	20.2
40	40	13.5	1000	60	97	-5	8	4	0.2	21.1
40	40	15.5	1000	60	97	-4	7	4	0.6	22.4
40	40	17.5	1000	60	97	-4	8	4	0.9	22.2
40	40	20	1000	60	97	-4	7	4	0.8	21.7
40	40	28	1000	60	96	-3	7	1	0.1	16.8
60	40	13	1000	60	96	-5	12	1	4.0	12.3
60	40	15.5	1000	60	96	-4	10	5	5.1	7.8
60	40	17.5	1000	60	97	-4	8	1	4.6	6.3
60	40	20.3	1000	60	97	-4	5	1	4.1	2.0
80	40	13.3	1000	60	96	-2	19	5	6.8	11.4

SOI (bTDC)	PR (%)	Total Fuel mass (mg/cycle)	Engine Speed (rpm)	Intake air temperature (Deg c)	Intake air Pressure (kPa)	CA_Start of Main HR (aTDC)	CA_End of Main HR (aTDC)	Heat release type	Fraction of early (%)	Fraction of Late (%)
80	40	15	1000	60	97	-3	16	5	6.8	6.0
80	40	16	1000	60	97	-4	12	2	7.4	3.8
80	40	18	1000	60	97	-5	7	2	7.3	-1.0
80	40	20	1000	60	97	-4	6	5	6.2	-7.0
30	60	19.3	1000	60	97	0	12	3	-0.1	33.4
30	60	21	1000	60	97	1	12	3	0.6	33.2
30	60	24	1000	60	96	0	11	3	0.0	32.1
30	60	29	1000	60	97	1	14	4	-0.2	21.7
40	60	19	1000	60	96	-4	8	3	1.2	28.6
40	60	21	1000	60	96	-4	7	3	0.8	28.3
40	60	24	1000	60	96	-3	7	3	0.8	23.6
40	60	29	1000	60	96	-2	7	4	0.4	17.9
60	60	19	1000	60	96	-4	12	1	2.8	8.2
60	60	21	1000	60	97	-2	11	1	2.8	6.1
60	60	25	1100	60	96	-2	11	1	2.4	6.4
80	60	19.3	1100	60	95	-1	17	1	3.2	12.4
80	60	20	1100	60	96	-1	17	1	3.3	6.0
80	60	21.5	1100	60	97	1	20	1	3.8	3.8
80	60	23	1100	60	96	2	22	1	3.9	3.7
20	20	10	900	79	97	-2	10	4	-4.3	17.8
20	20	11	900	80	96	-5	11	1	-4.4	16.4
20	20	14.7	900	80	96	-1	11	4	-3.2	21.3
20	20	19.5	900	80	97	-2	13	4	-2.7	21.1
20	20	27	900	80	97	1	17	1	-2.1	16.9
30	20	10	900	80	97	-6	2	1	-0.6	15.0

SOI (bTDC)	PR (%)	Total Fuel mass (mg/cycle)	Engine Speed (rpm)	Intake air temperature (Deg c)	Intake air Pressure (kPa)	CA_Start of Main HR (aTDC)	CA_End of Main HR (aTDC)	Heat release type	Fraction of early (%)	Fraction of Late (%)
30	20	11	900	80	97	-6	3	1	-0.3	13.6
30	20	12.3	900	80	98	-7	3	1	-0.9	16.3
30	20	14.6	900	80	103	-7	3	4	-0.5	18.4
30	20	19.5	900	80	100	-7	3	4	-0.1	21.1
30	20	27	1000	80	99	-5	5	1	-0.8	16.5
40	20	10	900	80	96	-9	0	1	0.8	12.1
40	20	11	900	80	96	-9	1	1	0.2	12.0
40	20	12.4	900	80	96	-9	0	1	0.8	14.9
40	20	14.6	900	80	97	-9	-1	1	2.5	15.6
40	20	19.5	900	80	98	-9	-1	4	1.9	18.3
40	20	27.5	900	80	96	-9	1	1	1.1	9.8
60	20	10.5	900	80	96	-9	6	5	5.1	9.2
60	20	11.8	900	80	97	-9	5	5	5.3	8.4
60	20	12.6	900	80	97	-9	4	5	5.5	8.1
60	20	14.6	900	80	96	-10	0	2	7.2	2.9
60	20	19	900	80	96	-9	-2	2	7.6	-6.1
80	20	13	900	80	96	-8	8	2	7.2	5.9
80	20	14	900	80	97	-8	6	2	9.4	1.8
80	20	15	900	80	98	-9	1	2	11.9	-6.5
80	20	17	900	80	95	-9	-2	2	12.1	-14.9
20	40	13	900	80	97	1	15	4	-3.7	21.0
20	40	15	900	80	97	2	15	4	-2.7	20.7
20	40	19	900	80	97	2	16	4	-2.2	22.1
20	40	28	1000	80	97	4	18	4	-1.4	22.0
30	40	13	900	80	96	-5	7	4	-1.9	22.4
30	40	15.2	900	80	97	-5	5	3	-1.1	23.7
30	40	19.3	1000	80	97	-5	7	3	-0.8	26.1
30	40	28	1000	80	97	-4	6	4	-0.9	21.1

SOI (bTDC)	PR (%)	Total Fuel mass (mg/cycle)	Engine Speed (rpm)	Intake air temperature (Deg c)	Intake air Pressure (kPa)	CA_Start of Main HR (aTDC)	CA_End of Main HR (aTDC)	Heat release type	Fraction of early (%)	Fraction of Late (%)
40	40	13.3	1000	80	97	-7	2	3	0.9	23.6
40	40	15.2	1000	80	97	-8	1	3	1.7	24.1
40	40	19.3	1000	80	99	-7	2	4	2.4	19.7
40	40	28	1000	80	104	-5	1	1	2.4	16.2
60	40	13.3	1000	80	97	-9	6	1	4.6	8.1
60	40	15.3	1000	80	98	-8	5	5	5.8	4.3
60	40	19.3	1000	80	106	-8	2	5	6.3	-5.8
80	40	13.3	1000	80	97	-8	7	5	5.1	7.9
80	40	14	1000	80	97	-8	8	5	6.0	3.9
80	40	15.8	1000	80	97	-9	5	5	6.2	1.3
80	40	18.5	1000	80	103	-8	2	2	8.5	-9.4
30	60	19.5	1000	80	100	-5	7	3	-0.2	33.1
30	60	20.5	1000	80	97	-5	5	3	0.1	35.5
30	60	24.5	1000	80	98	-4	5	3	-0.2	28.8
30	60	28.5	1000	80	97	-2	6	4	0.3	21.8
40	60	19.5	1000	80	99	-8	3	3	0.7	25.5
40	60	20.5	1000	80	98	-7	2	3	0.8	26.0
40	60	24.5	1000	80	99	-5	3	4	1.2	19.4
40	60	28.5	1000	80	97	-4	4	4	0.5	17.8
60	60	19.5	1000	80	97	-5	9	1	1.9	10.6
60	60	20.5	1000	80	96	-5	10	1	2.0	5.4
60	60	22.5	1000	80	97	-3	8	1	1.8	5.1
60	60	25.5	1000	80	97	-3	8	1	1.5	6.4
80	60	19.5	1000	80	97	-5	11	1	2.8	12.7
80	60	20.5	1000	80	96	-4	13	1	2.8	3.1

SOI (bTDC)	PR (%)	Total Fuel mass (mg/cycle)	Engine Speed (rpm)	Intake air temperature (Deg c)	Intake air Pressure (kPa)	CA_Start of Main HR (aTDC)	CA_End of Main HR (aTDC)	Heat release type	Fraction of early (%)	Fraction of Late (%)
80	60	22.5	1000	80	97	-2	12	1	2.8	0.8
80	60	25.5	1000	80	96	0	10	1	2.9	0.8
20	60	20.4	1000	80	97	3	15	3	-1.3	33.7
20	60	21.5	1000	80	97	2	15	3	-1.7	34.9
20	60	24	1000	80	97	2	15	3	-1.5	34.2
20	60	28	1000	80	97	5	18	3	-1.1	27.4

Appendix B

LTC engine model data used for LPV-SVM system identification

In the below set of data engine speed was set constant to 1000 rpm, intake manifold temperature was set to 60°C and Intake manifold pressure was set to 96.5 kPa. The data was generated by using a physics based LTC engine plant [5].

Cycle number	SOI (bTDC)	FQ (mg/cycle)	PR (%)	Fraction of early HR modelled (%)	Fraction of late HR modelled (%)	CA50 (aTDC)	MPRR (bar/CAD)	Tsoc (K)	Psoc (kPa)	IMEP (kPa)
1	38.5	19.3	0	7.2	14.6	8	0	777	1800	610
2	38.5	19.3	0	7.2	14.6	2.3	4.1	715	1834	557
3	38.6	20.5	0	7	14	4.8	4.3	713	1813	564
4	38.6	20.5	0.1	7	14	3.5	4.3	728	1779	528
5	38.8	21.8	0.2	6.7	13.2	3.6	4.6	731	1773	513
6	38.9	23	0.2	6.4	12.3	3.6	4.8	731	1770	546
7	38.9	23	0.4	6.3	12.3	3.6	4.8	732	1767	573
8	39	24	0.5	6.1	11.4	3.8	5	732	1764	567
9	39	24	0.6	6	11.5	3.9	5	733	1764	593
10	39	25	0.8	5.7	10.6	3.9	5.2	733	1761	589
11	39	25	1	5.6	10.7	4.1	5.2	733	1761	616
12	39.1	26	1.2	5.3	9.7	4.2	5.4	734	1761	612
13	39.1	26	1.4	5.2	9.7	4.1	5.4	734	1758	638
14	39.1	27	1.6	4.9	8.7	4.2	5.6	735	1758	634
15	39.1	27	1.9	4.8	8.8	4.4	5.6	735	1758	660
16	39.1	27	2.2	4.7	8.9	4.4	5.6	736	1758	656
17	39.1	27	2.5	4.6	8.9	4.5	5.6	736	1758	656
18	39.1	27	2.8	4.4	9	4.7	5.6	736	1758	657
19	39.1	27	3.1	4.3	9.1	4.8	5.6	736	1758	657
20	39.1	27	3.5	4.2	9.2	4.8	5.6	736	1758	658
21	39.1	27	3.8	4.1	9.2	5.1	5.6	736	1761	659
22	39.1	27	4.2	3.9	9.3	5.1	5.6	736	1761	659
23	39.1	27	4.6	3.8	9.4	5.3	5.6	736	1761	660
24	39	27	5	3.6	9.6	5.3	5.6	736	1761	661
25	38.9	27	5.4	3.5	9.7	5.6	5.6	737	1765	662
26	38.9	27	5.9	3.4	9.8	5.9	5.6	737	1768	663
27	38.9	27	6.3	3.2	9.9	5.9	5.6	737	1768	663

Cycle number	SOI (bTDC)	FQ (mg/cycle)	PR (%)	Fraction of early HR modelled (%)	Fraction of late HR modelled (%)	CA50 (aTDC)	MPRR (bar/CAD)	Tsoc (K)	Psoc (kPa)	IMEP (kPa)
28	38.9	27	6.8	3.1	10	6	5.6	737	1768	664
29	38.8	27	7.3	2.9	10.2	6.2	5.6	737	1771	665
30	38.8	27	7.7	2.8	10.3	6.2	5.6	737	1771	666
31	38.8	25.9	8.2	2.9	11.6	6.5	5.4	738	1774	667
32	38.8	25.9	8.8	2.8	11.7	6.6	5.4	738	1774	639
33	38.8	24.8	9.3	2.8	12.9	6.8	5.2	737	1777	645
34	38.8	24.8	9.8	2.7	13	7.1	5.2	737	1780	618
35	38.8	23.6	10.4	2.8	14.3	7.2	4.9	737	1783	624
36	38.8	23.6	10.9	2.7	14.4	7.4	4.9	736	1783	593
37	38.8	22.5	11.5	2.8	15.5	7.7	4.7	736	1786	600
38	38.8	22.5	12.1	2.7	15.6	7.8	4.7	736	1788	572
39	38.9	21.4	12.6	2.8	16.5	8.1	4.5	735	1791	578
40	38.9	21.4	13.2	2.6	16.6	8.3	4.5	735	1791	550
41	39.1	20.3	13.8	2.8	17.3	8.4	4.3	734	1794	556
42	39.2	19.1	14.4	2.9	18	8.6	4.1	734	1794	528
43	39.2	19.1	15	2.8	18.2	8.9	4.1	734	1797	502
44	39.5	18	15.6	2.9	18.6	9	3.9	733	1799	509
45	39.5	18	16.3	2.8	18.7	9.2	3.9	732	1799	481
46	39.8	18	16.9	2.8	18.7	9.3	3.9	732	1802	487
47	39.8	18	17.5	2.7	18.8	9.3	3.9	731	1799	489
48	40.1	18	18.1	2.7	18.8	9.5	3.9	732	1802	490
49	40.1	18	18.7	2.6	19	9.5	3.9	732	1802	491
50	40.5	18	19.4	2.7	18.9	9.6	3.9	732	1802	492
51	40.5	18	20	2.6	19	9.5	3.9	731	1799	494
52	40.9	18	20.6	2.6	18.9	9.6	3.9	732	1802	495

Cycle number	SOI (bTDC)	FQ (mg/cycle)	PR (%)	Fraction of early HR modelled (%)	Fraction of late HR modelled (%)	CA50 (aTDC)	MPRR (bar/CAD)	Tsoc (K)	Psoc (kPa)	IMEP (kPa)
53	40.9	18	21.3	2.6	19.1	9.5	3.9	731	1799	496
54	41.4	18	21.9	2.6	18.9	9.8	3.9	732	1802	497
55	41.8	18	22.5	2.7	18.8	9.6	4	731	1799	499
56	41.8	18	23.1	2.6	19	9.6	4	731	1799	500
57	42.9	18	23.7	2.8	18.5	9.8	4	731	1799	501
58	43.4	19.3	24.4	2.7	17.6	9.5	4.3	731	1793	502
59	43.4	19.3	25	2.7	17.8	9.3	4.3	730	1791	539
60	43.9	20.5	25.6	2.6	16.7	9.3	4.5	731	1791	535
61	43.9	20.5	26.2	2.6	16.9	9.2	4.5	731	1788	567
62	44.4	21.8	26.8	2.5	15.5	9.2	4.8	732	1788	563
63	44.4	21.8	27.4	2.5	15.7	9	4.8	732	1785	599
64	44.8	23	27.9	2.4	14.3	9	5.1	734	1785	594
65	44.8	23	28.5	2.4	14.4	8.9	5.1	733	1782	627
66	45	24	29.1	2.3	13.3	8.9	5.3	734	1782	623
67	45	24	29.6	2.3	13.4	8.9	5.3	735	1783	650
68	45	25	30.2	2.2	12.3	8.9	5.5	735	1783	646
69	45	25	30.7	2.2	12.4	8.9	5.5	736	1783	673
70	45	26	31.2	2.1	11.2	8.9	5.7	737	1783	670
71	45	26	31.8	2.1	11.3	9	5.7	737	1786	697
72	45	27	32.3	2	10	9	5.9	738	1786	694
73	45	27	32.7	2	10.1	9	5.9	738	1786	720
74	45	27	33.2	2.1	10.2	9.2	5.9	739	1786	717
75	45	27	33.7	2.1	10.3	9.2	5.9	739	1786	717
76	45	27	34.1	2.1	10.4	9.3	5.9	739	1789	718
77	45	27	34.6	2.1	10.4	9.3	5.9	739	1789	719
78	45	27	35	2.1	10.5	9.5	9.3	740	1792	720
79	45	27	35.4	2.2	10.6	9.5	9.3	740	1792	721
80	45	27	35.8	2.2	10.7	9.8	9.3	740	1795	722

Cycle number	SOI (bTDC)	FQ (mg/cycle)	PR (%)	Fraction of early HR modelled (%)	Fraction of late HR modelled (%)	CA50 (aTDC)	MPRR (bar/CAD)	Tsoc (K)	Psoc (kPa)	IMEP (kPa)
81	45	27	36.2	2.2	10.7	9.8	9.3	740	1795	722
82	45	27	36.5	2.2	10.8	9.8	9.3	740	1795	723
83	45	27	36.9	2.2	10.9	9.9	9.3	740	1798	724
84	44.9	27	37.2	2.3	11	9.9	9.3	740	1798	724
85	44.9	27	37.5	2.3	11.1	10.1	9.3	741	1801	725
86	44.4	27	37.8	2.2	11.5	10.2	9.2	741	1801	726
87	44.4	27	38.1	2.2	11.6	10.4	9.2	741	1804	726
88	43.8	25.9	38.4	2.3	13.6	10.5	8.6	741	1806	727
89	43.8	25.9	38.6	2.3	13.6	10.7	8.6	741	1809	698
90	43.1	24.8	38.8	2.3	15.6	10.8	8	741	1812	704
91	43.1	24.8	39	2.3	15.7	11.3	8	741	1817	676
92	42.4	23.6	39.2	2.3	17.7	11.4	7.4	741	1820	681
93	42.4	23.6	39.4	2.3	17.7	11.7	7.4	741	1825	650
94	41.6	22.5	39.5	2.3	19.5	11.9	6.9	740	1827	656
95	41.6	22.5	39.6	2.3	19.6	12.3	6.9	741	1832	627
96	40.8	21.4	39.8	2.2	21.2	12.5	6.3	740	1835	632
97	40.8	21.4	39.8	2.2	21.2	12.9	6.3	741	1842	604
98	40	20.3	39.9	2.2	22.7	12.9	5.8	740	1842	609
99	40	20.3	40	2.2	22.7	13.5	5.8	740	1849	580
100	39.1	19.1	40	2.1	24.1	13.5	5.3	739	1849	585
101	39.1	19.1	40	2.1	24.1	14	5.3	740	1856	553
102	38.3	18	40	2	25.2	14.1	4.8	739	1858	558
103	38.3	18	40	2	25.2	14.6	4.8	739	1862	529
104	37.4	18	39.9	1.9	25.6	14.7	4.7	738	1864	533
105	37.4	18	39.8	1.9	25.6	15.2	4.7	739	1870	534

Cycle number	SOI (bTDC)	FQ (mg/cycle)	PR (%)	Fraction of early HR modelled (%)	Fraction of late HR modelled (%)	CA50 (aTDC)	MPRR (bar/CAD)	Tsoc (K)	Psoc (kPa)	IMEP (kPa)
106	36.6	18	39.8	1.8	26	15.2	4.5	739	1870	534
107	35.8	18	39.6	1.7	26.4	15.5	4.4	739	1874	534
108	35.8	18	39.5	1.7	26.4	15.9	4.4	740	1880	533
109	35.1	18	39.4	1.6	26.7	15.9	4.3	740	1880	533
110	35.1	18	39.2	1.6	26.7	16.2	4.3	740	1883	533
111	34.4	18	39	1.4	27	16.2	4.1	740	1883	532
112	34.4	18	38.8	1.4	26.9	16.7	4.1	741	1888	532
113	33.8	18	38.6	1.3	27.2	16.5	4	741	1887	532
114	33.8	18	38.4	1.3	27.1	16.7	4	741	1890	531
115	33.3	18	38.1	1.2	27.3	16.7	4	741	1890	531
116	32.9	18	37.8	1.2	27.4	17	3.9	741	1893	530
117	32.9	18	37.5	1.2	27.3	17.1	3.9	742	1894	530
118	32.6	19.3	37.2	1.1	26.8	17.1	4.2	742	1894	529
119	32.6	19.3	36.9	1	26.7	17.1	4.2	742	1896	564
120	32.3	21.8	36.5	0.9	25.1	17	4.7	743	1895	557
121	32.3	21.8	36.2	0.9	25	17	4.7	743	1897	623
122	32.2	23	35.8	0.8	23.9	16.7	5	745	1894	612
123	32.2	23	35.4	0.8	23.9	16.5	5	745	1894	642
124	32.3	24	35	0.7	22.7	16.4	5.2	746	1892	636
125	32.3	24	34.6	0.7	22.7	16.1	5.2	746	1891	661
126	32.5	25	34.1	0.6	21.4	15.9	5.5	747	1889	656
127	32.8	26	33.7	0.6	20	15.8	5.9	747	1888	681
128	33.1	27	33.2	0.5	18.6	15.3	6.2	748	1885	702
129	33.1	27	32.7	0.5	18.5	15	6.2	748	1881	722
130	33.5	27	32.3	0.5	18.2	14.9	6.3	749	1879	716
131	33.5	27	31.8	0.5	18.1	14.3	6.3	748	1874	715
132	34	27	31.2	0.5	17.7	14.3	6.4	748	1874	714
133	34	27	30.7	0.5	17.6	14	6.4	748	1870	713

Cycle number	SOI (bTDC)	FQ (mg/cycle)	PR (%)	Fraction of early HR modelled (%)	Fraction of late HR modelled (%)	CA50 (aTDC)	MPRR (bar/CAD)	Tsoc (K)	Psoc (kPa)	IMEP (kPa)
134	34.5	27	30.2	0.5	17.2	13.8	6.6	748	1868	712
135	35	27	29.6	0.5	16.7	13.4	5.5	747	1863	711
136	35	27	29.1	0.5	16.7	12.9	5.5	747	1857	710
137	35.6	27	28.5	0.6	16.2	12.9	5.5	747	1857	709
138	35.6	27	27.9	0.5	16.1	12.5	5.5	746	1850	707
139	36.1	27	27.4	0.6	15.6	12.3	5.5	746	1850	707
140	36.1	27	26.8	0.6	15.5	11.9	5.5	745	1843	705
141	36.6	27	26.2	0.6	15.1	11.9	5.5	745	1843	704
142	36.6	27	25.6	0.6	15	11.4	5.5	744	1836	703
143	37.1	27	25	0.7	14.6	11.3	5.6	744	1836	702
144	37.1	27	24.4	0.7	14.4	11	5.6	744	1831	701
145	37.5	25.9	23.7	0.9	15.4	10.8	5.4	744	1828	699
146	37.5	25.9	23.1	0.9	15.3	10.5	5.4	743	1823	669
147	37.9	24.8	22.5	1.1	16.1	10.5	5.2	742	1823	673
148	38.1	23.6	21.9	1.3	17.1	10.2	4.9	741	1817	643
149	38.1	23.6	21.3	1.3	16.9	10.2	4.9	740	1817	615
150	38.3	22.5	20.6	1.5	17.7	10.1	4.7	739	1817	620
151	38.5	21.4	20	1.7	18.3	10.1	4.5	739	1814	590
152	38.5	21.4	19.4	1.8	18.2	9.9	4.5	737	1811	564
153	38.5	20.3	18.7	2	18.8	9.8	4.3	736	1811	568
154	38.5	20.3	18.1	2.1	18.7	9.8	4.3	736	1811	538
155	38.4	19.1	17.5	2.3	19.2	9.8	4.1	735	1811	542
156	38.3	18	16.9	2.5	19.5	9.8	3.8	735	1811	509
157	38.3	18	16.3	2.6	19.4	10.1	3.8	734	1813	483
158	38.1	18	15.6	2.6	19.4	9.9	3.8	733	1813	487

Cycle number	SOI (bTDC)	FQ (mg/cycle)	PR (%)	Fraction of early HR modelled (%)	Fraction of late HR modelled (%)	CA50 (aTDC)	MPRR (bar/CAD)	Tsoc (K)	Psoc (kPa)	IMEP (kPa)
159	37.8	18	15	2.7	19.4	9.9	3.8	733	1813	486
160	37.8	18	14.4	2.8	19.2	10.1	3.8	733	1816	485
161	37.5	18	13.8	2.8	19.2	9.8	3.8	733	1813	484
162	37.5	18	13.2	2.9	19.1	9.9	3.8	733	1816	483
163	37.1	18	12.6	2.9	19.2	9.6	3.8	733	1813	481
164	37.1	18	12.1	3.1	19	9.8	3.8	733	1816	480
165	36.7	18	11.5	3.1	19.1	9.8	3.8	733	1816	479
166	36.2	18	10.9	3.1	19.2	9.8	3.8	733	1819	478
167	36.2	18	10.4	3.3	19.1	9.9	3.8	734	1821	477
168	35.8	18	9.8	3.3	19.1	9.9	3.8	734	1821	476
169	35.8	18	9.3	3.4	19	9.9	3.8	734	1824	475
170	35.4	18	8.8	3.5	19.1	9.8	3.8	734	1821	473
171	35.4	18	8.2	3.6	18.9	9.8	3.8	734	1824	473
172	35	19.3	7.7	3.5	18.7	9.8	4	734	1824	471
173	35	19.3	7.3	3.6	18.5	9.8	4	734	1827	506
174	34.7	20.5	6.8	3.5	18.1	9.5	5	735	1824	499
175	34.7	20.5	6.3	3.6	18	9.5	5	736	1827	530
176	34.4	21.8	5.9	3.5	17.3	9.3	5.3	736	1824	524
177	34.4	21.8	5.4	3.6	17.2	9.3	5.3	737	1827	557
178	34.2	23	5	3.5	16.4	9	5.6	738	1825	551
179	34.2	23	4.6	3.6	16.3	8.9	5.6	738	1825	581
180	34	25	4.2	3.3	14.7	8.9	6.1	739	1825	575
181	34	25	3.8	3.4	14.6	8.7	6.1	739	1825	627
182	34.1	26	3.5	3.4	13.5	8.4	6.4	741	1822	617
183	34.3	27	3.1	3.4	12.3	8.1	6.7	741	1820	642
184	34.6	27	2.8	3.5	12.1	7.8	6.8	741	1817	663
185	34.6	27	2.5	3.7	12	7.5	6.8	742	1812	658
186	34.9	27	2.2	3.8	11.7	7.2	6.9	742	1809	657

Cycle number	SOI (bTDC)	FQ (mg/cycle)	PR (%)	Fraction of early HR modelled (%)	Fraction of late HR modelled (%)	CA50 (aTDC)	MPRR (bar/CAD)	Tsoc (K)	Psoc (kPa)	IMEP (kPa)
187	34.9	27	1.9	3.9	11.7	6.9	6.9	741	1806	656
188	35.4	27	1.6	4.1	11.3	6.8	5.5	741	1806	655
189	36	27	1.4	4.4	10.8	6.5	5.5	741	1801	655
190	36.6	27	1.2	4.6	10.4	5.9	5.5	740	1792	654
191	36.6	27	1	4.7	10.3	5.3	5.5	739	1783	654
192	37.3	27	0.8	4.9	9.8	5.1	5.5	739	1783	654
193	37.3	27	0.6	5	9.8	4.7	5.5	738	1777	653
194	38.1	27	0.5	5.2	9.2	4.5	5.6	738	1777	653
195	38.1	27	0.4	5.2	9.1	3.9	5.6	737	1768	653
196	38.9	27	0.2	5.5	8.6	3.6	5.6	737	1768	653
197	38.9	27	0.2	5.5	8.5	3	5.6	736	1758	652
198	39.7	25.9	0.1	6	9.1	2.7	5.4	736	1758	652
199	39.7	25.9	0	6	9.1	2	5.4	735	1748	623
200	40.6	24.8	0	6.4	9.5	1.7	5.2	734	1752	628
201	40.6	24.8	0	6.4	9.5	0.8	5.2	733	1742	599
202	41.4	23.6	0	6.9	10	-2	5	735	1771	605
203	42.3	22.5	0	7.4	10.3	0.5	4.8	731	1735	572
204	42.3	22.5	0.1	7.3	10.3	0.9	4.8	729	1728	549
205	43.1	21.4	0.2	7.8	10.6	1.4	4.7	728	1728	555
206	43.1	21.4	0.2	7.7	10.6	1.4	4.7	727	1721	526
207	43.8	20.3	0.4	8.1	10.9	1.7	4.5	726	1721	531
208	44.5	19.1	0.5	8.5	11.1	1.7	4.2	725	1714	502
209	44.5	19.1	0.6	8.4	11.1	1.8	4.2	724	1710	475
210	45	18	0.8	8.7	11.2	2.1	4	723	1714	481
211	45	18	1	8.6	11.3	2.3	4	722	1710	452

Cycle number	SOI (bTDC)	FQ (mg/cycle)	PR (%)	Fraction of early HR modelled (%)	Fraction of late HR modelled (%)	CA50 (aTDC)	MPRR (bar/CAD)	Tsoc (K)	Psoc (kPa)	IMEP (kPa)
212	45	18	1.2	8.6	11.3	2.6	4	722	1713	457
213	45	18	1.4	8.4	11.4	2.7	4	722	1713	458
214	45	18	1.6	8.3	11.5	2.9	4	722	1713	459
215	45	18	1.9	8.2	11.6	2.9	4	722	1713	459
216	45	18	2.2	8.1	11.6	3	4	722	1713	460
217	45	18	2.5	8	11.7	3.2	4	722	1713	460
218	45	18	2.8	7.8	11.8	3.5	4	722	1717	461
219	45	18	3.1	7.7	11.9	3.5	4	722	1717	461
220	45	18	3.5	7.5	12	3.6	4	722	1717	462
221	45	18	3.8	7.4	12.1	3.6	4	722	1717	463
222	45	18	4.2	7.2	12.2	3.9	4	722	1720	463
223	45	18	4.6	7.1	12.3	4.1	4	722	1720	464
224	45	18	5	6.9	12.5	4.1	4	722	1720	465
225	45	19.3	5.4	6.5	12.1	4.4	4.3	723	1724	466
226	45	19.3	5.9	6.3	12.2	4.2	4.3	723	1724	502
227	45	20.5	6.3	5.9	11.6	4.4	4.6	724	1724	497
228	45	20.5	6.8	5.7	11.7	4.4	4.6	724	1724	530
229	45	21.8	7.3	5.3	10.9	4.2	4.8	725	1721	525
230	45	21.8	7.7	5.1	11	4.4	4.8	725	1724	561
231	45	23	8.2	4.7	10.1	4.4	5.1	726	1721	556
232	45	23	8.8	4.6	10.2	4.5	5	727	1725	588
233	44.4	24	9.3	4.1	9.8	4.4	5.2	728	1721	584
234	44.4	24	9.8	4	9.9	4.7	5.2	728	1728	611
235	43.7	25	10.4	3.5	9.5	4.8	5.4	729	1728	608
236	43.7	25	10.9	3.4	9.6	5.3	5.4	731	1738	635
237	43	26	11.5	2.9	9.1	5.1	5.6	731	1735	631
238	43	26	12.1	2.8	9.2	5.6	5.6	732	1745	659
239	41.4	27	12.6	2.2	9.4	5.7	5.7	733	1745	655

Cycle number	SOI (bTDC)	FQ (mg/cycle)	PR (%)	Fraction of early HR modelled (%)	Fraction of late HR modelled (%)	CA50 (aTDC)	MPRR (bar/CAD)	Tsoc (K)	Psoc (kPa)	IMEP (kPa)
240	41.4	27	13.2	2.1	9.5	6.5	5.7	735	1761	682
241	40.6	27	13.8	1.9	10.2	6.5	5.7	736	1761	679
242	40.6	27	14.4	1.8	10.3	6.9	5.7	737	1771	679
243	39.7	27	15	1.6	11	7.1	5.6	737	1771	680
244	39.7	27	15.6	1.5	11.1	7.7	5.6	739	1783	682
245	38.9	27	16.3	1.3	11.8	7.7	5.6	739	1783	683
246	38.9	27	16.9	1.3	11.9	8.3	5.6	740	1792	684
247	38.1	27	17.5	1.1	12.6	8.4	5.6	740	1795	685
248	38.1	27	18.1	1	12.7	8.9	5.6	741	1804	686
249	37.3	27	18.7	0.8	13.4	9	5.6	741	1804	687
250	37.3	27	19.4	0.8	13.5	9.6	5.6	742	1815	689
251	36.5	27	20	0.6	14.1	9.6	5.5	742	1815	690
252	36.5	27	20.6	0.6	14.2	10.4	5.5	743	1825	691
253	35.9	27	21.3	0.5	14.7	10.4	5.5	743	1825	692
254	35.9	27	21.9	0.5	14.8	10.8	5.5	744	1833	694
255	42.3	23	22.5	2.1	15	11	5	744	1833	695
256	43	24	23.1	2	13.6	8.1	5.2	738	1776	589
257	43.7	25	23.7	2	12	8.3	5.4	735	1780	635
258	43.7	25	24.4	1.9	12.2	8	5.4	735	1774	661
259	44.3	26	25	1.9	10.6	8	5.7	735	1774	658
260	44.3	26	25.6	1.9	10.7	7.8	5.7	735	1771	685
261	44.8	27	26.2	1.8	9.1	8	5.9	736	1771	682
262	44.8	27	26.8	1.8	9.2	8	5.9	736	1771	708
263	45	27	27.4	1.9	9.2	8	5.9	737	1771	705
264	45	27	27.9	1.9	9.3	8	5.9	737	1771	706

Cycle number	SOI (bTDC)	FQ (mg/cycle)	PR (%)	Fraction of early HR modelled (%)	Fraction of late HR modelled (%)	CA50 (aTDC)	MPRR (bar/CAD)	Tsoc (K)	Psoc (kPa)	IMEP (kPa)
265	45	27	28.5	1.9	9.4	8	5.9	737	1771	707
266	45	27	29.1	1.9	9.5	8.3	5.9	738	1774	708
267	45	27	29.6	1.9	9.6	8.3	5.9	738	1774	709
268	45	27	30.2	1.9	9.7	8.4	5.9	738	1777	710
269	45	27	30.7	2	9.8	8.4	5.9	738	1777	711
270	45	27	31.2	2	9.8	8.7	5.9	738	1780	712
271	45	27	31.8	2	9.9	8.7	5.9	738	1780	713
272	45	27	32.3	2	10	8.9	5.9	739	1783	714
273	45	27	32.7	2	10.1	8.9	5.9	739	1783	715
274	45	27	33.2	2.1	10.2	9.2	5.9	739	1786	716
275	45	27	33.7	2.1	10.3	9.2	5.9	739	1786	717
276	45	27	34.1	2.1	10.4	9.3	5.9	739	1789	718
277	45	25.9	34.6	2.2	11.9	9.3	5.7	739	1789	719
278	45	25.9	35	2.3	12	9.6	8.9	740	1792	691
279	44.9	24.8	35.4	2.4	13.6	9.8	8.5	739	1795	697
280	44.4	23.6	35.8	2.4	15.5	9.9	7.9	739	1798	669
281	44.4	23.6	36.2	2.4	15.6	10.4	7.9	739	1803	643
282	43.9	22.5	36.5	2.5	17.3	10.5	7.4	738	1806	649
283	43.9	22.5	36.9	2.5	17.4	11	7.4	738	1811	622
284	43.3	21.4	37.2	2.5	18.9	11.1	6.9	738	1814	627
285	43.3	21.4	37.5	2.5	19	11.4	6.9	738	1819	599
286	42.7	20.3	37.8	2.5	20.5	11.6	6.4	737	1822	604
287	42.7	20.3	38.1	2.5	20.5	11.9	6.4	738	1824	576
288	42	19.1	38.4	2.5	21.9	12	5.9	737	1827	581
289	41.4	18	38.6	2.5	23	12.6	5.4	737	1834	550
290	41.4	18	38.8	2.5	23.1	12.9	5.4	737	1839	526
291	40.7	18	39	2.4	23.5	13.2	5.3	736	1841	531
292	40.7	18	39.2	2.4	23.6	13.5	5.3	736	1846	532

Cycle number	SOI (bTDC)	FQ (mg/cycle)	PR (%)	Fraction of early HR modelled (%)	Fraction of late HR modelled (%)	CA50 (aTDC)	MPRR (bar/CAD)	Tsoc (K)	Psoc (kPa)	IMEP (kPa)
293	40.1	18	39.4	2.3	24	13.5	5.1	736	1846	533
294	40.1	18	39.5	2.3	24	13.8	5.1	737	1851	533
295	39.5	18	39.6	2.2	24.4	13.8	5	737	1851	533
296	39	18	39.8	2.1	24.7	14.1	4.9	737	1855	534
297	39	18	39.8	2.1	24.7	14.4	4.9	738	1860	534
298	38.5	18	39.9	2.1	25	14.4	4.9	738	1860	534
299	38.5	18	40	2.1	25	14.7	4.9	738	1864	534
300	37.6	18	40	1.9	25.6	14.7	4.7	738	1864	534
301	37.6	18	40	1.9	25.6	15	4.7	739	1868	534
302	37.3	18	40	1.9	25.7	15	4.6	739	1868	534
303	37.3	18	40	1.9	25.7	15.2	4.6	739	1870	534
304	37	19.3	39.9	1.8	25.2	15.2	4.9	739	1870	534
305	37	19.3	39.8	1.8	25.2	15.2	4.9	739	1872	569
306	36.8	20.5	39.8	1.7	24.4	15	5.2	740	1870	563
307	36.8	20.5	39.6	1.7	24.4	15.2	5.2	741	1873	595
308	36.6	21.8	39.5	1.6	23.4	15	5.6	741	1871	590
309	36.6	23	39.4	1.6	22.2	14.9	5.9	742	1871	623
310	36.6	23	39.2	1.6	22.2	14.9	5.9	743	1871	650
311	36.6	24	39	1.5	21.1	14.7	6.2	744	1869	643
312	36.6	24	38.8	1.5	21	14.4	6.2	744	1867	669
313	36.6	25	38.6	1.4	19.8	14.4	6.5	745	1867	664
314	36.6	25	38.4	1.4	19.8	14.3	6.5	745	1865	690
315	36.7	26	38.1	1.4	18.4	14.1	6.8	745	1865	685
316	36.7	26	37.8	1.3	18.4	14	6.8	745	1863	710
317	36.9	27	37.5	1.3	16.9	13.8	7.1	746	1861	705

Cycle number	SOI (bTDC)	FQ (mg/cycle)	PR (%)	Fraction of early HR modelled (%)	Fraction of late HR modelled (%)	CA50 (aTDC)	MPRR (bar/CAD)	Tsoc (K)	Psoc (kPa)	IMEP (kPa)
318	36.9	27	37.2	1.3	16.9	13.7	7.1	746	1859	730
319	37.1	27	36.9	1.3	16.7	13.4	7.2	747	1857	725
320	37.1	27	36.5	1.3	16.6	13.2	7.2	746	1855	724
321	37.3	27	36.2	1.3	16.4	13.2	7.3	746	1855	723
322	37.3	27	35.8	1.2	16.3	13.1	7.3	746	1852	723
323	37.6	27	35.4	1.2	16	13.1	7.3	746	1852	722
324	37.6	27	35	1.2	16	12.8	7.3	746	1848	721
325	37.9	27	34.6	1.2	15.7	12.6	5.6	746	1848	720
326	37.9	27	34.1	1.2	15.6	12.3	5.6	745	1843	719
327	38.2	27	33.7	1.2	15.3	12.3	5.6	745	1843	719
328	38.2	27	33.2	1.2	15.2	12.2	5.6	745	1841	718
329	38.5	27	32.7	1.2	14.9	12	5.6	745	1838	717
330	38.9	27	32.3	1.2	14.6	11.9	5.6	744	1836	716
331	38.9	27	31.8	1.2	14.5	11.4	5.6	744	1831	715
332	39.3	27	31.2	1.2	14.1	11.4	5.6	744	1831	714
333	39.3	27	30.7	1.2	14	11.1	5.6	743	1825	713
334	39.7	25.9	30.2	1.3	15	11	5.4	743	1823	712
335	39.7	25.9	29.6	1.3	14.9	10.8	5.4	743	1820	682
336	40.1	24.8	29.1	1.4	15.8	10.8	5.2	742	1820	686
337	40.5	23.6	28.5	1.6	16.8	10.5	5	741	1814	656
338	40.5	23.6	27.9	1.6	16.6	10.4	5	740	1811	628
339	40.9	22.5	27.4	1.8	17.4	10.4	4.8	739	1811	633
340	40.9	22.5	26.8	1.8	17.3	10.2	4.8	738	1808	603
341	41.4	21.4	26.2	2	17.8	10.1	4.6	737	1808	607
342	41.4	21.4	25.6	2	17.7	9.9	4.6	736	1803	577
343	41.9	20.3	25	2.3	18.1	9.8	4.4	735	1803	581
344	41.9	20.3	24.4	2.3	17.9	9.5	4.4	735	1797	550
345	42.3	19.1	23.7	2.5	18.3	9.5	4.2	734	1797	554

Cycle number	SOI (bTDC)	FQ (mg/cycle)	PR (%)	Fraction of early HR modelled (%)	Fraction of late HR modelled (%)	CA50 (aTDC)	MPRR (bar/CAD)	Tsoc (K)	Psoc (kPa)	IMEP (kPa)
346	42.3	19.1	23.1	2.6	18.2	9.3	4.2	733	1794	521
347	42.8	18	22.5	2.8	18.2	9.3	4	732	1794	525
348	42.8	18	21.9	2.9	18.1	9	4	731	1788	494
349	43.3	18	21.3	3	17.6	9	4	730	1788	498
350	43.7	18	20.6	3.2	17.2	8.7	4	729	1782	497
351	43.7	18	20	3.2	17.1	8.4	4	729	1779	496
352	44.2	18	19.4	3.4	16.6	8.3	4	729	1775	495
353	44.2	18	18.7	3.5	16.5	8	4	728	1769	494
354	44.6	18	18.1	3.6	16.1	8	4.1	728	1769	493
355	45	18	17.5	3.8	15.7	7.5	4.1	727	1763	491
356	45	18	16.9	3.9	15.5	7.4	4.1	727	1760	490
357	45	18	16.3	4	15.4	7.2	4.1	727	1757	489
358	45	18	15.6	4.1	15.2	7.1	4.1	726	1757	488
359	45	18	15	4.2	15.1	6.9	4.1	726	1753	486
360	45	18	14.4	4.3	14.9	6.8	4.1	726	1750	485
361	45	18	13.8	4.4	14.8	6.6	4.1	726	1750	484
362	45	18	13.2	4.5	14.6	6.5	4.1	725	1747	483
363	45	19.3	12.6	4.4	13.9	6.3	4.3	725	1747	482
364	45	19.3	12.1	4.5	13.8	6	4.3	725	1744	516
365	45	20.5	11.5	4.4	12.9	5.9	4.6	726	1741	509
366	45	20.5	10.9	4.6	12.7	5.6	4.6	726	1738	540
367	45	21.8	10.4	4.4	11.6	5.4	4.8	726	1734	533
368	45	21.8	9.8	4.6	11.5	5.1	4.8	726	1731	567
369	45	23	9.3	4.4	10.3	4.8	5.1	727	1728	560
370	45	23	8.8	4.6	10.2	4.8	5	727	1728	590

Cycle number	SOI (bTDC)	FQ (mg/cycle)	PR (%)	Fraction of early HR modelled (%)	Fraction of late HR modelled (%)	CA50 (aTDC)	MPRR (bar/CAD)	Tsoc (K)	Psoc (kPa)	IMEP (kPa)
371	45	24	8.2	4.5	9.1	4.4	5.2	728	1721	584
372	45	24	7.7	4.7	9	4.2	5.2	728	1721	609
373	45	25	7.3	4.6	7.9	4.1	5.4	728	1718	604
374	45	25	6.8	4.7	7.8	3.8	5.4	728	1715	628
375	45	26	6.3	4.6	6.6	3.6	5.6	728	1711	623
376	45	26	5.9	4.8	6.5	3.5	5.6	729	1711	648
377	45	27	5.4	4.7	5.2	3.2	5.8	729	1708	643
378	45	27	5	4.8	5.1	3.2	5.8	729	1708	668
379	45	27	4.6	5	5	2.9	5.8	730	1704	663
380	45	27	4.2	5.1	4.9	2.6	5.8	729	1701	661
381	45	27	3.8	5.3	4.9	2.6	5.8	729	1701	660
382	45	27	3.5	5.4	4.8	2.4	5.8	729	1701	660
383	44.6	27	3.1	5.4	5	2.3	5.8	729	1697	659
384	44.6	27	2.8	5.6	4.9	2.3	5.8	729	1701	658
385	44	27	2.5	5.6	5.3	2.3	5.8	729	1701	658
386	44	27	2.2	5.7	5.3	2.4	5.8	730	1708	657
387	43.4	27	1.9	5.7	5.6	2.1	5.7	730	1704	656
388	43.4	27	1.6	5.8	5.6	2.3	5.7	731	1711	656
389	42.8	27	1.4	5.8	6	2.3	5.7	731	1711	655
390	42.8	27	1.2	5.9	5.9	2.3	5.7	731	1715	655
391	42.2	27	1	5.8	6.3	2.1	5.7	731	1715	654
392	41.5	27	0.8	5.8	6.8	2.3	5.7	732	1722	654
393	41.5	27	0.6	5.8	6.8	2.4	5.7	732	1729	654
394	40.8	25.9	0.5	6	8.4	2.3	5.4	733	1729	653
395	40.8	25.9	0.4	6.1	8.4	2.4	5.4	733	1735	624
396	40.2	24.8	0.2	6.2	9.8	2.4	5.2	733	1738	629
397	40.2	24.8	0.2	6.3	9.8	2.6	5.2	733	1745	600
398	39.5	23.6	0.1	6.4	11.3	2.3	5	732	1745	605

Cycle number	SOI (bTDC)	FQ (mg/cycle)	PR (%)	Fraction of early HR modelled (%)	Fraction of late HR modelled (%)	CA50 (aTDC)	MPRR (bar/CAD)	Tsoc (K)	Psoc (kPa)	IMEP (kPa)
399	39.5	23.6	0	6.5	11.3	2.4	5	733	1754	573
400	38.9	22.5	0	6.6	12.6	2.1	4.7	733	1758	578
401	38.9	22.5	0	6.6	12.6	2.1	4.7	734	1767	550
402	38.4	21.4	0	6.7	13.6	-0.6	4.5	735	1791	555
403	38.4	21.4	0	6.7	13.6	2.4	4.5	733	1773	525
404	37.9	20.3	0.1	6.8	14.5	3	4.3	732	1773	530
405	37.9	20.3	0.2	6.8	14.5	3.9	4.3	733	1779	502
406	37.4	19.1	0.2	6.9	15.3	4.2	4	732	1779	506
407	37.4	19.1	0.4	6.9	15.4	4.8	4	732	1785	475
408	37	18	0.5	6.9	15.9	5.3	3.8	731	1788	480
409	36.6	18	0.6	6.8	16.1	5.7	3.8	731	1790	451
410	36.6	18	0.8	6.7	16.2	6.2	3.8	731	1796	456
411	36.3	18	1	6.5	16.4	6.5	3.8	731	1799	457
412	36.3	18	1.2	6.4	16.5	6.8	3.8	732	1802	457
413	35.9	18	1.4	6.2	16.7	6.9	3.8	732	1802	458
414	35.8	18	1.6	6.1	16.9	7.4	3.8	732	1808	458
415	35.8	18	1.9	6	16.9	7.4	3.8	732	1808	459
416	35.7	18	2.2	5.9	17.1	7.5	3.8	732	1808	459
417	35.7	18	2.5	5.7	17.2	7.8	3.8	732	1810	460
418	35.7	18	2.8	5.6	17.3	8	3.8	732	1810	460
419	35.7	18	3.1	5.5	17.4	8	3.8	732	1810	461
420	35.7	18	3.5	5.3	17.5	8.1	3.8	732	1810	461
421	35.8	19.3	3.8	5	17.2	8.3	4	733	1813	462
422	35.8	19.3	4.2	4.8	17.3	8.1	4	732	1811	498
423	35.9	20.5	4.6	4.5	16.8	8.3	4.3	734	1811	493

Cycle number	SOI (bTDC)	FQ (mg/cycle)	PR (%)	Fraction of early HR modelled (%)	Fraction of late HR modelled (%)	CA50 (aTDC)	MPRR (bar/CAD)	Tsoc (K)	Psoc (kPa)	IMEP (kPa)
424	35.9	20.5	5	4.3	16.9	8.3	4.3	734	1811	526
425	36	21.8	5.4	3.9	16.3	8.1	4.5	735	1808	521
426	36	21.8	5.9	3.8	16.4	8.1	4.5	735	1808	556
427	36.1	23	6.3	3.4	15.6	8.3	4.7	736	1808	552
428	36.3	24	6.8	3.2	14.7	8.3	4.9	736	1809	584
429	36.3	24	7.3	3	14.8	8.1	4.9	737	1806	606
430	36.5	25	7.7	2.7	13.9	8	5.1	738	1803	602
431	36.7	26	8.2	2.5	12.9	8.1	5.3	738	1803	629
432	36.7	26	8.8	2.3	13	8	5.3	739	1801	652
433	37	27	9.3	2.1	11.8	8	5.5	739	1801	648
434	37	27	9.8	2	12	7.8	5.5	739	1798	675
435	37.2	27	10.4	1.9	11.9	8	5.5	740	1798	672
436	37.2	27	10.9	1.8	12	8	5.5	740	1798	672
437	37.4	27	11.5	1.7	12	8	5.6	740	1798	673
438	37.4	27	12.1	1.6	12.1	8.1	5.6	740	1798	674
439	37.6	27	12.6	1.6	12.1	8.1	5.6	740	1798	675
440	37.6	27	13.2	1.5	12.2	8.3	5.6	740	1798	677
441	37.9	27	13.8	1.4	12.1	8.3	5.6	740	1798	678
442	37.9	27	14.4	1.3	12.2	8.3	5.6	740	1798	679
443	38.1	27	15	1.3	12.2	8.4	5.6	740	1798	680
444	38.1	27	15.6	1.2	12.3	8.4	5.6	740	1798	681
445	38.3	27	16.3	1.2	12.2	8.4	5.6	740	1798	683
446	38.3	27	16.9	1.1	12.3	8.6	5.6	740	1798	684
447	38.5	27	17.5	1.1	12.3	8.7	5.6	741	1801	685
448	38.5	27	18.1	1.1	12.4	8.7	5.6	741	1801	686
449	38.7	27	18.7	1.1	12.4	8.9	5.6	741	1801	687
450	38.9	25.9	19.4	1.2	13.6	8.9	5.4	741	1801	689
451	38.9	25.9	20	1.2	13.7	9	5.4	741	1801	661

Cycle number	SOI (bTDC)	FQ (mg/cycle)	PR (%)	Fraction of early HR modelled (%)	Fraction of late HR modelled (%)	CA50 (aTDC)	MPRR (bar/CAD)	Tsoc (K)	Psoc (kPa)	IMEP (kPa)
452	39.1	24.8	20.6	1.3	14.9	9.2	5.2	740	1803	667
453	39.1	24.8	21.3	1.3	15.1	9.3	5.2	740	1803	640
454	39.2	23.6	21.9	1.5	16.3	9.5	5	739	1806	646
455	39.2	23.6	22.5	1.4	16.5	9.6	5	739	1806	616
456	39.4	22.5	23.1	1.6	17.5	9.8	4.8	738	1809	622
457	39.4	22.5	23.7	1.6	17.6	9.9	4.8	738	1808	595
458	39.5	21.4	24.4	1.7	18.6	10.2	4.6	738	1814	601
459	39.5	21.4	25	1.7	18.7	10.4	4.6	738	1814	573
460	39.7	20.3	25.6	1.9	19.6	10.5	4.3	737	1817	579
461	39.7	20.3	26.2	1.8	19.7	10.7	4.3	737	1816	552
462	39.8	19.1	26.8	2	20.5	10.8	4.1	736	1819	558
463	39.8	19.1	27.4	2	20.6	11.1	4.1	736	1821	527
464	39.9	18	27.9	2.1	21.2	11.3	3.9	735	1824	533
465	39.9	18	28.5	2.1	21.4	11.4	3.9	735	1824	505
466	40	18	29.1	2.1	21.5	11.6	3.9	734	1826	511
467	40	18	29.6	2.1	21.6	11.7	3.9	734	1829	513
468	40	18	30.2	2.1	21.7	11.9	3.9	734	1829	514
469	40.1	18	30.7	2.1	21.8	12	3.9	735	1832	515
470	40.1	18	31.2	2.1	21.9	12	3.9	735	1832	516
471	40.1	18	31.8	2.1	22	12	3.9	735	1832	517
472	40.1	18	32.3	2.1	22.2	12.3	3.9	735	1834	518
473	40.1	18	32.7	2.2	22.3	12.3	3.9	735	1834	519
474	40.1	18	33.2	2.2	22.4	12.5	3.9	735	1837	520
475	40.1	18	33.7	2.2	22.5	12.5	3.9	735	1837	521
476	40.1	18	34.1	2.2	22.6	12.6	3.9	736	1839	522

Cycle number	SOI (bTDC)	FQ (mg/cycle)	PR (%)	Fraction of early HR modelled (%)	Fraction of late HR modelled (%)	CA50 (aTDC)	MPRR (bar/CAD)	Tsoc (K)	Psoc (kPa)	IMEP (kPa)
477	40.1	18	34.6	2.2	22.7	12.8	3.9	736	1839	523
478	40	19.3	35	2.1	22.2	12.9	5.5	736	1841	524
479	40	19.3	35.4	2.1	22.3	12.8	5.5	736	1842	559
480	39.9	20.5	35.8	2	21.6	12.8	5.9	737	1842	555
481	39.9	20.5	36.2	2	21.7	12.8	5.9	737	1842	587
482	39.8	21.8	36.5	1.9	20.7	12.8	6.3	738	1842	583
483	39.8	21.8	36.9	2	20.8	12.9	6.3	739	1845	618
484	39.6	23	37.2	1.9	19.8	12.8	6.6	740	1842	613
485	39.6	23	37.5	1.9	19.9	12.9	6.6	740	1845	645
486	39.5	24	37.8	1.8	18.9	12.9	6.9	741	1845	640
487	39.5	24	38.1	1.8	19	12.9	6.9	741	1845	667
488	39.3	25	38.4	1.8	18	12.9	7.1	742	1845	663
489	39.3	25	38.6	1.8	18	12.8	7.1	742	1845	689
490	39	26	38.8	1.7	17	12.9	7.4	743	1845	685
491	39	26	39	1.7	17.1	12.9	7.4	744	1848	712
492	38.8	27	39.2	1.6	15.9	12.9	7.6	745	1848	708
493	38.8	27	39.4	1.7	16	12.9	7.6	745	1848	734
494	38.5	27	39.5	1.6	16.2	12.9	7.5	746	1848	730
495	38.5	27	39.6	1.6	16.2	13.1	7.5	746	1850	729
496	38.2	27	39.8	1.6	16.5	13.1	7.5	746	1850	730
497	38.2	27	39.8	1.6	16.5	13.2	7.5	746	1852	730
498	37.9	27	39.9	1.6	16.7	13.2	7.4	746	1852	730
499	37.5	27	40	1.5	17	13.5	7.3	746	1855	730
500	37.5	27	40	1.5	17	13.8	7.3	747	1859	730
501	37.2	27	40	1.5	17.2	13.8	7.2	747	1859	730
502	36.8	27	40	1.5	17.5	14	7.1	747	1861	730
503	36.4	27	40	1.4	17.7	14.1	7	747	1863	730
504	36.4	27	39.9	1.4	17.7	14.3	7	748	1866	730

Cycle number	SOI (bTDC)	FQ (mg/cycle)	PR (%)	Fraction of early HR modelled (%)	Fraction of late HR modelled (%)	CA50 (aTDC)	MPRR (bar/CAD)	Tsoc (K)	Psoc (kPa)	IMEP (kPa)
505	36	27	39.8	1.4	18	14.3	6.9	748	1866	730
506	36	27	39.8	1.4	18	14.4	6.9	748	1870	730
507	35.6	25.9	39.6	1.3	19.6	14.4	6.5	748	1870	730
508	35.6	25.9	39.5	1.3	19.6	14.7	6.5	748	1871	701
509	35.1	24.8	39.4	1.3	21.2	14.7	6.1	747	1871	705
510	35.1	24.8	39.2	1.3	21.1	15	6.1	748	1875	677
511	34.7	23.6	39	1.3	22.6	15.2	5.6	747	1877	681
512	34.7	23.6	38.8	1.3	22.6	15.3	5.6	747	1879	649
513	34.3	22.5	38.6	1.3	23.9	15.3	5.3	746	1879	654
514	34.3	22.5	38.4	1.2	23.8	15.6	5.3	746	1882	625
515	33.9	21.4	38.1	1.2	24.9	15.6	4.9	745	1882	629
516	33.9	21.4	37.8	1.2	24.9	16.1	4.9	745	1886	600
517	33.5	20.3	37.5	1.2	25.8	16.1	4.6	744	1886	604
518	33.5	20.3	37.2	1.2	25.8	16.2	4.6	744	1887	575
519	33.1	19.1	36.9	1.1	26.6	16.4	4.2	744	1889	579
520	32.8	18	36.5	1.1	27.1	16.5	3.9	744	1890	547
521	32.8	18	36.2	1.1	27	17	3.9	743	1893	521
522	32.5	18	35.8	1	27.1	16.8	3.9	742	1893	526
523	32.2	18	35.4	1	27.1	17	3.8	742	1894	526
524	32.2	18	35	1	27	17.1	3.8	742	1896	525
525	32	18	34.6	0.9	27	17.1	3.8	742	1896	524
526	32	18	34.1	0.9	26.9	17.1	3.8	742	1896	523
527	31.8	18	33.7	0.8	26.9	17.1	3.8	742	1896	522
528	31.8	18	33.2	0.8	26.8	17	3.8	742	1896	521
529	31.7	18	32.7	0.8	26.7	17	3.8	742	1896	520

Cycle number	SOI (bTDC)	FQ (mg/cycle)	PR (%)	Fraction of early HR modelled (%)	Fraction of late HR modelled (%)	CA50 (aTDC)	MPRR (bar/CAD)	Tsoc (K)	Psoc (kPa)	IMEP (kPa)
530	31.7	18	32.3	0.8	26.6	17	3.8	742	1896	520
531	31.7	18	31.8	0.8	26.4	16.8	3.8	742	1894	519
532	31.7	18	31.2	0.7	26.3	16.7	3.8	742	1894	518
533	31.7	18	30.7	0.7	26.2	16.5	3.8	741	1893	517
534	31.7	18	30.2	0.7	26.1	16.5	3.8	741	1893	516
535	31.8	18	29.6	0.7	25.9	16.5	3.8	741	1893	514
536	32.1	20.5	29.1	0.6	24.5	16.4	4.4	741	1891	513
537	32.1	20.5	28.5	0.6	24.4	15.8	4.4	741	1889	580
538	32.4	21.8	27.9	0.5	23.2	15.5	4.8	743	1885	568
539	32.4	21.8	27.4	0.5	23.1	15	4.8	743	1882	601
540	32.7	23	26.8	0.4	21.8	14.9	5.1	744	1880	594
541	32.7	23	26.2	0.4	21.7	14.4	5.1	744	1877	624
542	33.1	24	25.6	0.4	20.4	14.3	5.5	745	1875	618
543	33.1	24	25	0.4	20.3	13.8	5.5	744	1871	642
544	33.5	25	24.4	0.3	19	13.7	5.8	745	1869	637
545	33.5	25	23.7	0.3	18.9	13.2	5.8	745	1865	661
546	33.9	26	23.1	0.3	17.5	13.1	6.2	745	1863	656
547	33.9	26	22.5	0.3	17.4	12.6	6.2	745	1857	680
548	34.3	27	21.9	0.3	15.9	12.3	6.6	745	1854	675
549	34.3	27	21.3	0.3	15.8	12	6.6	745	1850	699
550	34.8	27	20.6	0.4	15.4	11.7	6.7	746	1848	694
551	35.2	27	20	0.4	15	11.4	5.5	745	1843	692
552	35.2	27	19.4	0.5	14.9	11.1	5.5	745	1838	691
553	35.7	27	18.7	0.6	14.4	10.8	5.5	744	1836	690
554	35.7	27	18.1	0.6	14.3	10.5	5.5	744	1831	688
555	36.1	27	17.5	0.7	14	10.4	5.5	744	1828	687
556	36.1	27	16.9	0.8	13.9	9.9	5.5	743	1823	686
557	36.4	27	16.3	0.9	13.5	9.9	5.5	743	1823	685

Cycle number	SOI (bTDC)	FQ (mg/cycle)	PR (%)	Fraction of early HR modelled (%)	Fraction of late HR modelled (%)	CA50 (aTDC)	MPRR (bar/CAD)	Tsoc (K)	Psoc (kPa)	IMEP (kPa)
558	36.4	27	15.6	0.9	13.4	9.6	5.5	742	1817	683
559	36.7	27	15	1.1	13.1	9.4	5.5	742	1817	682
560	36.7	27	14.4	1.1	13	9.2	5.5	742	1812	681
561	37	27	13.8	1.3	12.7	9.1	5.5	742	1812	680
562	37	27	13.2	1.4	12.6	8.7	5.5	741	1806	679
563	37.2	27	12.6	1.5	12.3	8.6	5.5	741	1804	678
564	37.2	27	12.1	1.6	12.2	8.4	5.5	741	1801	677
565	37.3	25.9	11.5	1.9	13.3	8.2	5.3	741	1801	675
566	37.3	25.9	10.9	2	13.1	8.1	5.3	740	1798	645
567	37.4	24.8	10.4	2.3	14.1	8.1	5.1	739	1798	649
568	37.4	24.8	9.8	2.4	14	8	5.1	739	1795	620
569	37.4	23.6	9.3	2.8	14.9	8	4.9	738	1798	623
570	37.4	23.6	8.8	2.9	14.8	7.8	4.9	738	1794	591
571	37.4	22.5	8.2	3.3	15.6	7.8	4.7	737	1794	595
572	37.3	21.4	7.7	3.6	16.3	7.8	4.5	737	1794	566
573	37.3	21.4	7.3	3.7	16.2	8	4.5	736	1797	540
574	37.1	20.3	6.8	4	16.8	7.8	4.3	735	1797	544
575	37.1	20.3	6.3	4.2	16.7	7.8	4.3	735	1797	515
576	37	19.1	5.9	4.5	17.1	8	4	734	1800	518
577	37	19.1	5.4	4.7	17	8	4	734	1799	486
578	36.7	18	5	5	17.4	8	3.8	733	1799	490
579	36.7	18	4.6	5.1	17.3	8.1	3.8	733	1802	460
580	36.5	18	4.2	5.2	17.2	8	3.8	732	1802	464
581	36.5	18	3.8	5.4	17.1	8.1	3.8	732	1805	464
582	36.2	18	3.5	5.4	17.2	8	3.8	732	1805	463

Cycle number	SOI (bTDC)	FQ (mg/cycle)	PR (%)	Fraction of early HR modelled (%)	Fraction of late HR modelled (%)	CA50 (aTDC)	MPRR (bar/CAD)	Tsoc (K)	Psoc (kPa)	IMEP (kPa)
583	35.9	18	3.1	5.5	17.3	8	3.8	732	1808	462
584	35.9	18	2.8	5.6	17.2	8.1	3.8	732	1810	461
585	35.7	18	2.5	5.7	17.2	7.8	3.8	732	1808	461
586	35.7	18	2.2	5.9	17.1	8	3.8	732	1810	460
587	35.4	18	1.9	5.9	17.2	7.8	3.8	732	1810	460
588	35.4	18	1.6	6	17.1	7.8	3.8	733	1813	459
589	35.1	18	1.4	6.1	17.2	7.7	3.8	733	1813	458
590	35.1	18	1.2	6.2	17.1	7.8	3.8	733	1816	458
591	34.9	18	1	6.2	17.1	7.7	4.4	733	1816	458
592	34.9	18	0.8	6.3	17.1	7.5	4.4	733	1816	457
593	34.7	18	0.6	6.3	17.1	7.4	4.3	733	1816	457
594	34.7	18	0.5	6.4	17.1	7.4	4.3	733	1819	457
595	34.5	19.3	0.4	6.1	16.9	7.2	4.6	733	1819	456
596	34.5	19.3	0.2	6.2	16.9	7.1	4.6	734	1821	491
597	34.3	20.5	0.2	5.9	16.5	6.6	4.9	735	1819	485
598	34.3	20.5	0.1	6	16.5	6.5	4.9	735	1822	517
599	34.2	21.8	0	5.7	15.9	6.2	5.3	736	1822	512
600	34.2	21.8	0	5.7	15.8	5.6	5.3	736	1822	546
601	34.1	24	0	5.2	14.4	5	5.8	738	1822	540
602	34.1	24	0	5.2	14.4	2.3	5.8	740	1845	599
603	34	25	0	5	13.6	4.7	6.1	740	1820	588
604	34	25	0.1	4.9	13.7	5.3	6.1	740	1820	614
605	34.1	26	0.2	4.7	12.7	5.5	6.4	740	1817	610
606	34.1	26	0.2	4.7	12.7	5.7	6.4	740	1817	636
607	34.1	27	0.4	4.4	11.8	5.9	6.7	741	1815	631
608	34.1	27	0.5	4.4	11.9	6	6.7	741	1815	657
609	34.2	27	0.6	4.3	11.8	6.3	6.7	742	1815	653
610	34.2	27	0.8	4.2	11.9	6.3	6.7	742	1812	653

Cycle number	SOI (bTDC)	FQ (mg/cycle)	PR (%)	Fraction of early HR modelled (%)	Fraction of late HR modelled (%)	CA50 (aTDC)	MPRR (bar/CAD)	Tsoc (K)	Psoc (kPa)	IMEP (kPa)
611	34.2	27	1	4.2	11.9	6.5	6.7	742	1812	653
612	34.2	27	1.2	4.1	12	6.6	6.7	742	1812	654
613	34.4	27	1.4	4	11.9	6.7	6.7	742	1812	654
614	34.4	27	1.6	3.9	11.9	6.9	6.7	742	1812	654
615	34.5	27	1.9	3.9	11.9	7	6.8	742	1812	655
616	34.6	27	2.2	3.8	11.9	6.9	6.8	742	1809	655
617	34.6	27	2.5	3.7	12	7.1	6.8	742	1809	656
618	34.7	27	2.8	3.6	12	7.2	6.8	742	1809	657
619	34.7	27	3.1	3.4	12.1	7.4	6.8	742	1809	657
620	34.9	27	3.5	3.4	12	7.3	6.8	742	1809	658
621	34.9	27	3.8	3.2	12.1	7.5	6.8	742	1809	658
622	35	27	4.2	3.1	12.1	7.5	5.5	742	1809	659
623	35.1	25.9	4.6	3.2	13.2	7.6	5.3	742	1809	660
624	35.1	25.9	5	3.1	13.3	7.8	5.3	742	1809	632
625	35.2	24.8	5.4	3.2	14.4	7.8	5.1	741	1809	637
626	35.2	24.8	5.9	3	14.5	8	5.1	740	1809	610
627	35.3	23.6	6.3	3.2	15.6	8.3	4.8	740	1812	616
628	35.3	23.6	6.8	3	15.7	8.4	4.8	740	1811	585
629	35.4	22.5	7.3	3.1	16.6	8.6	4.6	739	1814	591
630	35.4	22.5	7.7	3	16.7	8.7	4.6	739	1814	564
631	35.4	21.4	8.2	3	17.6	8.9	4.4	738	1817	569
632	35.4	21.4	8.8	2.9	17.7	9	4.4	738	1817	542
633	35.4	20.3	9.3	3	18.4	9.3	4.2	737	1819	547
634	35.4	20.3	9.8	2.8	18.5	9.6	4.2	737	1822	519
635	35.3	19.1	10.4	2.9	19.2	9.8	4	737	1824	525

Cycle number	SOI (bTDC)	FQ (mg/cycle)	PR (%)	Fraction of early HR modelled (%)	Fraction of late HR modelled (%)	CA50 (aTDC)	MPRR (bar/CAD)	Tsoc (K)	Psoc (kPa)	IMEP (kPa)
636	35.3	19.1	10.9	2.8	19.4	10.1	4	737	1827	495
637	35.2	18	11.5	2.8	19.9	10.2	3.8	736	1829	501
638	35.2	18	12.1	2.7	20	10.5	3.8	736	1832	473
639	35.1	18	12.6	2.5	20.2	10.8	3.8	735	1834	478
640	35.1	18	13.2	2.4	20.4	11	3.8	735	1837	480
641	35	18	13.8	2.3	20.6	11	3.8	735	1837	481
642	35	18	14.4	2.2	20.7	11.3	4.3	736	1839	482
643	34.8	18	15	2	21	11.3	4.3	736	1839	484
644	34.8	18	15.6	2	21.1	11.6	4.3	736	1844	485
645	34.5	18	16.3	1.8	21.4	11.7	4.3	736	1844	486
646	34.5	18	16.9	1.7	21.6	12	4.3	737	1848	487
647	34.3	18	17.5	1.6	21.8	12.2	4.2	737	1848	488
648	33.8	18	18.1	1.5	22.2	12.5	4.1	737	1853	490
649	33.8	18	18.7	1.4	22.4	12.8	4.1	738	1857	491
650	33.5	18	19.4	1.3	22.7	13.1	4.1	738	1860	492
651	33.5	18	20	1.2	22.8	13.2	4.1	738	1862	493
652	33.2	19.3	20.6	1	22.7	13.4	4.3	738	1864	495
653	33.2	19.3	21.3	1	22.8	13.5	4.3	738	1866	531
654	33	20.5	21.9	0.8	22.5	13.5	4.6	740	1866	527
655	33	20.5	22.5	0.7	22.6	13.8	4.6	740	1871	560
656	32.7	21.8	23.1	0.5	22	13.7	4.9	741	1869	556
657	32.7	21.8	23.7	0.5	22.2	14	4.9	742	1873	591
658	32.5	23	24.4	0.4	21.4	14	5.1	743	1873	587
659	32.5	23	25	0.4	21.6	14.1	5.1	743	1875	619
660	32.3	24	25.6	0.3	20.9	14.1	5.3	745	1875	615
661	32.3	24	26.2	0.3	21	14.3	5.3	745	1877	642
662	32.2	25	26.8	0.2	20.2	14.4	5.5	746	1877	639
663	32.2	25	27.4	0.2	20.3	14.6	5.5	746	1879	666

Cycle number	SOI (bTDC)	FQ (mg/cycle)	PR (%)	Fraction of early HR modelled (%)	Fraction of late HR modelled (%)	CA50 (aTDC)	MPRR (bar/CAD)	Tsoc (K)	Psoc (kPa)	IMEP (kPa)
664	32.1	26	27.9	0.1	19.4	14.6	5.7	747	1879	663
665	32.1	26	28.5	0.2	19.5	14.7	5.7	747	1881	690
666	32.1	27	29.1	0.1	18.5	14.7	6	748	1881	687
667	32.1	27	29.6	0.1	18.6	14.7	6	748	1881	714
668	32.1	27	30.2	0.2	18.7	14.7	6	749	1881	710
669	32.1	27	30.7	0.2	18.8	14.9	6	749	1883	711
670	32.2	27	31.2	0.3	18.8	15	6	749	1883	712
671	32.2	27	31.8	0.3	18.9	15	6	749	1883	713
672	32.3	27	32.3	0.4	18.9	15	6	749	1883	714
673	32.5	27	32.7	0.4	18.9	15	6.1	749	1883	715
674	32.5	27	33.2	0.4	19	15.2	6.1	749	1883	716
675	32.7	27	33.7	0.5	18.9	15.2	6.1	749	1883	717
676	32.7	27	34.1	0.5	19	15.2	6.1	749	1883	718
677	33	27	34.6	0.6	18.9	15.2	6.2	749	1883	719
678	33	27	35	0.6	19	15	6.2	749	1881	719
679	33.4	27	35.4	0.7	18.8	15.2	6.3	749	1883	720
680	33.4	27	35.8	0.8	18.9	15.2	6.3	749	1881	721
681	33.7	27	36.2	0.8	18.8	15.2	6.3	749	1881	722
682	34.2	25.9	36.5	1	19.8	15	6.2	749	1879	723
683	34.2	25.9	36.9	1	19.9	14.7	6.2	749	1875	694
684	34.6	24.8	37.2	1.1	21	15	6	748	1877	700
685	34.6	24.8	37.5	1.1	21.1	14.9	5.9	748	1875	672
686	35.1	23.6	37.8	1.3	22.1	15	5.7	747	1877	678
687	35.1	23.6	38.1	1.3	22.2	14.9	5.7	746	1873	647
688	35.6	22.5	38.4	1.4	23.1	15	5.5	745	1875	653

Cycle number	SOI (bTDC)	FQ (mg/cycle)	PR (%)	Fraction of early HR modelled (%)	Fraction of late HR modelled (%)	CA50 (aTDC)	MPRR (bar/CAD)	Tsoc (K)	Psoc (kPa)	IMEP (kPa)
689	35.6	22.5	38.6	1.4	23.1	14.9	5.5	745	1873	625
690	36.1	21.4	38.8	1.5	23.9	15	5.3	744	1875	630
691	36.1	21.4	39	1.6	23.9	14.9	5.3	744	1871	602
692	36.6	20.3	39.2	1.7	24.5	15	5.1	743	1873	607
693	36.6	20.3	39.4	1.7	24.6	15	5.1	743	1870	578
694	37.1	19.1	39.5	1.8	25.1	15	4.9	742	1870	583
695	37.6	18	39.6	1.9	25.5	14.9	4.7	741	1868	552
696	37.6	18	39.8	1.9	25.5	14.9	4.7	740	1866	527
697	38	18	39.8	2	25.3	15	4.8	739	1868	533
698	38.5	18	39.9	2.1	25	14.8	4.9	739	1866	534
699	38.5	18	40	2.1	25	14.6	4.9	738	1862	534
700	38.9	18	40	2.1	24.8	14.7	4.9	738	1864	534
701	38.9	18	40	2.1	24.8	14.4	4.9	738	1860	534
702	39.2	18	40	2.2	24.7	14.4	5	738	1860	534
703	39.2	18	40	2.2	24.6	14.3	5	738	1857	534
704	39.6	18	39.9	2.2	24.4	14.3	5.1	738	1857	534
705	39.6	18	39.8	2.2	24.4	14.1	5.1	737	1855	534
706	39.8	18	39.8	2.3	24.2	14.1	5.1	737	1855	534
707	39.8	18	39.6	2.3	24.2	14.1	5.1	737	1855	534
708	40.1	18	39.5	2.3	24	13.9	5.1	737	1853	533
709	40.3	18	39.4	2.3	23.9	13.8	5.2	737	1851	533
710	40.3	18	39.2	2.3	23.8	13.8	5.2	737	1851	533
711	40.5	20.5	39	2.2	22	13.8	6	737	1851	533
712	40.5	20.5	38.8	2.2	21.9	13.4	6	737	1849	600
713	40.5	21.8	38.6	2.1	20.7	13.1	6.4	738	1844	589
714	40.5	21.8	38.4	2.1	20.7	13.1	6.4	739	1845	622
715	40.5	23	38.1	2	19.4	12.9	6.8	740	1842	616
716	40.4	24	37.8	1.9	18.3	12.6	7.1	740	1840	646

Cycle number	SOI (bTDC)	FQ (mg/cycle)	PR (%)	Fraction of early HR modelled (%)	Fraction of late HR modelled (%)	CA50 (aTDC)	MPRR (bar/CAD)	Tsoc (K)	Psoc (kPa)	IMEP (kPa)
717	40.4	24	37.5	1.9	18.2	12.5	7.1	740	1838	667
718	40.3	25	37.2	1.8	17	12.3	7.4	742	1838	662
719	40.3	25	36.9	1.8	17	12.2	7.4	741	1835	687
720	40.2	26	36.5	1.7	15.7	12.2	7.7	742	1835	682
721	40	27	36.2	1.6	14.5	11.9	8	742	1833	707
722	40	27	35.8	1.6	14.4	11.9	8	743	1833	728
723	39.8	27	35.4	1.5	14.5	11.7	7.9	744	1831	723
724	39.2	27	35	1.4	14.8	11.7	7.8	744	1831	721
725	39.2	27	34.6	1.4	14.8	11.9	5.6	744	1836	721
726	38.9	27	34.1	1.3	14.9	11.7	5.6	744	1833	720
727	38.9	27	33.7	1.3	14.8	11.9	5.6	744	1836	719
728	38.6	27	33.2	1.2	14.9	11.7	5.6	744	1833	718
729	38.3	27	32.7	1.2	15.1	11.9	5.6	744	1836	717
730	38.3	27	32.3	1.1	15	11.9	5.6	744	1836	716
731	37.9	27	31.8	1	15.2	11.7	5.6	744	1836	715
732	37.6	27	31.2	1	15.3	11.9	5.6	745	1838	714
733	37.6	27	30.7	0.9	15.2	11.9	5.6	745	1838	713
734	37.2	25.9	30.2	1	16.7	11.9	5.3	745	1838	712
735	37.2	25.9	29.6	0.9	16.6	12	5.3	745	1840	682
736	36.9	24.8	29.1	1	18	12	5.1	744	1840	686
737	36.9	24.8	28.5	0.9	17.9	12.2	5.1	744	1843	656
738	36.5	23.6	27.9	1	19.3	12	4.9	743	1843	660
739	36.5	23.6	27.4	1	19.1	12.3	4.9	743	1845	628
740	36.2	22.5	26.8	1	20.2	12.2	4.7	742	1845	632
741	36.2	22.5	26.2	1	20.1	12.2	4.7	742	1845	602

Cycle number	SOI (bTDC)	FQ (mg/cycle)	PR (%)	Fraction of early HR modelled (%)	Fraction of late HR modelled (%)	CA50 (aTDC)	MPRR (bar/CAD)	Tsoc (K)	Psoc (kPa)	IMEP (kPa)
742	35.9	21.4	25.6	1.1	21.1	12.3	4.4	741	1847	606
743	35.9	21.4	25	1.1	20.9	12.3	4.4	741	1847	576
744	35.6	20.3	24.4	1.2	21.7	12.3	4.2	740	1847	579
745	35.6	20.3	23.7	1.2	21.6	12.5	4.2	740	1849	549
746	35.3	19.1	23.1	1.3	22.2	12.5	4	739	1849	553
747	35.3	19.1	22.5	1.3	22.1	12.6	4	739	1851	520
748	35.1	18	21.9	1.4	22.5	12.6	3.8	738	1851	523
749	34.9	18	21.3	1.4	22.4	12.6	4.3	738	1851	493
750	34.9	18	20.6	1.5	22.3	12.8	4.3	737	1853	496
751	34.7	18	20	1.5	22.2	12.6	4.3	737	1853	496
752	34.7	18	19.4	1.5	22.1	12.6	4.3	737	1853	495
753	34.6	18	18.7	1.6	22	12.5	4.3	737	1851	493
754	34.6	18	18.1	1.6	21.8	12.5	4.3	737	1851	492
755	34.5	18	17.5	1.7	21.7	12.3	4.2	737	1851	491
756	34.5	18	16.9	1.7	21.6	12.3	4.3	737	1851	490
757	34.4	18	16.3	1.8	21.5	12.2	4.2	737	1848	488
758	34.4	18	15.6	1.9	21.3	12	4.2	737	1848	487
759	34.3	18	15	1.9	21.2	12	4.2	737	1848	486
760	34.3	18	14.4	2	21.1	11.9	4.2	737	1848	485
761	34.3	18	13.8	2.1	20.9	11.7	4.2	736	1846	483
762	34.3	18	13.2	2.2	20.8	11.7	4.2	736	1846	482
763	34.3	18	12.6	2.4	20.6	11.4	4.2	736	1844	481
764	34.3	18	12.1	2.5	20.5	11.4	4.2	736	1844	480
765	34.4	19.3	11.5	2.4	19.9	11.3	4.6	736	1841	479
766	34.5	20.5	10.9	2.4	19.2	11	4.9	736	1839	513
767	34.5	20.5	10.4	2.5	19.1	10.7	4.9	737	1837	539
768	34.5	21.8	9.8	2.4	18.2	10.4	5.3	738	1835	532
769	34.5	21.8	9.3	2.5	18.1	10.1	5.3	738	1832	565

Cycle number	SOI (bTDC)	FQ (mg/cycle)	PR (%)	Fraction of early HR modelled (%)	Fraction of late HR modelled (%)	CA50 (aTDC)	MPRR (bar/CAD)	Tsoc (K)	Psoc (kPa)	IMEP (kPa)
770	34.8	24	8.8	2.3	16.1	9.9	5.9	738	1830	558
771	34.8	24	8.2	2.4	16	9.6	5.9	738	1828	615
772	34.9	25	7.7	2.4	14.9	9.2	6.2	740	1822	605
773	34.9	25	7.3	2.5	14.8	9	6.2	740	1820	629
774	35.1	26	6.8	2.5	13.6	8.7	5.3	740	1817	624
775	35.1	26	6.3	2.7	13.5	8.4	5.3	740	1815	649
776	35.2	27	5.9	2.6	12.4	8.3	5.5	741	1812	643
777	35.2	27	5.4	2.8	12.3	8.1	5.5	741	1812	668
778	35.4	27	5	2.9	12	7.9	5.5	741	1809	663
779	35.4	27	4.6	3.1	12	7.7	5.5	741	1806	662
780	35.5	27	4.2	3.2	11.8	7.3	5.5	741	1804	661
781	35.5	27	3.8	3.3	11.7	7.4	5.5	741	1804	660
782	35.6	27	3.5	3.5	11.6	7.1	5.5	741	1801	659
783	35.6	27	3.1	3.6	11.5	7.1	5.5	741	1801	659
784	35.8	27	2.8	3.8	11.3	6.9	5.5	741	1801	658
785	35.8	27	2.5	3.9	11.2	6.8	5.5	740	1798	657
786	36	27	2.2	4	11	6.5	5.5	740	1795	657
787	36	27	1.9	4.2	10.9	6.2	5.5	740	1792	656
788	36	27	1.6	4.3	10.9	6	5.5	740	1792	656
789	36	27	1.4	4.4	10.8	6	5.5	740	1792	655
790	36.1	27	1.2	4.5	10.7	5.8	5.5	740	1792	655
791	36.1	27	1	4.6	10.7	5.6	5.5	739	1789	654
792	36.1	25.9	0.8	4.9	11.7	5.4	5.3	739	1789	654
793	36.1	25.9	0.6	4.9	11.7	5.3	5.3	739	1789	624
794	36.1	24.8	0.5	5.2	12.6	5.3	5.1	739	1792	629
795	36.1	24.8	0.4	5.3	12.6	5.3	5.1	739	1792	600

Cycle number	SOI (bTDC)	FQ (mg/cycle)	PR (%)	Fraction of early HR modelled (%)	Fraction of late HR modelled (%)	CA50 (aTDC)	MPRR (bar/CAD)	Tsoc (K)	Psoc (kPa)	IMEP (kPa)
796	36.1	23.6	0.2	5.6	13.6	5	4.9	738	1792	605
797	36.1	23.6	0.2	5.7	13.5	5	4.9	738	1794	573
798	36.1	22.5	0.1	5.9	14.3	4.7	4.7	737	1794	578
799	36.1	21.4	0	6.2	15	4.5	4.4	737	1794	550
800	36.1	21.4	0	6.2	15	4.2	4.4	736	1797	525
801	36.1	20.3	0	6.5	15.5	3.8	4.2	735	1800	530
802	36.1	20.3	0	6.5	15.5	1.4	4.2	737	1824	502
803	36.1	19.1	0	6.7	16	4.1	4	734	1802	505
804	36.1	19.1	0.1	6.7	16	4.8	4	734	1802	474
805	36	18	0.2	6.8	16.3	5.3	3.8	733	1802	479
806	36	18	0.2	6.8	16.3	5.6	3.8	733	1802	450
807	36	18	0.4	6.8	16.4	6	3.8	732	1805	455
808	36	18	0.5	6.7	16.4	6.2	3.8	732	1805	456
809	36	18	0.6	6.6	16.5	6.5	3.8	732	1805	456
810	36	18	0.8	6.5	16.5	6.6	3.8	732	1805	456
811	36	18	1	6.5	16.6	6.8	3.8	732	1805	457
812	36	18	1.2	6.4	16.6	6.9	3.8	732	1805	457
813	36	18	1.4	6.3	16.7	7.1	3.8	732	1805	458
814	36	18	1.6	6.2	16.8	7.2	3.8	732	1805	458
815	36	18	1.9	6	16.8	7.2	3.8	732	1805	459
816	36	18	2.2	5.9	16.9	7.4	3.8	732	1805	459
817	36	18	2.5	5.8	17	7.7	3.8	732	1808	460
818	36	18	2.8	5.7	17.1	7.8	3.8	732	1808	460
819	36	18	3.1	5.5	17.2	7.8	3.8	732	1808	461
820	36	18	3.5	5.4	17.3	8	3.8	732	1808	461
821	36.1	18	3.8	5.3	17.4	8	3.8	732	1808	462
822	36.1	18	4.2	5.1	17.5	8.1	3.8	732	1808	463

Cycle number	SOI (bTDC)	FQ (mg/cycle)	PR (%)	Fraction of early HR modelled (%)	Fraction of late HR modelled (%)	CA50 (aTDC)	MPRR (bar/CAD)	Tsoc (K)	Psoc (kPa)	IMEP (kPa)
823	36.1	19.3	4.6	4.7	17.2	8.3	4	732	1808	464
824	36.2	20.5	5	4.4	16.8	8.3	4.3	732	1811	500
825	36.2	21.8	5.4	4	16.1	8.1	4.5	733	1808	527
826	36.2	21.8	5.9	3.8	16.2	8	4.5	734	1806	557
827	36.3	23	6.3	3.5	15.4	8.1	4.8	736	1806	552
828	36.3	23	6.8	3.3	15.5	8.1	4.8	736	1806	584
829	36.4	24	7.3	3	14.8	8.1	4.9	737	1806	580
830	36.4	24	7.7	2.9	14.9	8	4.9	737	1803	606
831	36.6	25	8.2	2.6	14	8.1	5.1	738	1803	603
832	36.6	25	8.8	2.5	14.1	8.1	5.1	738	1803	630
833	36.8	27	9.3	2	12	8.1	5.5	739	1803	627
834	36.8	27	9.8	1.9	12.1	8	5.5	739	1801	680
835	37	27	10.4	1.9	12.1	8.1	5.5	740	1801	672
836	37	27	10.9	1.7	12.2	8	5.5	740	1798	672
837	37.1	27	11.5	1.7	12.2	8.1	5.5	741	1801	673
838	37.1	27	12.1	1.6	12.3	8.3	5.5	741	1801	674
839	37.3	27	12.6	1.5	12.3	8.3	5.5	741	1801	675
840	37.3	27	13.2	1.4	12.4	8.4	5.5	741	1801	677
841	37.5	27	13.8	1.4	12.4	8.4	5.6	741	1801	678
842	37.5	27	14.4	1.3	12.5	8.4	5.6	741	1801	679
843	37.7	27	15	1.2	12.4	8.7	5.6	741	1804	680
844	37.9	27	15.6	1.2	12.4	8.6	5.6	741	1801	681
845	38.1	27	16.3	1.2	12.4	8.5	5.6	741	1801	683
846	38.1	27	16.9	1.1	12.5	8.7	5.6	741	1801	684
847	38.5	25.9	17.5	1.3	13.6	8.7	5.4	741	1801	685

Cycle number	SOI (bTDC)	FQ (mg/cycle)	PR (%)	Fraction of early HR modelled (%)	Fraction of late HR modelled (%)	CA50 (aTDC)	MPRR (bar/CAD)	Tsoc (K)	Psoc (kPa)	IMEP (kPa)
848	38.5	25.9	18.1	1.2	13.7	8.9	5.4	741	1801	657
849	38.8	24.8	18.7	1.4	14.8	9	5.2	740	1803	663
850	38.8	24.8	19.4	1.4	14.9	9	5.2	740	1800	636
851	39	23.6	20	1.5	16.1	9.2	5	739	1803	642
852	39	23.6	20.6	1.5	16.2	9.3	5	739	1803	612
853	39.2	22.5	21.3	1.6	17.2	9.4	4.8	738	1806	619
854	39.2	22.5	21.9	1.6	17.4	9.6	4.8	738	1806	591
855	39.5	21.4	22.5	1.8	18.2	9.9	4.6	737	1811	597
856	39.5	21.4	23.1	1.8	18.4	9.9	4.6	737	1808	570
857	39.7	20.3	23.7	1.9	19.2	10.1	4.3	736	1811	576
858	39.7	20.3	24.4	1.9	19.3	10.2	4.3	736	1811	548
859	40	19.1	25	2.1	20	10.5	4.1	736	1816	554
860	40	19.1	25.6	2	20.1	10.5	4.1	735	1813	523
861	40.2	18	26.2	2.2	20.6	10.8	3.9	735	1819	530
862	40.5	18	26.8	2.2	20.6	11	3.9	735	1819	502
863	40.5	18	27.4	2.2	20.8	11	3.9	734	1819	508
864	40.7	18	27.9	2.2	20.8	11.3	3.9	734	1821	509
865	40.7	18	28.5	2.2	20.9	11.3	3.9	734	1821	510
866	41	18	29.1	2.3	20.9	11.3	3.9	734	1821	512
867	41	18	29.6	2.3	21	11.3	3.9	734	1821	513
868	41.2	18	30.2	2.3	21	11.4	3.9	734	1821	514
869	41.2	18	30.7	2.3	21.1	11.4	3.9	734	1821	515
870	41.5	18	31.2	2.4	21.1	11.5	3.9	734	1824	516
871	41.5	18	31.8	2.4	21.2	11.6	3.9	734	1824	517
872	41.7	18	32.3	2.4	21.2	11.7	4	734	1824	518
873	41.7	18	32.7	2.4	21.3	11.7	4	734	1824	519
874	41.9	18	33.2	2.5	21.3	11.7	4	734	1824	520
875	41.9	18	33.7	2.5	21.4	11.7	4	734	1824	521

Cycle number	SOI (bTDC)	FQ (mg/cycle)	PR (%)	Fraction of early HR modelled (%)	Fraction of late HR modelled (%)	CA50 (aTDC)	MPRR (bar/CAD)	Tsoc (K)	Psoc (kPa)	IMEP (kPa)
876	42.1	18	34.1	2.5	21.4	11.9	4	734	1826	522
877	42.1	18	34.6	2.5	21.5	12	4	734	1826	523
878	42.3	19.3	35	2.5	20.8	12	6	734	1826	524
879	42.3	19.3	35.4	2.5	20.9	11.9	6	734	1827	560
880	42.4	20.5	35.8	2.4	20	11.9	6.4	735	1827	555
881	42.4	20.5	36.2	2.4	20.1	11.9	6.4	736	1827	587
882	42.6	21.8	36.5	2.3	18.9	11.7	6.9	736	1824	583
883	42.6	21.8	36.9	2.4	19	11.7	6.9	737	1825	618
884	42.7	23	37.2	2.3	17.7	11.7	7.3	738	1825	613
885	42.8	24	37.5	2.2	16.6	11.6	7.7	738	1822	645
886	42.8	24	37.8	2.2	16.6	11.4	7.7	739	1822	667
887	42.8	25	38.1	2.2	15.5	11.4	8	740	1820	662
888	42.8	25	38.4	2.2	15.5	11.4	8	740	1822	689
889	42.9	26	38.6	2.2	14.2	11.3	8.4	741	1820	685
890	42.9	26	38.8	2.2	14.2	11.3	8.4	741	1820	711
891	42.8	27	39	2.1	13	11.3	8.7	742	1820	707
892	42.8	27	39.2	2.1	13	11.3	8.7	742	1820	733
893	42.8	27	39.4	2.1	13	11.3	8.7	743	1820	729
894	42.6	27	39.5	2.1	13.2	11.3	8.7	743	1820	729
895	42.6	27	39.6	2.1	13.2	11.4	8.7	743	1823	730
896	42.5	27	39.8	2.1	13.3	11.4	8.6	743	1823	730
897	42.5	27	39.8	2.1	13.4	11.4	8.6	743	1823	730
898	42.4	27	39.9	2.1	13.4	11.4	8.6	743	1823	730
899	42.4	27	40	2.1	13.5	11.6	8.6	743	1823	730
900	42.2	27	40	2.1	13.6	11.6	8.5	743	1823	730

Cycle number	SOI (bTDC)	FQ (mg/cycle)	PR (%)	Fraction of early HR modelled (%)	Fraction of late HR modelled (%)	CA50 (aTDC)	MPRR (bar/CAD)	Tsoc (K)	Psoc (kPa)	IMEP (kPa)
901	42.2	27	40	2.1	13.6	11.7	8.5	743	1825	730
902	42	27	40	2.1	13.8	11.7	8.5	743	1825	730
903	42	27	40	2.1	13.8	11.9	8.5	744	1828	730
904	41.7	27	39.9	2	14	11.9	8.4	744	1828	730
905	41.7	27	39.8	2	14	11.9	8.4	744	1828	730
906	41.4	25.9	39.8	2	15.6	11.7	8	744	1828	730
907	41.4	25.9	39.6	2	15.6	12	8	744	1830	701
908	41.1	24.8	39.5	2.1	17.2	12	7.5	743	1830	706
909	41.1	24.8	39.4	2.1	17.2	12.2	7.5	743	1833	677
910	40.5	22.5	39.2	2.1	20.2	12.3	6.6	742	1835	682
911	40.2	21.4	39	2.1	21.4	12.6	6.2	742	1837	621
912	40.2	21.4	38.8	2.1	21.4	12.9	6.2	741	1842	601
913	39.8	20.3	38.6	2.1	22.5	13.1	5.8	740	1844	606
914	39.8	20.3	38.4	2.1	22.4	13.2	5.8	740	1847	577
915	39.5	19.1	38.1	2.1	23.4	13.2	5.4	739	1847	581
916	39.5	19.1	37.8	2.1	23.3	13.5	5.4	739	1849	549
917	39.1	18	37.5	2.1	24.1	13.7	5	738	1851	554
918	39.1	18	37.2	2.1	24	13.8	5	738	1853	524
919	38.8	18	36.9	2	24.1	13.8	4.9	737	1853	528
920	38.8	18	36.5	2	24	14	4.9	737	1855	528
921	38.4	18	36.2	2	24.1	13.8	4.8	737	1853	527
922	38.4	18	35.8	1.9	24	13.8	4.9	737	1855	527
923	38.1	18	35.4	1.9	24.1	13.8	4.8	737	1855	526
924	38.1	18	35	1.9	24	13.8	4.8	737	1855	525
925	37.8	18	34.6	1.8	24	13.8	3.8	737	1855	524
926	37.8	18	34.1	1.8	23.9	14	3.8	738	1857	523

Appendix C

Mode Frontier

C.0.0.1 Optimization of hyper parameters of LS-SVM

Optimization of hyper parameters used to build the LPV-SVM model in Section 5.1.3.1 and Section 6.2 are carried out by using an optimization tool named Mode Frontier. Mode Frontier is a multi objective optimization tool. It is a multi-disciplinary optimization software developed by an Italian software house ESTECO SpA.

In simpler terms, design of experiments is generated by the tool based on the chosen optimization algorithm. Each combination of design input parameters i.e. the hyper parameters are fed to the design software and the outputs,i.e. the RMSE associated with prediction of CA_{50}, IMEP and MPRR are received back by the tool. Based on the optimization condition and objective set on the outputs, subsequent experiments are redesigned. Optimization of hyper parameters for LPV-SVM model, is carried out with Mode Frontier tool tied up with MATLAB LS-SVM code. Every combination of hyper parameters are evaluated for minimization of RMSE of CA_{50}, IMEP and MPRR prediction. The process is iterated till the maximum number of iterations are reached. Non-dominant sorting genetic algorithm (NSGA) is an extension of genetic

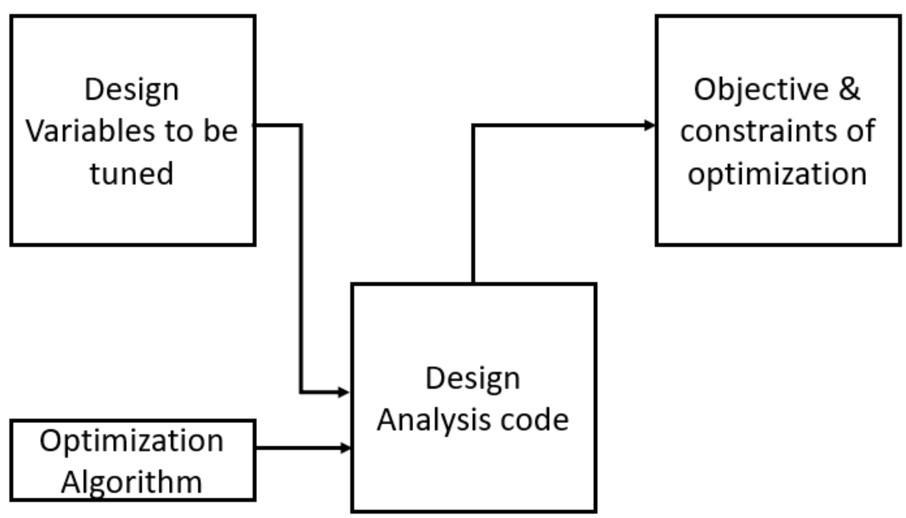

Figure C.1: Work flow of Mode Frontier tool

algorithm for optimization of multiple objective problem. Its is an adaptive algorithm, keeps redefining the inputs based on current population of data to optimise for the objectives. 4000 number of iterations are run for the model to optimise. If the result needs further improvement, the best design from current iterations are chosen and fed as initial combination for the next 4000 iterations.

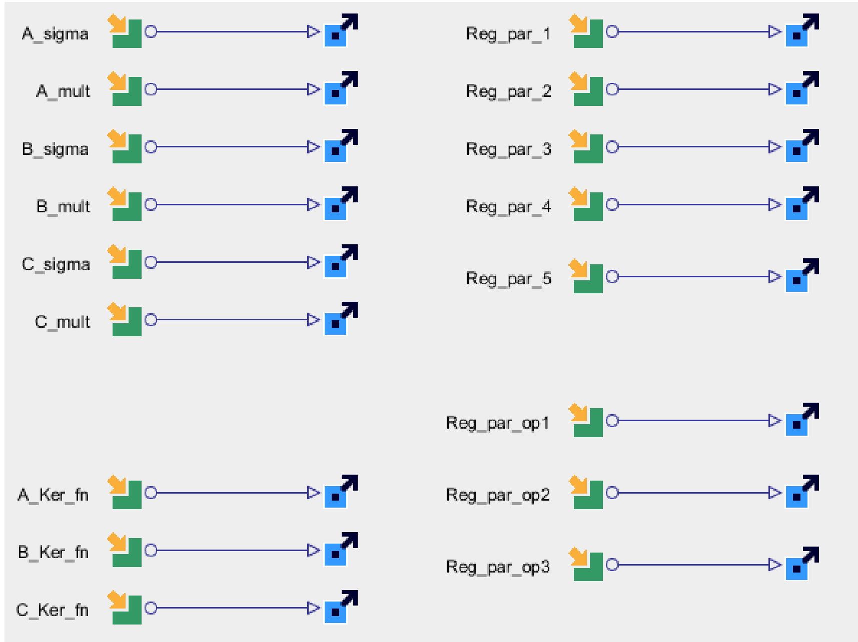

Figure C.2: Hyper parameters tuned in Mode Frontier for LPV- SVM model from Section 6.2

Figure C.2 is an example of the hyper parameters tuned for 6.2. Seven different kernel functions are used and they are linear function, radial basis function, polynomial function, sigmoid function, multi quadratic function, inverse multi quadratic function and rational multi quadratic function. Mode Frontier could choose one of it. The kernel functions are defined "unordered" for arrangement with a step size of 1. This helps the Mode Frontier tool to understand that each kernel function is independent of another even though they are numbered in a sequence.Other parameters sigma, multiplier, regularization parameter defined for the states and output are defined as "ordered" for arrangement. Range of these parameters were arrived by trial and error in order to provide a wide operating range for the Mode Frontier tool for optimization. The range of parameters are defined in the Mode Frontier, to optimize are defined in

Table C.1
Range of hyper parameters defined in Mode Frontier

	Name	Minimum	Maximum
1	Kernel Function	1	7
2	Sigma	0	1000
3	Multiplier	0	1000
4	Regularization parameter on states	0	1000000
5	Regularization parameter on output	0	1000000

Table C.1. For optimization, objective function is defined on the output parameters.

For the LPV- SVM model minimization objective was set on the RMSE of CA_{50}, IMEP and MPRR prediction, shown in Figure C.3. The downward arrow attached to RMSE of CA_{50}, IMEP and MPRR represents minimization.

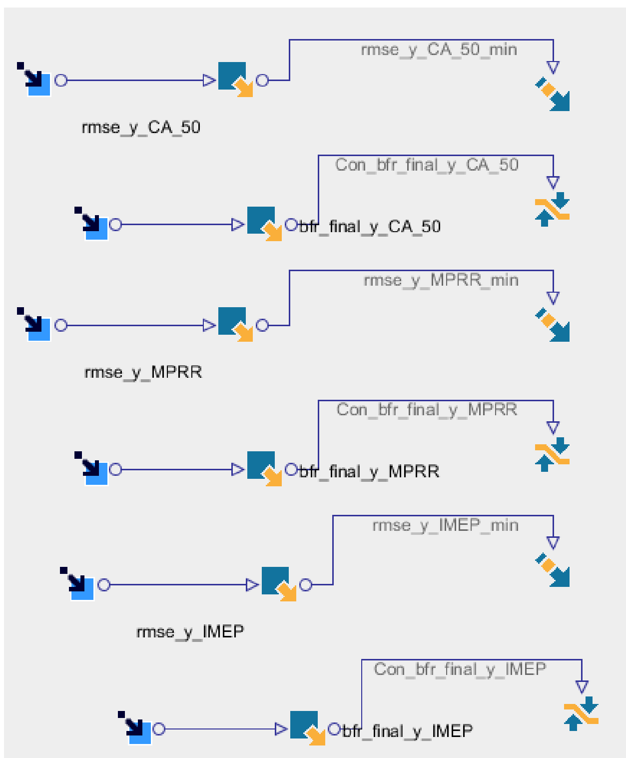

Figure C.3: Hyper parameters tuned in Mode Frontier for LPV- SVM model from Section 6.2

Appendix D

Hyper Parameters Used for System Identification

The combination of hyper parameters used for system identification of A,B,C from Chapter5, Section 5.1.3.2 is listed in Table D.1

Table D.1
Table of hyper parameters for System Identification with A,B and C matrices

Parameters	Value
Kernel Function A	Inverse multiquadratic function
Kernel function B	Radial basis function
Kernel Function C	Inverse multiquadratic function
Sigma A	915.2
Sigma B	445.2
Sigma C	151.9
Multiplier A	74.47
Multiplier B	445.9
Multiplier C	443.5
Regularisation parameter CA50	422210
Regularisation parameter MPRR	401080
Regularization parameter Tsoc	387890
Regularization parameter Psoc	424120
Regularization parameter IMEP	137420
Regularization Parameter_output CA50	3.8
Regularization parameter_output_MPRR	5.5
Regularization parameter_output_IMEP	8.0

Appendix E

Program and data files summary

E.1 Chapter 1

Table E.1
Figure Files

File	Description
Equivalence ratio to temp.png	File of Figure 1.1

Table E.2
Visio Files

File	Description
Chapter1_intro_flowchart.vsdx	Visio file of Figure 1.2
Content_thesis.vsdx	Visio file of Figure 1.3

E.2 Chapter 2

Table E.3
Figure Files

File	Description
New_LTC_Engine_Setup.png	File of Figure 2.1
Data_Setup.png	File of Figure 2.2

E.3 Chapter 3

Table E.4
Matlab Data File

Data File	Description
Combined_data_RCCI_Nitin _Kaushik_data.mat	Data used for classification

Table E.5
Matlab code Files

File Name	Description
find_peaks_rev3.m	Matlab code used to analyse and perform rule- based classification
Classification_plot.m	Matlab code used to plot classified traces
Plot_normal_dist_rev1.m	Matlab code used to analyse combustion parameters characteristics of classified traces
Decision_tree_5_bin.m	Matlab code used to create Decision tree model
Shifting_HRR_trace_rev1.m	Matlab code for shifting and normalising heat release rate to evaluate traces for k-means
HRR_K_Means_5_bin.m	Matlab code to do k-means classification

Table E.6
Python code

File	Description
regimeClass.py	Python code used to build CNN model

Table E.7
Visio Files

File	Description
Classification_flow_chart.vsdx	Visio file of the Figure 3.2

Table E.8
Figure Files

File	Description
flow_chart.png	Figure 3.2
emission_01.png	Figure 3.12
emission_02.png	Figure 3.13
emission_03.png	Figure 3.14
emission_04.png	Figure 3.15
emission_05.png	Figure 3.16
Presentation_CNN.png	Figure 3.17
CNN_data_size.png	Figure 3.18
CNN_Prediction_summary.png	Figure 3.19
Decision_tree.png	Figure 3.20
decision_tree_Prediction_summary.png	Figure 3.21

Table E.9
Matlab Figure Files

File	Description
heat release_C3.fig	Figure 3.1
Combustion regime_plot_rev1.fig	Figure 3.3
cov_imep.fig	Figure3.4
P_max_kPa.fig	Figure 3.5
MPRR.fig	Figure 3.6
CA_10_HR.fig	Figure 3.7
CA_90_HR.fig	Figure 3.8
IN_cy_Temp.fig	Figure 3.9
T_SOM_K.fig	Figure 3.10
T_EOM_K.fig	Figure 3.11
kmeans_5bin.fig	Figure 3.22

E.4 Chapter 4

Table E.10
Matlab code

Data File	**Description**
Plot_scatter.m	Matlab code for plotting Figure 4.1

Table E.11
Figures

Data File	**Description**
3clusters_exp_0.fig	Figure 4.1

Table E.12
Rstudio data and Code

Data File	**Description**
R_data_rev5_2804_type1_2_3.csv	Data with 3 clusters for PCA and Linear regression
project.R	RStudio code for PCA and Linear regression Table 4.1, 4.2
Plot_scatter.m	Matlab code for Figure 4.1

E.5 Chapter 5

Table E.13
Matlab code

Data File	Description
sch_par_model_mF_script_ver5_ABC.m and its sub functions	Matlab code for SVM- modelling of the system with ABC matrices and to generate Figure 5.1 to 5.4
contourplot_matrix_v2_2sch_var.m	Matlab code for generating contour plot of figure 5.5 to 5.7

Table E.14
Data file

Data File	Description
LPV_data_Aditya.mat	Dataset used to train SVM- LPV model and test it.

Table E.15
Figure files

Data File	Description
Input_1.fig	Figure 5.1
States.fig	Figure 5.2
scheduling_parameter.fig	Figure 5.3
normalised_Output_ABC.fig	Figure 5.4
A_matrix_ABC.fig	Figure 5.5
B_matrix_ABC.fig	Figure 5.6
C_matrix_ABC.fig	Figure 5.7

E.6 Chapter 6

Table E.16
Figure files

Filename	Description
Comparison_P1_P2_set2range_CA50.fig	Figure 6.1
Comparison_P1_P2_set2range_IMEP.fig	Figure 6.2
Comparison_P1_P2_set2range_MPRR.fig	Figure 6.3
MPC Control Model Schematic_0108_rev1.png	Figure 6.4
Case1.fig	Figure 6.5
Case2.fig	Figure 6.6
Case1_dist.fig	Figure 6.7
Case4_comp.fig	Figure 6.8
Case4.fig	Figure 6.9
Case3.fig	Figure 6.10

Table E.17
Visio files

Filename	Description
MPC Control Model Schematic_0108_rev1.vsdx	File for the Figure 6.4

Table E.18
Matlab code

File name	Description
Simulate_LPV_model.m	Simulink model to evaluate model accuracy
Surface_plot_prediction.m	Matlab code to create surface plots from Figure 6.1 to Figure 6.3

Table E.19
Simulink files

File name	Description
LPV_SVM_prediction.slx	Simulink for evaluating model accuracy
LPV_MPC_rev6.slx	Simulink with the designed MPC controller

Table E.20
Matlab Data

File name	Description
model_verification_set_to_Range.mat	Steady state data of model and RCCI engine
MPC_opt_workspace_rev9_thesis.mat	Matlab parameters for running MPC

E.7 Chapter 7

Table E.21
Figure file

File name	Description
Future_work.png	Figure 7.1

E.8 Appendix A

Table E.22
Data file

File name	Description
Combined_data_RCCI_Nitin _Kaushik_data.mat	Data used for classification of HRR

E.9 Appendix B

Table E.23
Data file

File name	Description
LPV_data_Aditya.mat	Data used for LPV-SVM identification of LTC engine

E.10 Appendix C

Table E.24
Figure file

File name	Description
Mode frontier.png	Figure C.1
mode_frontier_2.png	Figure C.2
output_constraints.png	FigureC.3